Modification of Amyloid-beta Peptide Aggregation *via* Photoactivation of Ru(II) Polypyridyl Complexes

by

Janaina C. Bataglioli

B.Sc. (Hons.), University of São Paulo, 2016

Thesis Submitted in Partial Fulfillment of the
Requirements for the Degree of
Master of Science

in the
Department of Chemistry
Faculty of Science

SIMON FRASER UNIVERSITY
Summer 2020

Approval

Name:	**Janaina C. Bataglioli**
Degree:	**Master of Science (Chemistry)**
Title:	**Modification of Amyloid-beta Peptide Aggregation *via* Photoactivation of Ru(II) Polypyridyl Complexes**
Examining Committee:	**Chair:** Dr. Corina Andreoiu Associate Professor
	Dr. Tim Storr Senior Supervisor Associate Professor
	Dr. Dipankar Sen Supervisor Professor
	Dr. Jeffrey Warren Supervisor Associate Professor
	Dr. Caterina Ramogida Internal Examiner Assistant Professor
Date Defended:	**July 28th, 2020**

Abstract

Alzheimer's disease (AD) is a chronic neurodegenerative disease characterized by progressive and irreversible damage to the brain. One of the hallmarks of the disease is the presence of both soluble and insoluble aggregates of the amyloid beta (Aβ) peptide in the brain. In this work we investigate how photoactivation of three Ru(II) polypyridyl complexes [Ru (6,6'-dimethyl-2,2'-dipyridyl)$_2$ (2-thiophen-2-yl-1H-imidazo (4,5-f) (1,10) phenanthroline)] (**Ru1**), [Ru (6,6'-dimethyl-2,2'-dipyridyl)$_2$ (2-phenyl-1H-imidazo (4,5-f) (1,10) phenanthroline)] (**Ru2**), and [Ru (6,6'-dimethyl-2,2'-dipyridyl)$_2$ (2,2'-bipyridine)] (**Ru3**), alters the aggregation profile of the Aβ peptide. Both **Ru1** and **Ru2** contain an extended planar (4,5-f) (1,10) phenanthroline ligand, as compared to a 2,2'-bipyridine ligand for **Ru3**, and we show that the presence of the phenanthroline ligand leads to a greater effect on peptide aggregation. The ability of photoactivated **Ru1-3** to bind to the Aβ peptide was evaluated by Nuclear Magnetic Resonance (NMR) which indicated the loss of the 6,6'-dimethyl-2,2'-bipyridyl (6,6'-dmb) ligand for all three complexes and the formation of a covalent bond with the Aβ peptide *via* His residue shifts for **Ru1** and **Ru2**. By comparison, no shift in His residues was observed for **Ru3**, or for the unactivated **Ru1-3** samples. The influence of **Ru1-3** on peptide aggregation was investigated using gel electrophoresis/Western blot, Transmission electron microscopy (TEM) and a Bicinchoninic acid assay (BCA assay). Upon photoactivation, the Aβ aggregation was greatly enhanced in the presence of **Ru1** and **Ru2** relative to **Ru3**, in agreement with initial binding studies by ^{1}H NMR. However, the three complexes resulted in a similar aggregate size distribution at 24 h, forming mostly insoluble amorphous aggregates. Excitingly, the complexes also changed A$\beta_{1\text{-}42}$ fibrils to amorphous aggregates upon photoactivation. The unactivated **Ru1** and **Ru2** complexes exhibited a much stronger binding affinity for Aβ (*via* Tyr^{10} fluorescence) in comparison to **Ru3**, further indicating the important role of hydrophobic interactions between the Ru complexes and the insoluble fibrillar peptide aggregates. Overall, our results show that upon photoactivation the extended planar ligand of **Ru1** and **Ru2** promotes immediate covalent binding and formation of soluble high molecular weight Aβ aggregates in comparison to **Ru3**, however similar aggregate size and morphology is observed after 24 h for all three Ru complexes.

Keywords: Alzheimer's Disease; Amyloid-β (Aβ); Ru(II) polypyridyl complexes; photoactivation; Aβ aggregation

Dedication

To my mom – thank you for showing me what a brave woman is capable of.

Acknowledgements

E como não poderia deixar de ser, meu primeiro e mais especial agradecimento é destinado à minha família. Ticiane, muito obrigada não somente por toda a ajuda em bioquímica e Pymol, mas também por sempre me proporcionar bons momentos e boas risadas. Às minhas irmãs, Daniela e Izabela, meu mais profundo agradecimento por terem estado comigo desde sempre. Nossas memórias muitas vezes são a fonte de um sorriso quando tudo parece não dar certo, e vocês são a certeza de que aconteça o que acontecer, eu nunca estarei sozinha. Sou imensamente grata também a você, Arthur, pela paciência e companheirismo diários ao longo desses últimos doze anos, e por ter me mostrado que sou capaz de muito mais do que eu poderia imaginar. Você me faz uma pessoa melhor, e sem você eu não teria conseguido. E por último, mas nunca menos importante, muito obrigada, mãezinha. Nem que eu falasse todas as línguas do mundo meu vocabulário seria extenso o suficiente para te agradecer por tudo que você fez e faz por mim. Cada conquista minha reflete a sua dedicação, o seu esforço e acima de tudo, o seu amor. Te amo!

To my supervisor Tim Storr, thank you for giving me the chance to be part of your group, and for guiding me during the last two years. It was an experience that changed me forever, and I'll carry all I learned with you for the rest of my life. To my committee members, Prof. Dipankar Sen and Prof. Jeffrey Warren, thank you for taking the time to be part of my committee, and for all the suggestions and advices that contributed to a better version of this work.

For the last two years I had the opportunity to work side by side with amazing people in the lab, and for that I'm very thankful to the Storr Group, in especial to three amazing girls. Jessica, thank you for all the ideas and discussions we had. I appreciate all your help, and I'll miss our adventures at Barre. Luiza, thank you very much for your kindness and generosity. You helped me and shared your knowledge from day one, and you for sure made this a better experience. Thank you for the long talks, for the advices, and for the fun moments punching Bob! I take our friendship to life. To amazing Khrystyna, I just have a gigantic gratitude for all the time we spent together, and I will be forever thankful for the friendship we have. For uncountable times your support and kind words gave me the strength I needed to keep going. Your friendship means much more than I'm able to describe.

To my dear friends, Arielle and Dimitri, there is no ocean big enough capable of tearing us apart. Your friendship is treasured beyond measures. I miss you, and I can't wait for the next opportunity to see you! To Dody, thank you very much for giving me my very first opportunity in Canada, for believing in me, and for always encouraging me to pursue my dreams. I hope one day I become a person as strong and intelligent as you are.

Table of Contents

List of Figures

List of Acronyms

℃	Degree Celsius
^{1}H	Proton
$^1O_2$	Singlet dioxygen
2-D	Two-dimensional
$^3O_2$	Triplet dioxygen
6,6'-dmb	6,6'-dimethyl-2,2'-dipyridyl
Aβ	Amyloid beta
AChE	Acetylcholinesterase
AD	Alzheimer's Disease
AICD	Amyloid precursor protein intracellular domain
Ala	Alanine
APP	Amyloid precursor protein
Asp	Aspartate
BBB	Blood-brain barrier
BCA	Bicinchoninic acid assay
bpy	2,2'-bipyridine
BSA	Bovine serum albumin
BSS	Pepto-bismol
C	C-terminal tail
ca.	circa
Cl^-	Chloride ion
CSF	Cerebrospinal fluid
CSP	Chemical shift perturbations
D_2O	Deuterium oxide
ddH_2O	Double distilled water
DFO	Desferrioxamine
DFT	Density functional theory
DMSO	Dimethyl sulfoxide
DMT	Disease-modifying therapies
dppz	Dipyridophenazine

EC_{50}	Half maximal effective concentration
eq.	Equivalent
ESI-MS	Electrospray ionization – mass spectrometry
FDA	Food and Drug Administration
Glu	Glutamate
GPX	Glutathione peroxidase
GS	Ground state
GSK-3β	Glycogen synthase kinase 3 beta
h	Hour
H_2O_2	Hydrogen peroxide
HCQ	Clioquinol
His	Histidine
HPLC	High pressure liquid chromatography
HSA	Human serum albumin
I	Intensity
ICP-MS	Inductively coupled plasma mass spectrometry
Ile	Isoleucine
Im	Imidazole
ISC	Intersystem crossing
K_d	Binding constant
kDa	Kilodalton
kV	Kilovolt
LD_{50}	Half maximal lethal dose
Leu	Leucine
M	Molar
MAP	Microtubule-associated proteins
MC	Metal center
MD	Molecular dynamics
Met	Methionine
MHz	Megahertz
min	Minutes
µL	Microliter
mL	Milliliter
µM	Micromolar
mM	Millimolar
MLCT	Metal-to-ligand charge-transfer
MOE	Molecular Operating Environment
MTBD	Microtubule binding domain
MW	Molecular weight

N	N-terminal acid projection domains
ND	Neurodegenerative Disease
NFTs	Neurofibrillary tangles
nm	Nanometer
$O_2^{\bullet -}$	Superoxide anion
OH$^\bullet$	Hydroxyl radical
P-tau	Hyperphosphorylated tau
PBS	Phosphate buffered saline
PBT2	5,7-Dichloro-2-[(dimethylamino)methyl]quinolin-8-ol
PDB	Protein data bank
PDT	Photodynamic therapy
PET	Positron emission tomography
Phe	Phenylalanine
phen	1,10-phenanthroline
PHF	Paired helical filaments
ppm	Parts per million
ppy	Phenylpyridine
Py	Pyridine
ROS	Reactive oxygen species
rpm	Revolutions per minute
Ru1	[Ru(6,6'-dimethyl-2,2'-dipyridyl)$_2$(2-thiophen-2-yl-1H-imidazo(4,5-f)(1,10)phenanthroline)]
Ru2	[Ru(6,6'-dimethyl-2,2'-dipyridyl)$_2$(2-phenyl-1H-imidazo(4,5-f)(1,10)phenanthroline)]
Ru3	[Ru(6,6'-dimethyl-2,2'-dipyridyl)$_2$(2,2'-bipyridine)]
sAPPβ	Soluble amyloid precursor protein beta
SAR	Structure-activity relationship
SDS	Sodium dodecyl sulfate
SOD	Superoxide dismutase
SOFAST-HMQC	Band-selective optimized flip-angle short transient heteronuclear multiple quantum correlation
STEM	Scanning TEM
TBS	Tris-buffered saline
TEM	Transmission electron microscopy
ThT	Thioflavin T
Tyr	Tyrosine
UV-Vis	Ultraviolet-visible
V	Volts
Val	Valine

WHO	World Health Organization
λem	Wavelength of emission
λex	Wavelength of excitation

Chapter 1

Introduction

Adapted from: Gomes, L. M. F.; Bataglioli, J. C.; Storr, T. Coord. Chem. Rev., 2020, 412, 213255. J. C. Bataglioli wrote the Ru(II) polypyridyl section and assisted with the literature review and figure preparation. L. M. F. Gomes wrote the V, Mn, Fe, Ru(III), Co, Rh, Ir, and Pt sections.

1.1 Alzheimer's Disease

Alzheimer's Disease (AD) is the most common progressive neurodegenerative disease (ND),[1] accounting for 60-80% of all cases of dementia, and is the fifth leading cause of death among those aged over 65 years.[2,3] Dementia is a clinical syndrome characterized by memory and cognitive decline, which prevents an individual from living a fully functional life.[3] Age is the most important risk factor for ND, with the highest incidence in people over the age of 65. In 2018 it was estimated that ND affected 50 million people worldwide, and due to an increase in global life expectancy, this number is expected to increase significantly over the next decade.[4,5] Currently more than half a million Canadians suffer from dementia, with an estimated annual cost of 11 billion dollars to care only for AD patients, which is a significant burden on the Canadian healthcare system, society, and economy.[6–8]

Alois Alzheimer was the first to describe AD more than 100 years ago,[9,10] and the search for a safe and effective therapy is still on-going.[11,12] The main histopathological features of AD in the brain are the extracellular accumulation of amyloid beta (Aβ) plaques and intracellular accumulation of neurofibrillary tangles (NFTs) of tau protein.[13–15] Opposed to other forms of dementia, the final diagnosis of AD requires post-mortem examination of the brain to determine the presence and severity of AD hallmarks: Aβ-plaques and NFTs, however ante-mortem diagnosis may soon be possible through the development of molecular neuroimaging agents.[16,17] A few positron emission tomography (PET) agents for the

detection of Aβ deposits are currently available, however, PET agents for the detection of tau accumulation are still in clinical development.[3,14] While there is no cure for AD, current FDA (Food and Drug Administration) approved treatments include four prescription drugs, (1) donepezil, (2) rivastigmine, (3) galantamine (Figure 1.1) - acetyl cholinesterase (AChE) inhibitors, and (4) memantine - a glutamate regulator, in addition to a drug combination (memantine and donepezil).[18–20] These treatments are insufficient since they only ameliorate and provide partial relief of the symptoms, and do not stop or reverse the progression of the disease.[21,22]

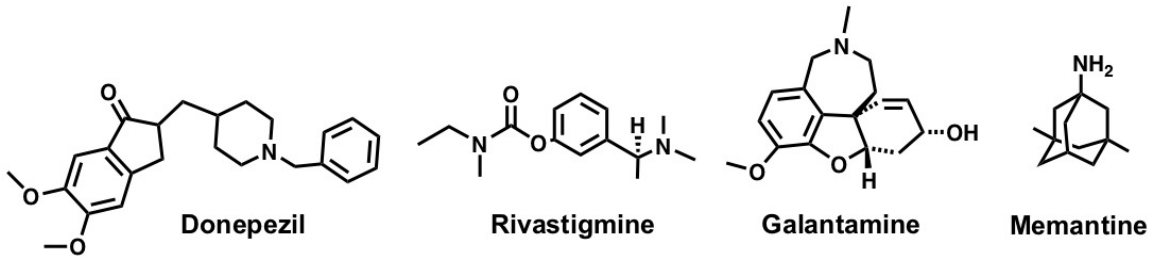

Figure 1.1 Structures of FDA-approved drugs to treat AD.

Drug discovery and development for AD is very difficult, and despite billions of dollars invested in clinical trials to develop new therapeutics for AD, there have been no new drugs approved since 2003.[23,24] The global impact of AD continues to increase, and the focus of drug development is now on disease-modifying therapies (DMTs), whose aim is to impact one or more of the characteristic brain changes caused by AD.[25] These treatments could delay or slow down the progression of the disease, and are of great interest for AD treatment.

1.2 AD Hypotheses

1.2.1 Amyloid Hypothesis

The amyloid hypothesis was first proposed almost 25 years ago, and still remains an important hypothesis in AD.[26–28] The Aβ hypothesis postulates that the progressive formation of oligomers and aggregates of the Aβ peptide is caused either by increased production or decreased clearance of Aβ, triggering a neurotoxic cascade in the brain.[8,27–29] Aβ is a low molecular-weight peptide (~4.5 kDa) derived from the proteolytic cleavage of the amyloid precursor protein (APP). APP contains 751 to 770 amino acids, and it is a single-pass transmembrane protein with a large extracellular domain containing the N-terminus and a small cytoplasmic domain containing the C-terminus. The physiological role of APP still remains unclear, but evidence suggests that APP plays an important role in cell growth, mobility, and cell survival.[27,30]

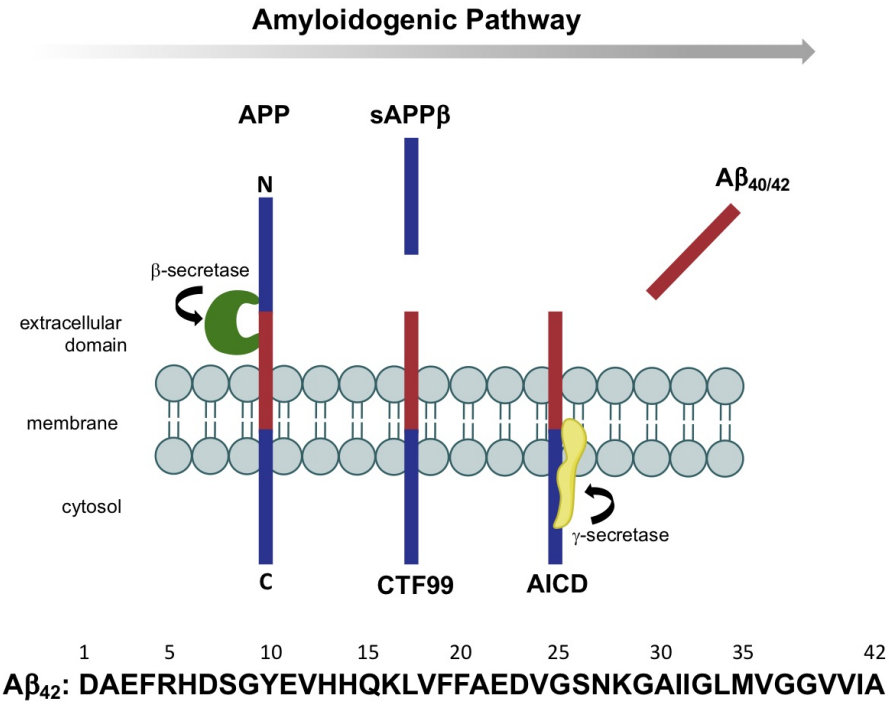

Figure 1.2 Diagram of the transmembrane protein APP and the amyloidogenic pathway showing the action of β- and γ-secretases producing $A\beta_{1\text{-}40}$ and $A\beta_{1\text{-}42}$. The amyloidogenic process also generates the soluble ectodomain sAPPβ and the intracellular -terminal fragment AICD. The full amino acid sequence for $A\beta_{1\text{-}42}$ is also shown.

Under physiological conditions, APP can be cleaved by three membrane-bound secretases, α-, β- and γ-secretase, through the amyloidogenic or non-amyloidogenic pathway. In the non-amyloidogenic pathway, APP is cleaved first by α-secretase and then by the γ-secretase, producing products that are hypothesized to have a role in brain development and in adult brain processes, such as synaptic plasticity and neurodegeneration protection.[31] The amyloidogenic pathway produces the Aβ peptide, however, it is not specific and results in different Aβ species, ranging from 38 to 43 amino acids, with the fragment ending at position 40 ($A\beta_{1\text{-}40}$) being the most abundant (~90%) followed by 42 ($A\beta_{1\text{-}42}$, ~9%) (Figure 1.2).[32–34] In this pathway, β-secretase first cleaves APP, releasing the large fragment sAPPβ.[30] A fragment containing 99 amino acids remains bound to the membrane, and when cleaved by γ-secretase, releases the Aβ peptide (Figure 1.2). While $A\beta_{1\text{-}40}$ is the most common form of the peptide found in the brain, $A\beta_{1\text{-}42}$ is more prone to aggregation due to the two additional hydrophobic amino acid residues (isoleucine and alanine) (Figure 1.2), and is more toxic.[35–37] The APP gene is located on chromosome 21, and genetic mutations on this gene have been associated with increased aggregation of Aβ through one of two mechanisms: increased overall production of all Aβ species or production of more

aggregation-prone $A\beta_{1\text{-}42}$.[38–40] A decrease in $A\beta_{1\text{-}42}$ in cerebrospinal fluid (CSF) was found to precede an increase in concentration of tau and hyperphosphorylated tau (P-tau), which suggests that Aβ plays a role in other brain processes that lead to AD.[14]

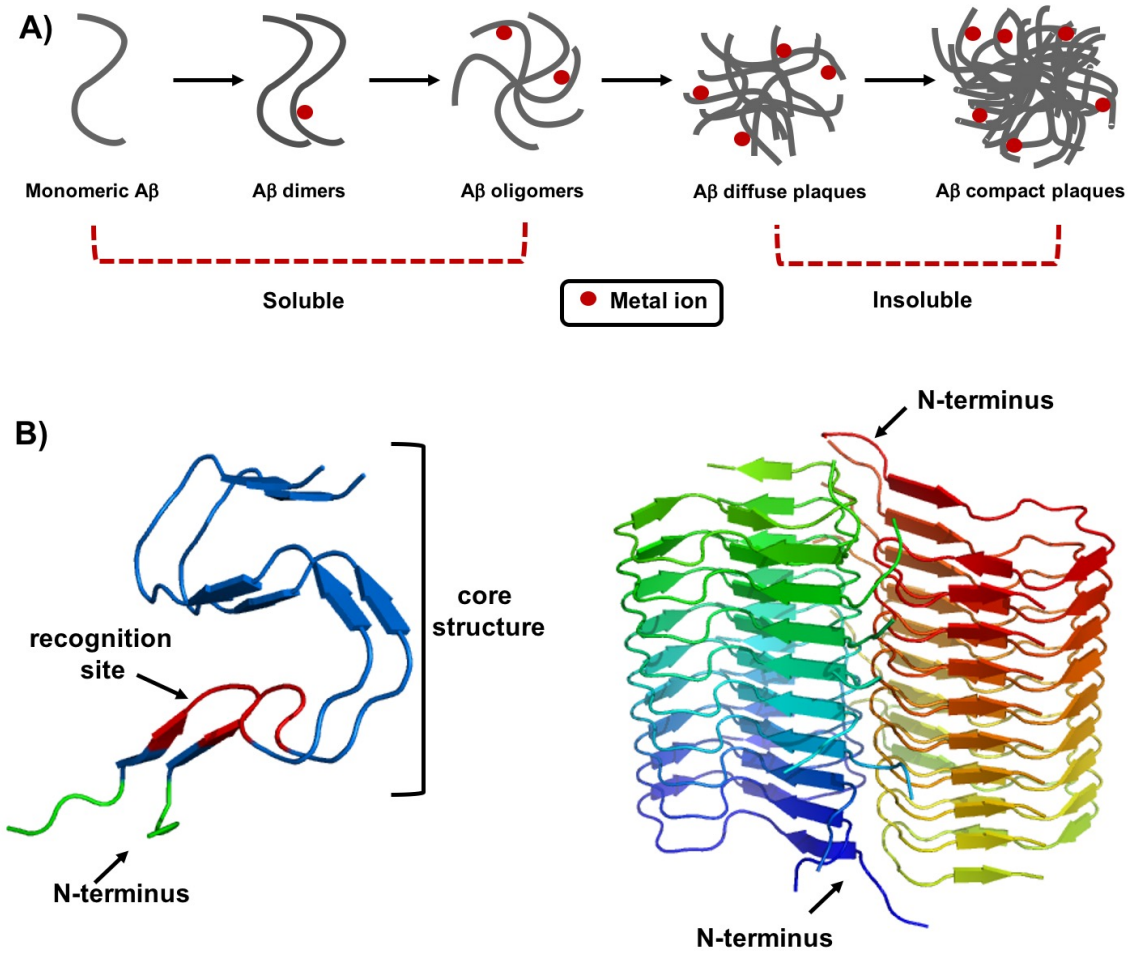

Figure 1.3 (A) Aggregation pathway of Aβ peptide including metal-ion interaction. (B) Protein data bank 5KK3 (PDB 5KK3) structure of a pair of peptides interacting, highlighting 15-42 core structure (blue) including the self-recognition portion (Leu^{17}-Ala^{21}) (red), and the unstructured N-terminus (residues 1-14) (green) (Left). PDB 5KK3 structure of $A\beta_{1\text{-}42}$ fibrils (Right).

Monomeric Aβ primarily exists as a random coil structure, however, when the monomer is converted from a random coil to a partially folded structure (α-helix and β-strand), its propensity to interact with other folded monomers *via* hydrophobic interactions is increased, leading to the formation of aggregates, such as oligomers and fibrils. Hydrophobic interactions are known to be a major driving force for Aβ aggregation, and typically occur at the hydrophobic C-terminus and/or at the self-recognition site (from Leu^{17} to Ala^{21})[41–46] (Figure 1.3).The Aβ peptide has been found in the brain in three general forms: (1) membrane

associated, (2) aggregated, and (3) soluble.[47,48] Soluble Aβ oligomers are hypothesized to induce toxicity *via* multiple mechanisms, and are reportedly more toxic as compared to other forms of Aβ, and are better correlated with memory impairment and AD progression.[42,44,45,49–51] In addition, metal ions such as Fe, Zn, and Cu have been shown to interact with Aβ, modifying the aggregation pathway of the peptide and increasing its toxicity (Figure 1.3).[52]

Three main strategies have been used to target Aβ-specific pathways to reduce aggregate formation: (1) decrease Aβ production *via* inhibition of β- or γ-secretases using secretase inhibitors or encourage other secretases to cut APP into fragments that will not produce the Aβ fragment; (2) expedite Aβ clearance by mobilizing the immune system to produce anti-bodies to target Aβ, (3) inhibit the formation of toxic Aβ aggregates by using small molecules designed to limit Aβ aggregation.[53–55]

Clinical trials of promising drugs targeting the amyloid pathway have so far failed, either due to off-target effects or a lack of efficacy.[56,57] There is considerable debate as to when drug treatments should be initiated in AD, and drug trials targeting the amyloid pathway and focused on healthy people at risk of AD are on-going.[25,58]

1.2.2 Metal Ions and Aβ

The brain contains essential d-block transition metals ions, such as Fe(II/III), Cu(I/II), and Zn(II), that are involved in the critical processes of a healthy brain.[59,60] Protein-bound cations are key elements in the maintenance of cell structures, gene expression, and cell signaling, and an imbalance in their homeostasis can affect brain function.[61] It is known that AD patients show altered metal ion homeostasis and that the insoluble Aβ plaques present in the brains of people affected by AD contain high levels of Cu, Fe, and Zn (3-5 times when compared to age-matched controls).[62–68] Monomeric Aβ is known to bind metal ions with dissociation constants (K_d) of ~10^{-10} M for Cu(II) and ~10^{-5} M for Zn(II).[69,70–76] The amino acid residues with high propensity for metal binding in the N-terminus segment include Asp^1, His^6, Tyr^{10}, Glu^{11} , His^{13}, and His^{14} (Figure 1.4)[77–80].

The binding of metal ions to Aβ is known to modulate the aggregation pattern of the peptide, for example, by reducing the electrostatic repulsion between two peptides. The presence of many Aβ peptides in the aggregate form increases the capacity for metal coordination, as several Aβ N-termini are oriented in close proximity for metal ion binding (Figure 1.3B).[60,81,82] Metal ion binding may potentiate the neurotoxicity of Aβ *via* redox-cycling and the production of reactive oxygen species (ROS) when in the presence of dioxygen, which plays an important role in oxidative stress.[83–85]

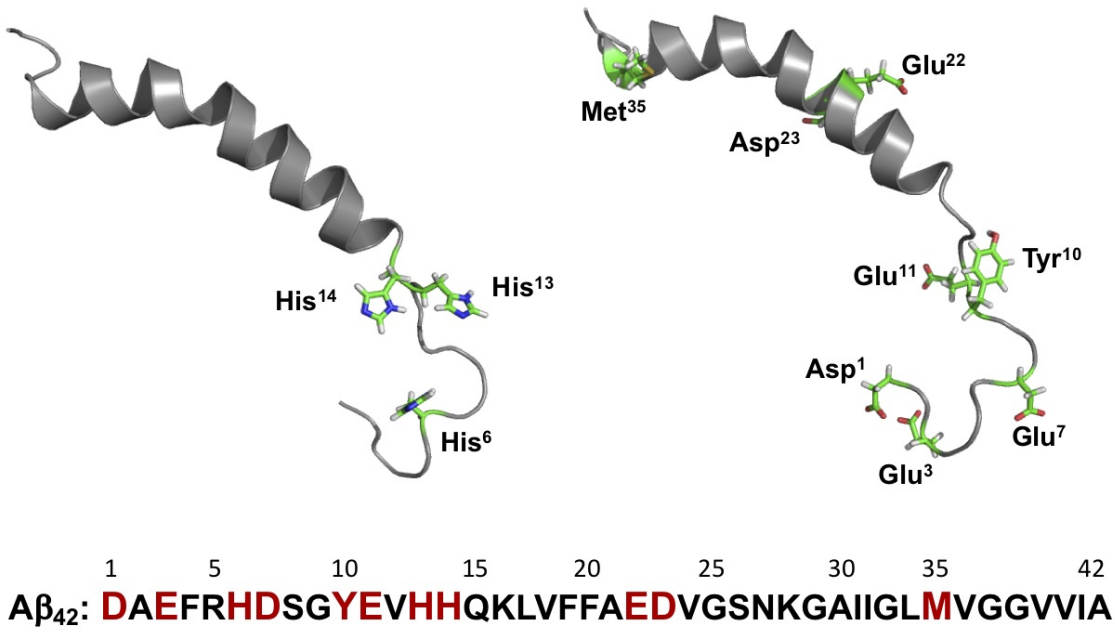

Figure 1.4 Solution structure of monomeric $A\beta_{1\text{-}40}$ (PDB 1BA4) highlighting the amino acid residues potentially involved in metal binding. (Left) Three highlighted histidine residues (His^{6}, His^{13}, and His^{14}) involved in metal binding. (Right) Negatively charged amino acids and Tyr^{10} that can also be involved in metal ion coordination, and peptide oxidation site (Met^{35}). (Bottom) Amino acid sequence of $A\beta_{1\text{-}42}$ highlighting the amino acids with propensity for metal binding.

The metal ion dyshomeostasis observed in AD and the involvement of these metal ions in Aβ aggregation are hypothesized to be important components in the development of AD.[83] One approach to limit metal binding to Aβ is the use of chelating agents. These ligands usually present moderate affinity for metal ions, and have shown promising results in the restoration of normal homeostasis and prevention of Aβ aggregation due to metal binding.[86] Desferrioxamine (DFO) (Figure 1.5) was shown to slow AD progression as one of the first examples of the use of a chelating agent to treat AD.[87] Unfortunately it failed a 24 month clinical trial, when probable AD patients presented no significant differences in memory recovery when compared to the control group.[88] Another example is Clioquinol (HCQ) (Figure 1.5), an 8-hydroxyquinoline derivative that demonstrated remarkable efficacy in animal models.[89] This ligand binds to Cu(II) and Zn(II), interacts with the Aβ peptide, crosses the blood-brain barrier (BBB), and reduces the deposition of Aβ in the brain. Importantly, clioquinol reduces the level of Cu(II) in the cortex of rats and does not alter the concentration of Cu(II) in blood, however, its purification on a large scale presented challenges.[90] In order to overcome this obstacle, an improved 8-hydroxyquinoline derivative, PBT2, was synthesized (Figure 1.5). PBT2 treatment reduced Aβ aggregation,

limited Aβ oligomer toxicity and redistributed Cu(II) and Zn(II) in mice brain tissue.[91] However, a recent phase II clinical trial failed when treatment with PBT2 did not show significant difference compared to placebo.[92,93]

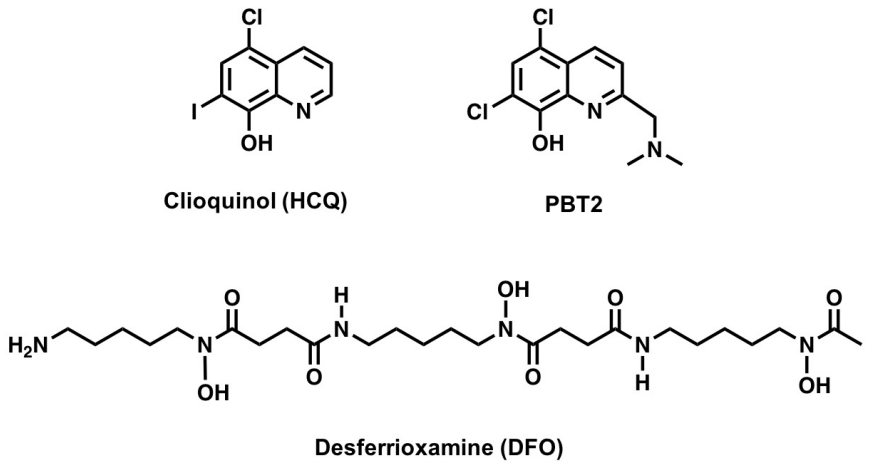

Figure 1.5 Metal-binding therapeutics tested as AD treatments.

1.2.3 Oxidative Stress

The brain requires high oxygen concentrations in order to function, in fact, approximately 20% of the oxygen supplied by the respiratory system is consumed by the brain.[94] As a result, the brain is the most vulnerable organ to the action of ROS,[85] in addition to the relatively low antioxidant capacity.[95] An increase in the levels of oxidative stress is associated with aging, with many NDs known to be linked to oxidative stress, such as in the case of AD.[84] ROS are involved in the maintenance of normal brain function, as they act as secondary messengers in the intracellular signaling cascade, and are by-products of normal cellular metabolism. Enzymes such as superoxide dismutase (SOD), glutathione peroxidase (GPX), and catalase regulate the scavenging of these ROS, however, an imbalance or dysfunction of this system can lead to cellular damage and apoptosis.[85]

Dysregulated redox-active metal ions, such as Cu and Fe, in the AD brain can interact with superoxide anion ($O_2^{\bullet -}$) and hydrogen peroxide (H_2O_2), leading to the formation of hydroxyl radical ($OH^{\bullet}$) *via* Fenton chemistry, which is harmful to living cells.[60,71,85] There is evidence linking the excessive levels of ROS to AD, as well as the abnormal levels of Aβ and oxidative stress.[96,97]

1.2.4 Tau Hypothesis

Another hallmark of AD was discovered in 1986 by Selkoe *et al.*, and consists of NFTs mainly formed by aggregation of paired helical filaments (PHFs) of phosphorylated tau protein (Figure 1.6).[38,98] Tau is one of the microtubule-associated proteins (MAP) that directly binds microtubules, regulating their assembly and stability. Phosphorylated tau dissociates from microtubules, however hyperphosphorylation of tau leads to aggregation, generating NFTs and causing neurodegeneration *via* synaptic dysfunction and neuronal loss.[99,100] Tau is found predominantly in the axons, but it is also present at lower levels in dendrites, the plasma membrane, and Golgi complex.[101] The gene that encodes the tau protein in humans is localized on chromosome 17, and six tau isoforms are expressed in the adult human brain as a result of mRNA alternative splicing, with or without exons 2, 3, and 10, with exon 10 containing the microtubule-binding region (Figure 1.6).[38,102]

Hyperphosphorylation occurs as a result of mutations in chromosome 17, leading to the expression of a protein that is more prone to phosphorylation, and also due to dysregulation of kinases and phosphatases, which trigger the neurotoxicity of tau.[103] The binding of metal ions, such as Zn(II), Cu(II), and Fe(II) to the microtubule binding domain (MTBD) of tau protein has also been shown to play a role in aggregation and hyperphosphorylation. The binding of these metal ions to the MTBD region of tau leads to the generation of ROS.[104,105]

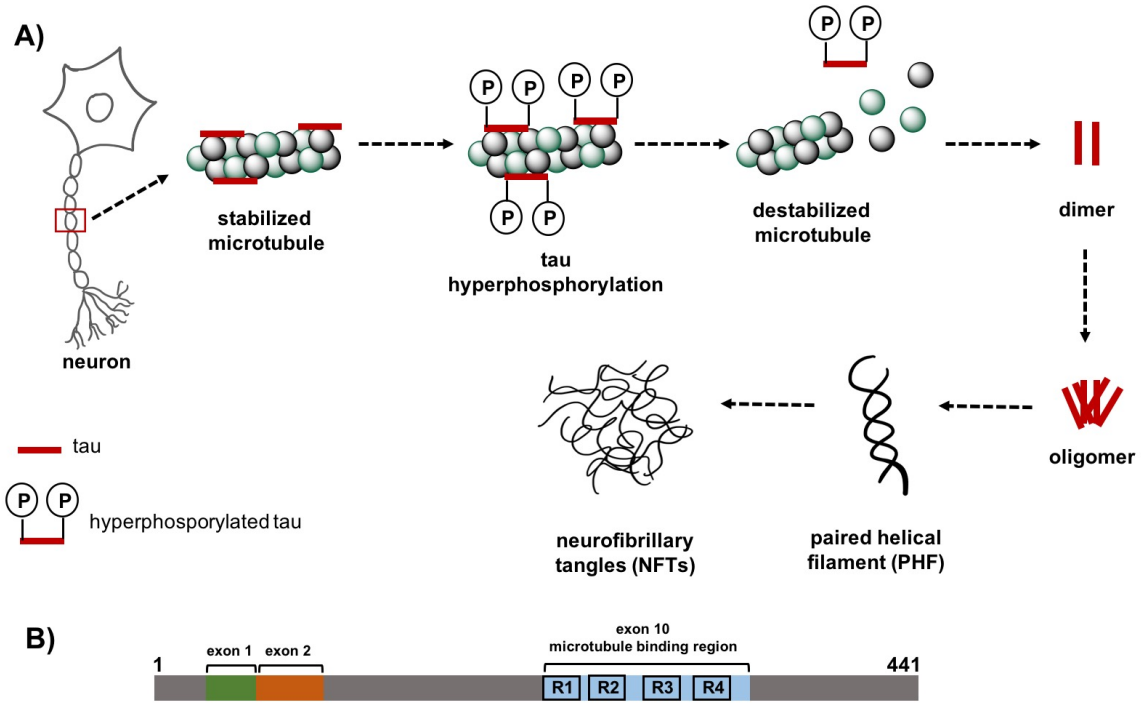

Figure 1.6 (A) Formation process of NFTs. (B) Schematic illustration of functional sites of tau showing the microtubule binding site (exon 10) and R3 and R4 – the core of tau fibrils.

Many anti-tau therapies have failed in clinical trials. Glycogen synthase kinase 3 beta (GSK-3β) is a protein kinase that facilitates tau phosphorylation and is therefore, an attractive target for anti-tau therapy. However, the GSK-3β inhibitor Tideglusib (Figure 1.7) did not show significant clinical benefit in a phase II clinical trial.[106,107] Anti-aggregation agents have also been developed, such as methylene blue dye derivatives Trx0014 and LMTM (Figure 1.7). These dye derivatives appeared to slow cognitive decline in phase III clinical trials, but the claims and the methodology of these studies remain controversial.[108,109]

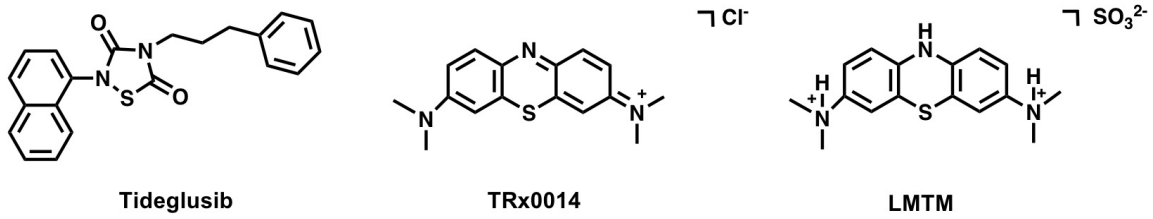

Figure 1.7 Examples of anti-tau compounds.

1.3 Medicinal Inorganic Chemistry

Metal ions play an important role in biological processes, providing charge balance, catalyzing enzymatic reactions, and facilitating electron transport.[110] These natural systems provide inspiration for the development of active agents that target and/or mimic these same natural mechanisms. Medicinal inorganic chemistry is therefore a very attractive field and can be divided into two main categories: (1) drugs that target metal ions and (2) metal-based drugs in which the central metal ion plays an important role for the desired clinical application. Although medicinal inorganic chemistry is still considered a young field, it has been present in our society for over 5000 years, with evidence of its use tracing back to the ancient civilizations of Mesopotamia, Egypt, India, and China. There is evidence of the use of silver to treat wounds and ulcers by the Greek physician Hippocrates, and the use of gold in a number of different treatments in Asia almost 3500 years ago.[111,112]

In the modern era, the first studied metallodrug was salvarsan (Figure 1.8), an arsenic based antimicrobial agent develop by Paul Ehrlich,[113,114] however, the most successful metallodrug is cisplatin (Figure 1.8), an anticancer agent discovered by Barnett Rosenberg and Loretta VanCamp in 1965,[115] which also led to the development of many other cisplatin derivatives, such as carboplatin and oxaliplatin (Figure 1.8). Platinum metallodrugs targeting cancer are not the only example of metal complexes being used in modern medicine.[116,117] One arsenic drug that is currently used to treat trypanosomiasis is melarsoprol, a second stage treatment for the human African sleeping sickness (Figure 1.8).[118] Other metallodrugs include auranofin, an Au(I) compound that received FDA approval in

1985 to treat arthritis, BEOV, a vanadium (IV) complex that is being tested as an antidiabetic drug, and pepto-bismol (BSS), a bismuth complex used to treat gastrointestinal disorders (Figure 1.8).[119–121] The idea of using metal-based drugs to modulate the progression of AD has also been explored in the last few decades, and the results will be discussed in more detail in the following sections.

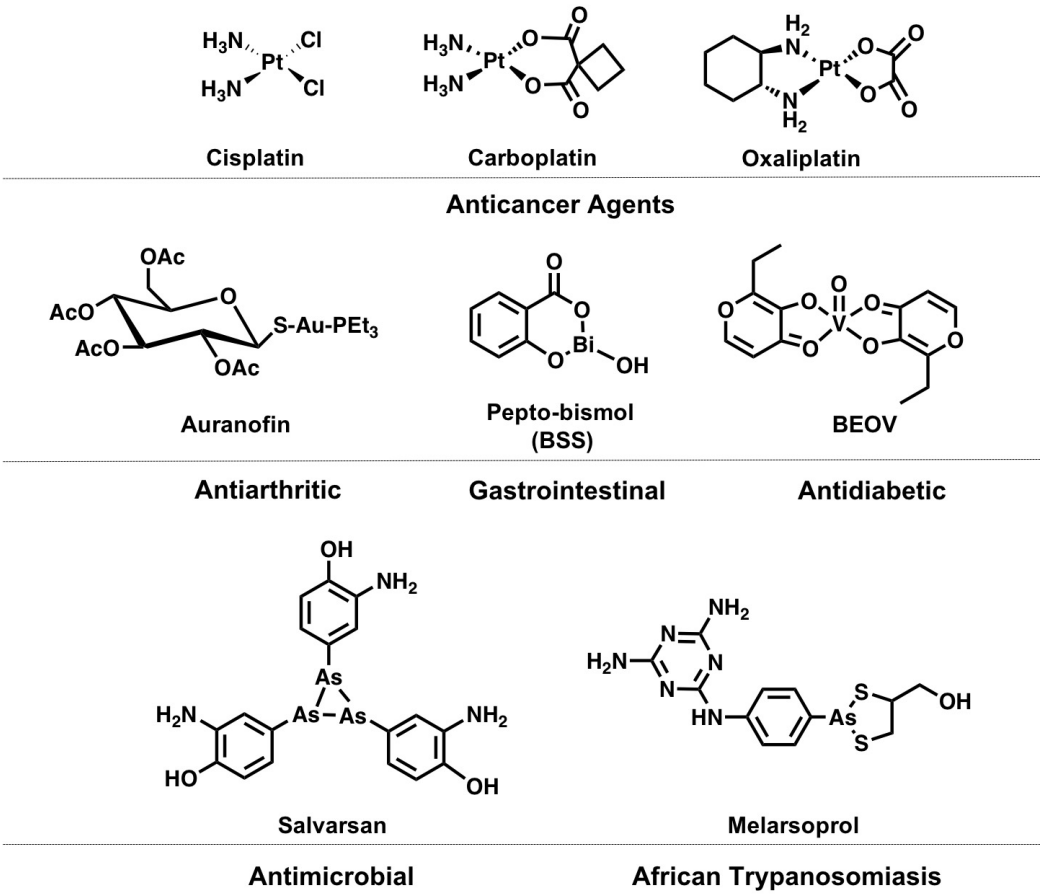

Figure 1.8 Selected examples of medicinally relevant metal-based drugs and their applications.

1.4 Ru Complexes as Cancer Therapeutics

According to the World Health Organization (WHO) cancer is the leading cause of death worldwide, with cancer-related deaths projected to rise above 13 million by 2030.[122] In Canada, cancer presents a large and growing impact on our population and health care system. Nearly half of Canadians are expected to be diagnosed with cancer in their lifetime, and although the treatments are now more advanced compared to a few decades ago, cancer remains the leading cause of death in Canada.[123] Most of the FDA approved anticancer drugs are organic molecules, but since the discovery of cisplatin, a new era in the application

of transition metal complexes has emerged.[124] Although cisplatin and its derivatives are considered by the WHO as essential drugs, they have their drawbacks, such as fast resistance build up in tumors, and side-effects caused by their cytotoxicity and lack of specificity, which leads to undesirable interactions with other biomolecules.[125,126] These limitations have triggered a search for metal-based compounds that exhibit lower toxicity compared to cisplatin and its derivatives and higher selectivity.[127] Ruthenium complexes have shown promising antitumor activity, and they present certain desired advantages over platinum drugs, and are expected to become a new generation of antitumor drugs.[128] The study of Ru-based complexes started in 1980, when chloro-ammine Ru(III) compounds (Figure 1.9) were reported to have anticancer activity in rats, however, their action was limited due to low solubility.[129] Four years later a DMSO-Ru(II) complex (Figure 1.9) (DMSO = dimethyl sulfoxide) was shown to be active in both primary and metastatic cancers, although it was less effective than cisplatin, but exhibited fewer side effects.[120]

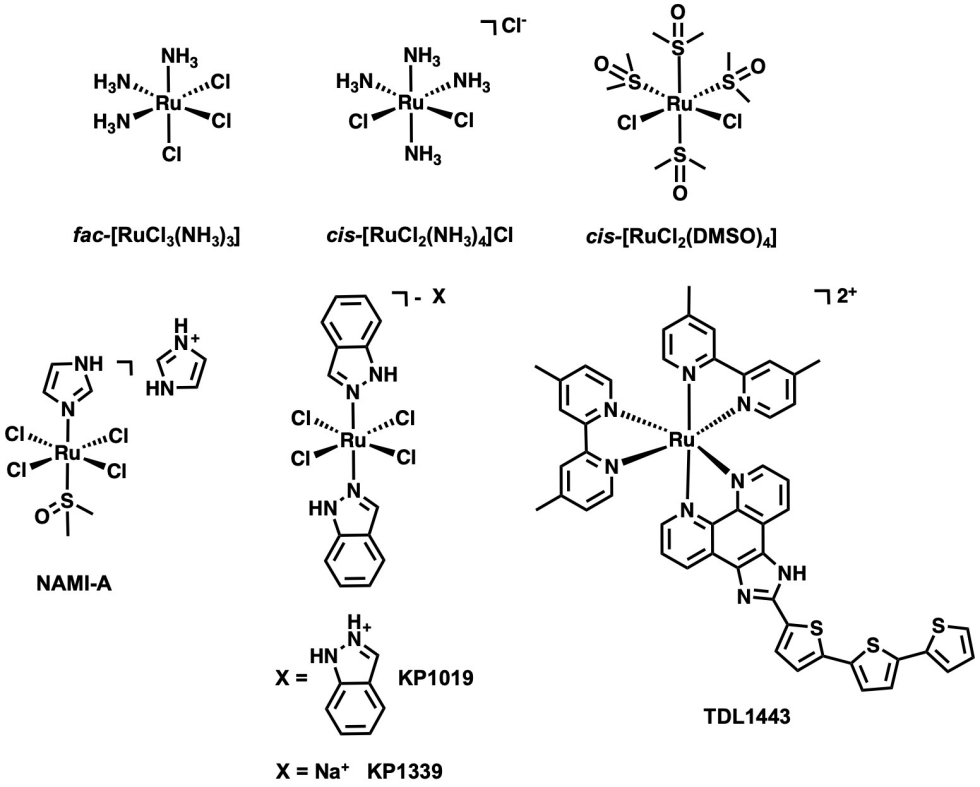

Figure 1.9 Top: structure of first ruthenium complexes with anticancer activity. Bottom: structure of four Ru(II/III) complexes that have entered into clinical trials.

To date there are four Ru(II/III) complexes that have entered clinical trials.[130] The first Ru(III) complex in clinical trials was NAMI-A (Figure 1.9). This complex showed low potency in terms of direct cytotoxicity towards cancer cells in vitro, however, it had significant efficacy in inhibiting tumor metastasis in vivo.[124,131] Studies suggest that NAMI-A is

capable of binding to DNA and RNA, and also to histidine residues of serum albumin (human - HSA or bovine - BSA) under physiological conditions,[132,133] however its mechanism of action still remains unclear.[124] The low therapeutic efficiency and its partial response in phase I/II clinical trials limited further clinical use of NAMI-A.[128] Another Ru(III) complex that underwent clinical trials is KP1019 (Figure 1.9), however trials were discontinued due to poor aqueous solubility and severe side effects.[128,134,135] In order to improve the water solubility of KP1019, a more soluble sodium complex was synthetized, KP1339 (Figure 1.9) and it is currently being tested in clinical trials, and has showed the ability to stabilize tumor size while presenting mild side-effects.[136] The only Ru(II) complex currently in clinical trials is TDL1443 (Figure 1.9). This octahedral Ru(II) is chelated by polypyridyl ligands, and exhibits potent photophysical properties that are being explored in photodynamic therapy (PDT). TDL1443 has shown significant therapeutic efficacy in bladder cancer and is currently in phase II clinical trials.[128,137] Based on the results indicating the interaction of Ru complexes and DNA, RNA, and His residues present in proteins, these Ru complexes have also been studied for their ability to interact with the Aβ peptide.

1.4.1 Ru(II) Complexes and their Photophysical Properties

Ru(II) polypyridyl complexes have been extensively studied because of their interesting electrochemical and photophysical properties (Figure 1.10).[138,139] These complexes find broad application in several research areas, such as conversion of solar energy, fabrication of molecular devices, DNA intercalation, and protein binding.[140] In terms of the application of these complexes in the medicinal field, photoactivation is of considerable interest as it allows the controlled conversion of a non-toxic drug into an active cytotoxic species. Photoactivation provides a mechanism to discriminate between the targeted area and surrounding healthy tissue, which reduces the dose-limiting side effects and increases specificity.[141] Ru(II) polypyridyl complexes absorb visible light and their photochemical properties can vary depending on the nature and the number of the polypyridyl ligands around the metal centers.[139]

A metal-to-ligand charge-transfer (MLCT) transition (450-480 nm)[142] is of interest for the photophysical properties.[143] An electron is promoted from a dπ orbital (t_{2g} orbital in the case of Ru(II) complexes) to a π* orbital on the polypyridyl ligand, ($d\pi^6$) → ($d\pi^5\pi^*$) transition , followed by relaxation to a ^{3}MLCT state (Figure 1.10). The ^{3}MLCT state can be quenched by molecular oxygen ($^3O_2$), generating singlet oxygen ($^1O_2$) (Figure 1.10) that can quickly react with biomolecules in close proximity. The incorporation of substituents on the polypyridyl ligands can influence the excited states of the complex. The energy of the triplet metal center (^{3}MC) state can be lowered below the ^{3}MLCT state if simple methyl- or phenyl-substituents are added at the 6,6' positions of the polypyridyl ligand.[144,145] The addition of

these substituents causes steric crowding at the metal center, resulting in distortion of the octahedral geometry of the complex, and a lowering of the ^{3}MC state relative to the ^{1}MLCT state. In this case, a ligand dissociative pathway is the major pathway for relaxation to the ground state (GS) (Figure 1.10).[141,144,146–148]

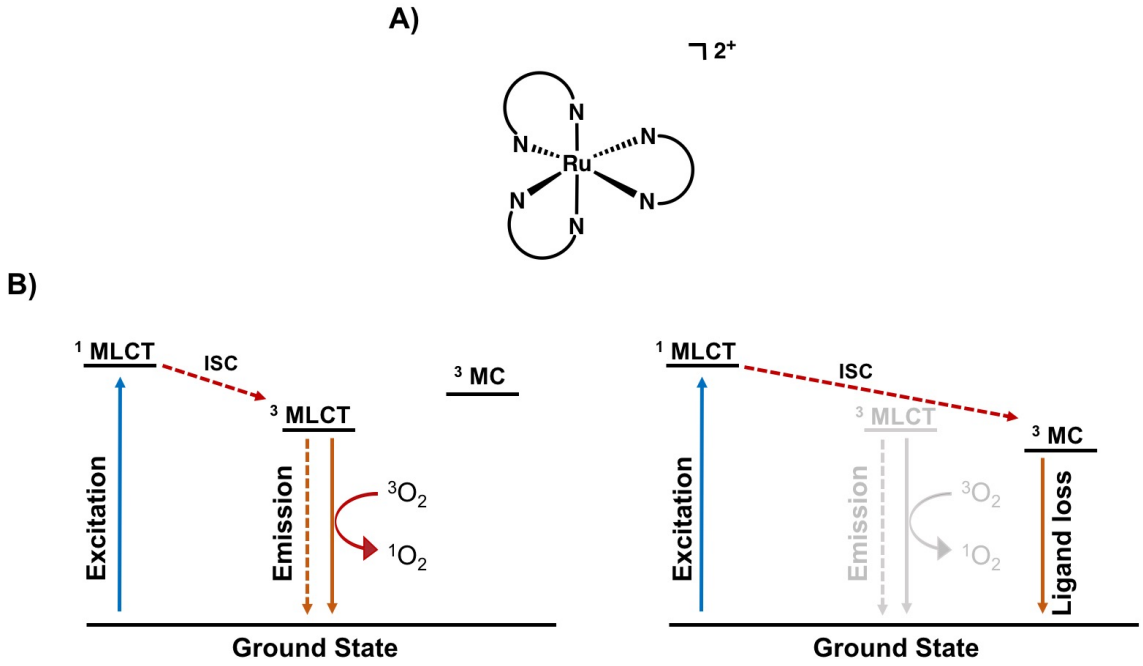

Figure 1.10 (A) Figure of a general Ru(II) polypyridyl complex, wherein the half-circle connecting the two N donors signifies bipyridyl ligands or analogues; (B) Simplified Jablonski diagram showing the excited state decay process of Ru(II) polypyridyl complexes *via* either emission or formation of $^1O_2$ (left), and the ligand dissociative pathway (right) that occurs with steric crowding of the metal center. ISC – intersystem crossing.

1.4.2 Ru(II) Polypyridyl Complexes Targeting Cancer

DNA damage can lead to an interruption in DNA transcription and replication, which is essential for cell proliferation.[149] One of the hallmarks of cancer is the increased cell division, and therefore targeting the DNA transcription and replication of damaged cells could lead to a method to control the development of some cancers.[150] The structure and chemical composition of DNA provides many opportunities for interaction with metal complexes *via* reversible or irreversible interactions.[151] Molecules can form covalent bonds (defined as irreversible binding) to DNA bases and sugar residues.[152] The induction of DNA damage caused by these covalent interactions is the basis of classical chemotherapy with cisplatin (Figure 1.8).[153,154]

Ru(II) polypyridyl complexes interact reversibly with DNA, *via* electrostatic binding, intercalation, and groove binding. Negatively charged DNA attracts cationic molecules, and as the majority of Ru polypyridyl complexes are cationic, electrostatic interactions contribute to the binding affinity between the complexes and DNA, however, the most important modes of interaction are intercalation or groove binding. One example of a metal complex that interacts with DNA predominantly through electrostatic effects is $[Ru(bpy)_3]^{2+}$ (where bpy = 2,2'-bipyridine)[151,155] (Figure 1.11).

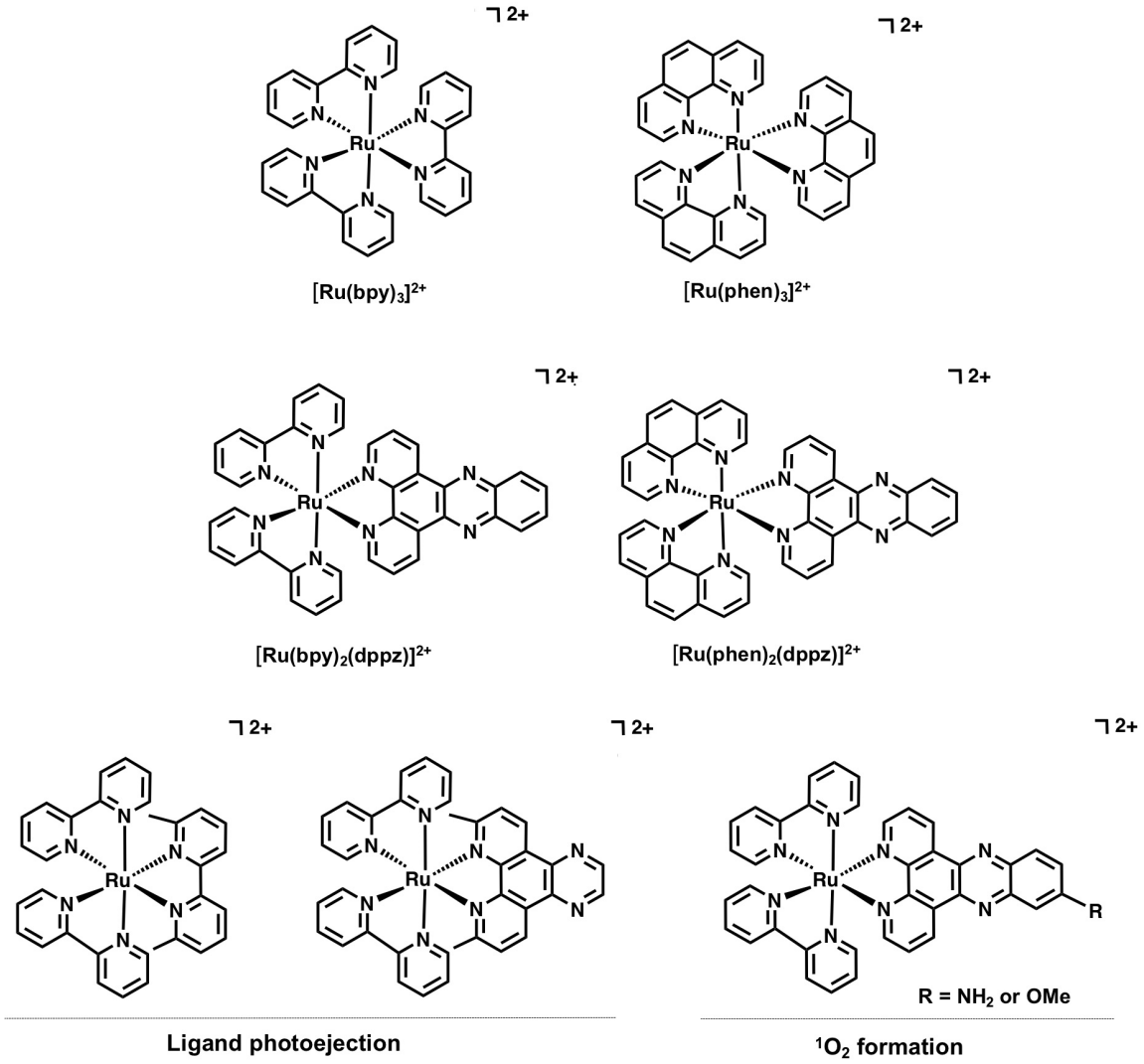

Figure 1.11 Ru(II) polypyridyl complexes that target cancer.

Intercalation occurs when an aromatic compound is inserted between adjacent base pairs in the DNA double helix, which involves the π-π interactions between the DNA bases and the complex, and is the most explored binding mode.[124] In 1990, the Barton and Sauvage

research groups reported the use of $[Ru(bpy)_2(dppz)]^{2+}$ and $[Ru(phen)_2(dppz)]^{2+}$ (where phen = 1,10-phenanthroline and dppz = dipyridophenazine) (Figure 1.11) as DNA intercalators.[156] These complexes show intense MLCT-based luminescence upon addition of DNA, however, the luminescence is quenched in the absence of DNA. This phenomenon is known as the DNA "light switch" effect and is commonly used to study the interaction of metal polypyridyl complexes with DNA.[151,157] Many transition metal complexes can also interact with DNA by binding to DNA grooves. Groove binding is dependent on a combination of hydrogen bonding, van der Waals, hydrophobic, and electrostatic interactions. Usually groove binders are positively charged and incorporate planar aromatic ligands that can interact with DNA. The first confirmed Ru(II) polypyridyl groove binder was $[Ru(phen)_3]^{2+}$ (Figure 1.11), although this complex exhibited low DNA binding affinity, a fact that limits its applications.[158]

Light activation of Ru(II) polypyridyl complexes can cause DNA damage *via* the production of $^1O_2$ (Figure 1.10), preventing transcription and replication, which leads to cell death.[144] For example, Gasser *et al.* investigated Ru(II) polypyridyl complexes (Figure 1.11) and their ability to generate $^1O_2$ upon exposure to visible light, leading to DNA damage, including double strand breaks and guanine oxidation, ultimately resulting in cell apoptosis.[140] These results show the promise of Ru(II) polypyridyl complexes as photodynamic therapeutic compounds for cancer treatment.[140]

In addition, covalent binding of Ru(II) complexes to DNA is an irreversible mechanism[124] that usually occurs *via* binding of the Ru(II) center to the N7 atom of guanosine. The covalent adduct results in distortion of the DNA backbone, which impairs DNA replication and transcription. For example, Glazer *et al.* synthesized a group of Ru(II) polypyridyl complexes (Figure 1.11) that undergo ligand photoejection upon irradiation with visible light.[141] They describe the rapid and selective ejection of one of the ligands due to steric crowding at the metal center, and the advantages of using the complexes, such as high aqueous solubility and a high light/dark therapeutic index. Interestingly, the compounds demonstrated higher potency in comparison to cisplatin when light activated. The interesting photophysical properties of Ru(II) polypyridyl complexes as well as the interaction of these complexes with DNA raised attention to the possibility of using these same complexes to interact with Aβ.

1.5 Metal Complexes Targeting AD

Aβ aggregation is an important factor in AD pathogenesis, and the design of metal complexes that target this peptide and modify its aggregation process is an active area of research.[159–161] Several metal complexes have been shown to interact with Aβ at different

aggregation stages, modifying the overall aggregation pathway and toxicity in cells and animal models.[44,162–165]

A series of Pt(II) phenanthroline complexes, Pt(phen)Cl_2 and Pt(ϕ-phen)Cl_2 (Figure 1.12), showed the ability to bind to Aβ and modify its aggregation process and neurotoxicity.[159] The phenanthroline ligands are able to facilitate π-π stacking interaction with residues present in the peptide sequence (Phe^4, Tyr^{10}, and Phe^{19}), which also facilitates the formation of covalent bonds between the metal complex and the peptide due to the proximity of the Pt(II) complex to His residues.[166] The influence of these complexes on the Aβ aggregation process was associated with almost complete rescuing of cell viability in primary cortical neuron cells. In this same study, cisplatin was used as a control complex. In contrast to the phenanthroline complexes, cisplatin targeted the Met^{35} residue, and did not show any activity when exposed to the neuron cells, which indicates that the π-π stacking interaction between the peptide and the phenanthroline ligands is essential for the formation of the adduct that modifies the aggregation process of Aβ. In fact, NMR, X-ray absorption spectroscopy (XAS), MS, and molecular modeling investigations confirmed that the planar hydrophobic ligands stabilized His-protein adducts. The study also suggests that when these Pt(II) complexes bind covalently to the His residues present in Aβ, the complexes are able to inhibit the binding of metal ions such as Cu(II) to the peptide, which may lead to a decrease in the concentration of ROS generated.[159] Pt(IV) complexes have also been studied for their ability to modulate aggregation and reduce the toxicity of Aβ. Pt1 (Figure 1.12) showed increased brain uptake when compared to the Pt(II) analogue Pt2 (Figure 1.12) and the Pt1 complex significantly reduced levels of $Aβ_{1\text{-}42}$ plaques in an AD mouse model.[163]

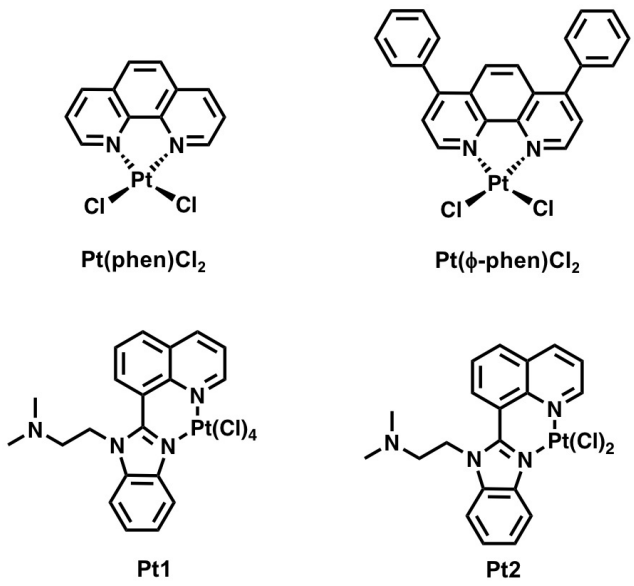

Figure 1.12 Platinum complexes that target Aβ and promote modulation of the Aβ aggregation pathway.

Complexes containing metals from group 9 (Co, Rh, and Ir) can be also used as Aβ aggregation modulators.[164] The first application of Rh(III) complexes as inhibitors of Aβ aggregation was reported by Ma *et al.* in 2011.[167] The Rh(III) complex (Figure 1.13) incorporates phenylpyridine (ppy) ligands and labile water molecules to facilitate non-covalent interactions with the N-terminal region of the peptide and covalent binding to His residues of Aβ, respectively. Electrospray ionization – mass spectrometry (ESI-MS) confirmed 1:1 Aβ:Rh(III) adduct formation, and Transmission electron microscopy (TEM) confirmed that the metal complex almost completely inhibited $A\beta_{1\text{-}40}$ aggregation.[164,167] As for Ir complexes, Lu *et al.* prepared an Ir(III) complex with three bidentate ligands that interacts with $A\beta_{1\text{-}40}$ in a non-covalent manner (Figure 1.13). Even without covalent binding, the non-covalent interaction was strong enough to completely inhibit the aggregation of $A\beta_{1\text{-}40}$ and reduce peptide toxicity in human neuroblastoma SH-SY5Y cells and mouse primary cortical cells.[168] More recently, Lim *et al.* reported a series of cyclometallated Ir(III) complexes with two exchangeable cis-aqua ligands (Figure 1.13) that coordinate to the Aβ peptide and promote the photo-induced peptide oxidation in the presence of O_2.[169] A number of Co(III) complexes have also been investigated for their ability to interact with Aβ and modify the peptide aggregation pathway.[74,170,171] A Co(III) Schiff base complex (Figure 1.13) was designed to covalently bind to the Aβ peptide *via* His residues. It was reported that the complex binds to one or two His residues present in the peptide, with a preference for His^6 and one of $His^{13/14}$, through dissociative ligand exchange at the axial positions.[74] As a result of the binding, the Co(III) complex can induce the formation of large soluble

oligomeric species and reduce the levels of small Aβ oligomers. Additionally, the complex also reduced the binding of $A\beta_{1\text{-}42}$ to differentiated hippocampal neurons.[74]

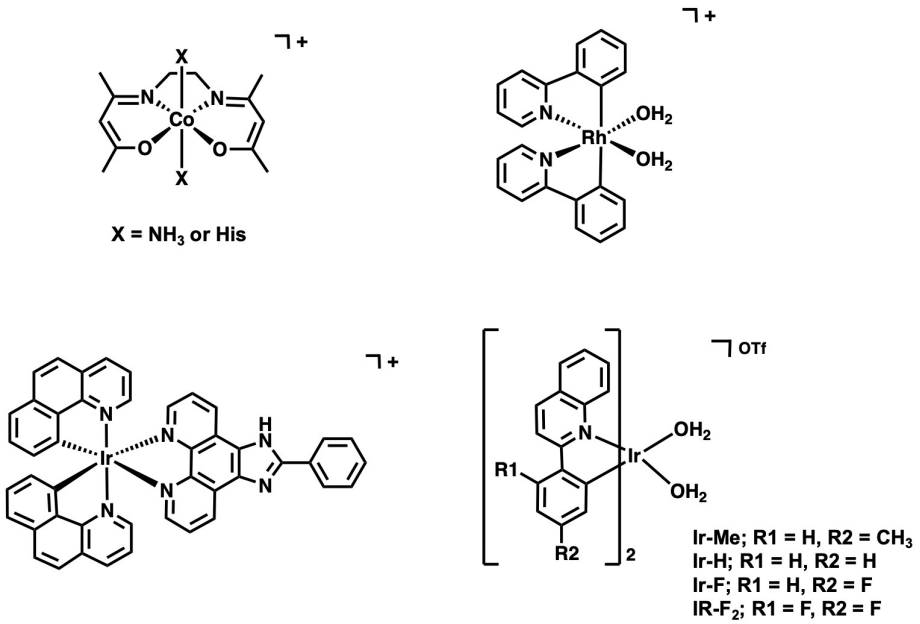

Figure 1.13 Structure of complexes containing group 9 metals that are Aβ aggregation modulators.

Martí *et al.* reported the use of a Re complex as a light switch model to detect Aβ fibrils.[172] When Aβ fibrils are in solution, the photoluminescence of $[Re(CO)_3(dppz)(Py)]^+$ (Py = pyridine) (Figure 1.14) is increased by ~18-fold in comparison to complex in the absence of fibrils. In addition to this first light switch effect, it was observed that consecutive photoluminescence measurements resulted in increased emission intensity over time. The increased photoluminescence of $[Re(CO)_3(dppz)(Py)]^+$ in the presence of fibrillar Aβ after repeated irradiation was up to 2 orders of magnitude higher than in buffer. Molecular dynamics (MD) simulations predict that the increased photoluminescence is due to the binding of $[Re(CO)_3(dppz)(Py)]^+$ to Aβ fibrils *via* the hydrophobic cleft formed by Val^{18} and Phe^{20}. The close proximity of the hydrophobic cleft and the Met^{35} residue was hypothesized to promote Met^{35} oxidation by the complex.[173]

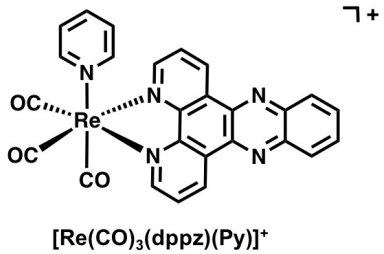

Figure 1.14 Structure of a rhenium complex that act as light switch model to detect Aβ fibrils.

The focus of iron complexes and their influence on AD is mostly centered on naturally occuring iron phorphirins.[174,175] An increase in the production of porphyrin complexes, heme-a and heme-b (Figure 1.15), has been observed in the brains of AD patients, while there is a depletion of complex V, a cell enzyme containing heme-a, resulting from the interaction of heme and Aβ,[176–178] and several studies have shown that heme binds to Aβ peptide.[179–181] Dey *et al.* showed that a His residue is essential for heme binding to Aβ, and the study also suggested that the binding likely occurs at either His^{13} or His^{14}.[178] In a different study, Yuan and Gao suggested that residues Phe^{19} and Phe^{20} are also important for the interaction between Aβ and heme.[175] Additionally, Thioflavin T (ThT) fluorescence has shown that heme can change the aggregation pattern of Aβ, leading to the formation of smaller fibrils as confirmed by TEM.[175,176] Heme and Cu are known to be co-localized in Aβ plaques, and under physiological conditions both Cu(II) and heme could be bound to Aβ, presenting biologically-accessible redox responses that could generate ROS and associated oxidative stress.[182] Most recently, a Fe corrole complex (Figure 1.15) was determined to have moderate affinity for Aβ, binding to the peptide *via* a His residue to form a 5-coordinate complex, and limiting the aggregation of Aβ in solution.[183] Previously to this study, Gross *et al.* had reported the exceptional catalase and superoxide dismutase activity of the corrole even when bound to an axial His (and albumin).[184,185] Interestingly, the Fe corrole maintains its exceptional antioxidant activity when bound to the Aβ peptide, limiting the generation of ROS from Cu-Aβ.[183]

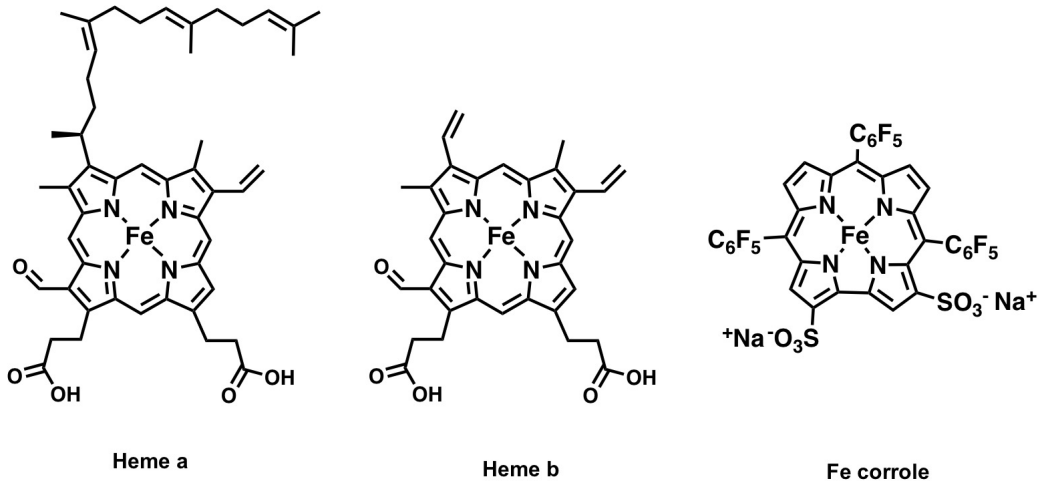

Figure 1.15 Structure of iron complexes that interact with Aβ fibrils.

1.5.1 Ru Complexes Targeting AD

Ru(II/III) complexes have been reported to interact with the Aβ peptide, and due to their general lower toxicity in comparison to Pt(II) compounds,[186–189] Ru(II/III) complexes have been studied as potential candidates for AD treatment.[129] The concept of Ru(III) complexes as AD therapeutics was first introduced by Valensin *et al.* with the report of the *fac*−[$Ru(CO)_3Cl_2(N^1-thz)$] (Figure 1.16) complex binding to His residues present in the Aβ peptide.[190] This study shows that the complex loses both Cl^- and the N^1-thz ligand, allowing the *fac*−$Ru(CO)_3^{2+}$ unit to bind to Aβ His residues.

The well-studied anticancer candidates PMru20[191] (Figure 1.16) and KP1019[192] (Figure 1.9) were also investigated for their ability to interact with Aβ and modify the aggregation process. PMru20 (Figure 1.16) protected rat cortical neurons from toxicity caused by Aβ using both full length peptide and the fragment $Aβ_{25\text{-}35}$ (without His), likely due to the inhibition of peptide aggregation. KP1019 (Figure 1.9) showed a concentration-dependent effect on the aggregation of full-length peptide *via* covalent interaction with His residues, which modulated the aggregation process of monomeric and pre-formed aggregates by inducing the formation of soluble high molecular weight aggregates. The complex also limited Aβ toxicity in SH-SY5Y neuroblastoma cells. A series of NAMI-A analogues (Figure 1.13) were reported by Walsby *et al.* to bind covalently to HSA *via* a His residue.[193] The axial DMSO ligand was rapidly replaced by a water molecule at physiological pH, and Cl^- ligand loss was also observed. The ligand exchange processes are reported to facilitate the covalent interaction of these complexes and HSA.[193] Based on these results, our group investigated a series of NAMI-A analogues for their potential to interact with Aβ.[194] ^1H NMR and ESI-MS showed that the complexes are able to bind to the peptide, likely *via* a His residue, and

they are able to modulate the aggregation process by stabilizing insoluble fibrils at 24 h time point.

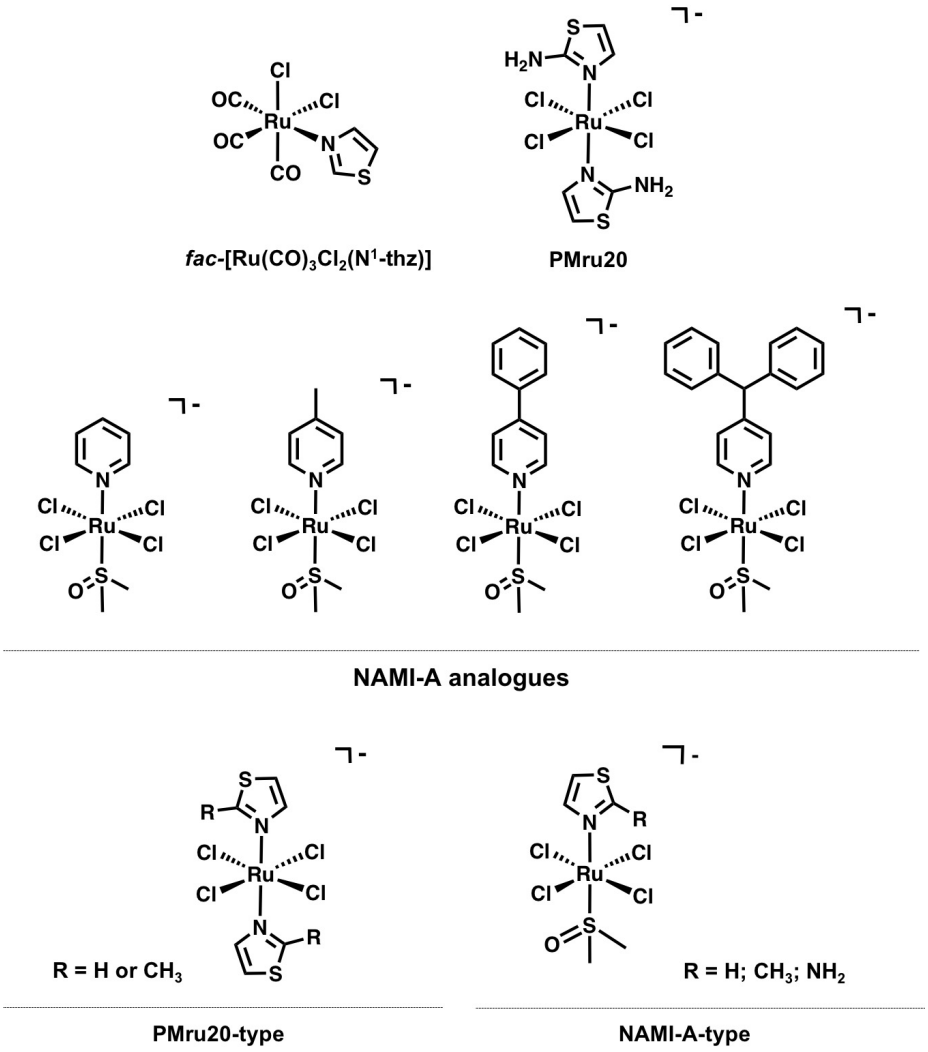

Figure 1.16 Examples of Ru complexes that interact with the Aβ peptide, modulating aggregation and limiting toxicity.

Most recently, Webb *et al.* reported the study of a series of NAMI-A- and PMru20-type complexes (Figure 1.16) in order to establish a structure-activity relationship (SAR) for these Ru(III) complexes.[195] Different functional groups were installed at the 2' position on the thiazole ring, and the interaction of these complexes with Aβ was investigated. All complexes were shown to bind to the peptide *via* a His residue and demonstrated peptide aggregation inhibition, as confirmed by TEM and ThT fluorescence.

1.5.2 Ru(II) Polypyridyl Complexes Targeting AD

As mentioned previously in this chapter, Ru(II) polypyridyl complexes have been extensively investigated due to their electrochemical and photophysical properties.[138] This class of Ru(II) complexes is stable under physiological conditions, and thus is being investigated for DNA and protein targeting.[196] The hydrophobic nature of the bpy/phen ligands facilitates the interaction of the complexes with proteins and peptides, such as Aβ. For example, photoactivation of $[Ru(bpy)_3]^{2+}$ (Figure 1.11) in the presence of Aβ leads to amino acid oxidation and destabilization of peptide secondary structure.[197] After exposure to light, $[Ru(bpy)_3]^{2+}$ demonstrated the ability to disassemble highly stable Aβ aggregates, generating small Aβ fragments, suggesting that Ru(II) complexes can be used as anti-Aβ agents.

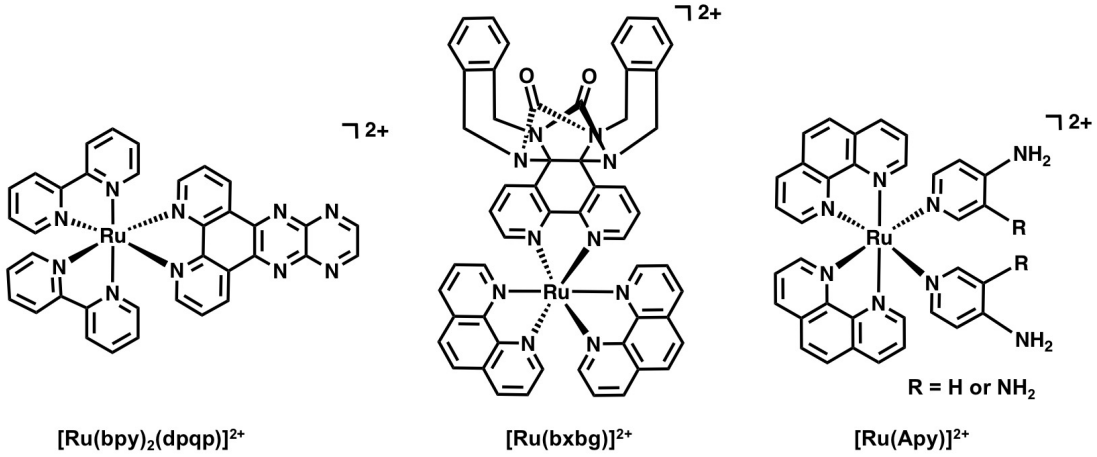

Figure 1.17 Structures of Ru(II) polypyridyl complexes that target the Aβ peptide.

Ru(II) polypyridyl complexes can also be used as sensitive fluorescent probes for Aβ aggregates. The interaction of $[Ru(bpy)_2(dppz)]^{2+}$ (Figure 1.11) with Aβ fibrils results in an enhancement of luminescence, likely due to the limited ability of water to quench the excited state of the complex once bound to the peptide aggregates.[198] A similar process occurs with $[Ru(bpy)_2(dpqp)]^{2+}$, however, this complex can be used to monitor oligomer formation (Figure 1.17).[199,200] Another Ru(II) complex containing an extended polypyridyl ligand, ($[Ru(bxbg)]^{2+}$ (Figure 1.17), inhibited acetylcholinesterase (AChE), showing inhibitory values similar to that of the FDA approved drug tacrine.[201] This complex can also inhibit Aβ aggregation completely, as demonstrated by ThT fluorescence and TEM. Another series of Ru(II) complexes, $[Ru(Apy)]^{2+}$ (Figure 1.17), were shown to protect against ROS and had an inhibitory effect against AChE.[202] Interestingly, the luminescence of $[Ru(Apy)]^{2+}$ increases in the presence of Aβ aggregates, allowing for the visualization of these species

within 3 hours of aggregation, making this a promising compound for the visualization of Aβ aggregates in the early stages of fibrillization.

1.6 Thesis Overview

In this thesis three Ru(II) polypyridyl complexes (Figure 1.18) were studied for their ability to interact with the Aβ peptide and modulate its aggregation process. The influence of a covalent bond formed between the complexes and the peptide upon photoactivation and comparison to unactivated complexes are described in Chapter 2. As expected, the 6,6'-methyl- substituents on the bpy ligands promoted ligand loss upon photoactivation, providing exchangeable coordination sites for the complexes to interact covalently with the peptide, while unactivated samples did not show any evidence of changes to Aβ aggregation relative to peptide alone. All three complexes modulated the aggregation of monomeric Aβ by stabilizing high molecular weight species, preventing peptide fibrillization, and promoting the formation of insoluble amorphous aggregates after photoactivation. It was demonstrated in this study that **Ru1-3** were also able to interact with mature Aβ fibrils, leading to the same structures obtained in the presence of monomeric Aβ. It is interesting to note that **Ru1** and **Ru2** were able to induce these changes in both monomeric and fibrillar Aβ immediately after photoactivation, while **Ru3** demonstrated a more moderate modulation of the peptide after activation, taking more time to promote the same changes observed for **Ru1-2**. We hypothesize that the differences are related to the extended phenanthroline ligand of **Ru1-2**, in comparison to **Ru3**, that facilitates the interaction between complexes and peptide. Finally, future research directions based on these studies will be discussed in Chapter 3.

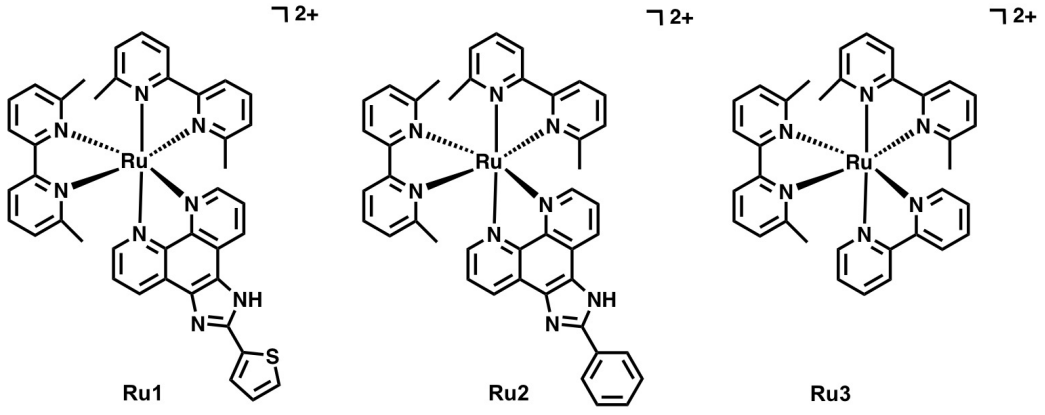

Figure 1.18 The structure of Ru(II) polypyridyl complexes studied in Chapter 2.

Chapter 2

Impact of photoactivation on the interaction between Ru(II) Polypyridyl Complexes and the Amyloid-beta Peptide

J. C. Bataglioli performed the ^{1}H NMR, gel electrophoresis/Western blotting, TEM imaging, BCA assay, the binding constant experiments, and the synthesis of $Ru(bpy)_2CO_3$. C. Maunoir assisted with experiments involving **Ru3**, Dr. J. R. Smith assisted with ESI-MS and completed docking experiments, and Professor Sherri McFarland's research team synthesized **Ru1-3**.

2.1 Introduction

Globally, an increase in life expectancy has led to a higher number of dementia cases.[203] Alzheimer's disease (AD) is the most common cause of irreversible dementia, accounting for 60-80% of diagnosed dementia cases,[204] resulting in a significant disruption of normal brain structure and function. At a cellular level, AD is characterized by the progressive loss of neurons, affecting memory and cognition, and eventually leading to mood fluctuation and death.[203,205,206] The two hallmarks of AD are the aggregation of tau protein leading to the generation of neurofibrillary tangles (NFTs) in neurons, and the aggregation of the amyloid beta (Aβ) peptide in the extracellular environment of the brain.[207,208]

The amyloid hypothesis stems from the cleavage of the membrane-bound amyloid precursor protein (APP), which is cleaved by a series of secretases, affording the 38- to 43- amino acid residue Aβ peptide.[209] The Aβ peptide exists predominantly in $A\beta_{1\text{-}40}$ form (~90%) and $A\beta_{1\text{-}42}$ (~9%), with the latter more prone to aggregation and presenting a higher toxic-

ity.[30,42,50,192,210,211] After APP cleavage, Aβ monomers are formed, which rapidly aggregate in solution to form oligomers, leading to diffuse, compact plaques. The fibrils are the final stage of the aggregation pathway of Aβ, although recent studies have suggested that soluble oligomers are the most toxic form of the peptide, due to their ability to interact with cellular membranes, initiating events that can lead to cell dysfunction and death.[37,71,212] The amyloid hypothesis also suggests that Aβ can induce hyperphosphorylation and aggregation of tau protein, leading to the formation of NFTs, causing neuronal damage.[38,213–215] In addition, oxidative stress has been linked with the amyloid hypothesis, through the binding of His residues present in Aβ to metal ions such as iron, and copper, producing reactive oxygen species (ROS).[71,216–220]

There are many strategies that have been investigated to inhibit Aβ aggregation, such as the breakdown of pre-formed plaques. However, this approach could lead to the formation of toxic Aβ oligomers. Thus, the development of a strategy that can regulate the aggregation pattern of Aβ is of current interest. Transition metal complexes incorporating Pt,[159,163] V,[221] Mn,[222] Re,[223–226] Fe,[183,227] Co,[71,74,170] Rh,[167] and Ir[168,169] metal ions have been shown to interact with different forms of Aβ and modify the aggregation pattern and toxicity of the peptide, emerging as therapeutic candidates against AD.[164,228,229]

Ru(II) polypyridyl complexes are an interesting class of transition metal complexes that have been the focus of many different research groups due to their electrochemical, photophysical, and biological properties.[138,139] These complexes find wide application in several research areas, such as conversion of solar energy,[230,231] fabrication of molecular devices,[232] DNA intercalation,[233–235] and protein binding.[236–238] Stable Ru(II) polypyridyl complexes can be activated with light, leading to ligand dissociation to afford a metal complex capable of binding to biological targets, and/or generation of ROS such as singlet oxygen ($^1O_2$).[140] A number of Ru(II) polypyridyl complexes have been investigated for their ability to interact with the Aβ peptide.[197,198,200–202] For example, the photoactivation of $[Ru(bpy)_3]^{2+}$ (Figure 2.1) leads to the formation of $^1O_2$ (quantum yield = 0.22)[239,240], and in the presence of the Aβ peptide, the complex is able to disassemble Aβ aggregates, generating smaller oxidized fragments.[197] Another example of a Ru(II) polypyridyl complex that can interact with Aβ is $[Ru(bpy)_2(dppz)]^{2+}$ (Figure 2.1). This complex interacts with a hydrophobic cleft on the surface of the peptide, and provides evidence of the importance of molecules with extended aromatic ligands for the interaction between Aβ and metal complex.[198] Here we investigate the interaction of photoactivated **Ru1**, **Ru2**, and **Ru3** (Figure 2.1) with Aβ to determine if the complexes are able to bind covalently to the peptide upon photoactivation, leading to modulation of the aggregation pattern of the peptide. **Ru1-2** have been previously reported to dissociate one 6,6'-dimethyl-2,2'-dipyridyl (6,6'-dmb) ligand upon photoactivation,[143,241] while the photochemical ligand dissociation process for **Ru3** has not yet been reported. **Ru1-2** present limited overall toxicity in the dark (EC_{50}

= 37 µM in HL 60 cells for **Ru1** and 101 µM in SKMEL 28 cells for **Ru2**),[143,241] and these two complexes incorporate planar aromatic ligands that we hypothesized would exhibit hydrophobic interactions with the Aβ peptide, thereby enhancing the metal complex-Aβ interaction.[228,242]

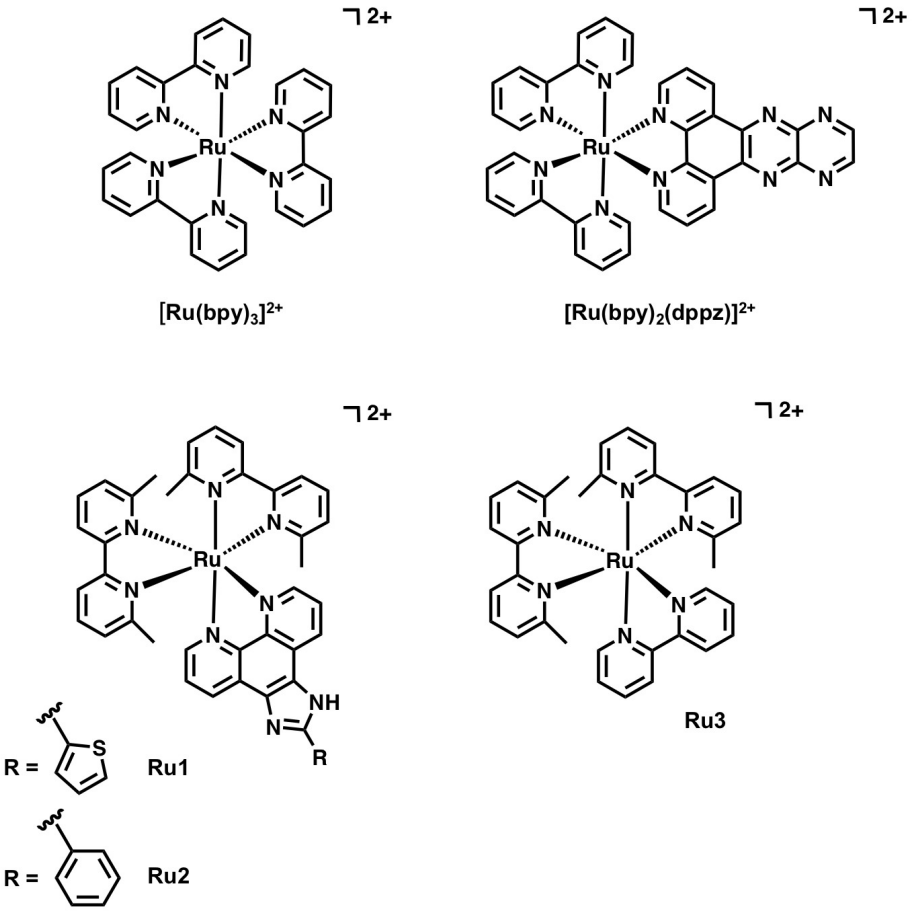

Figure 2.1 Structures of example Ru(II) polypyridyl complexes investigated for their ability to interact with the Aβ peptide and modulate aggregation (top), and the structure of the complexes investigated in this study (bottom).

2.2 Results and Discussion

2.2.1 Photoejection

The stability of unactivated **Ru1-3** in solution was investigated by ^{1}H Nuclear Magnetic Resonance (NMR) and Electrospray ionization – mass spectrometry (ESI-MS). As expected, **Ru1** and **Ru2** were stable in solution over 24 h, and did not exhibit ligand dissociation when not exposed to light (Figure 2.2 and 2.3 A, B). Surprisingly, a different result was obtained for **Ru3**, where a small quantity (~6% based on ^{1}H NMR integration) of free

6,6'-dmb ligand was observed for the unactivated sample at 24 h (Figure 2.2 and Figure 2.3 C), indicating that **Ru3** is not as stable as **Ru1** and **Ru2** in buffer solution.

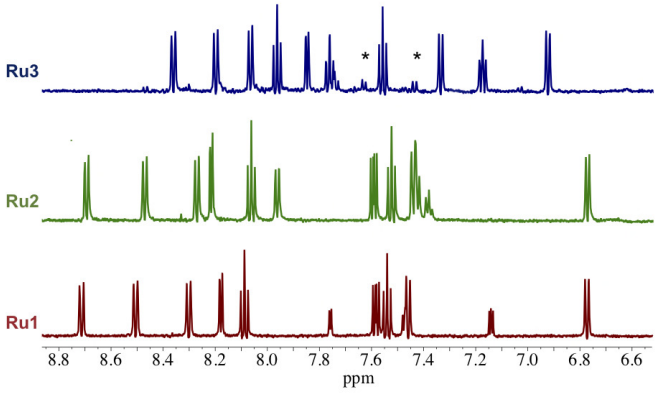

Figure 2.2 ^{1}H NMR spectra showing the absence of 6,6'-dmb free ligand after 24 h of incubation of unactivated **Ru1** (red) and **Ru2** (green) (200 µM) and an indication of free 6,6'-dmb ligand for unactivated **Ru3** (blue) (200 µM) in phosphate buffered solution (PBS) (0.01 M, pH 7.4). * 6,6'-dmb ligand.

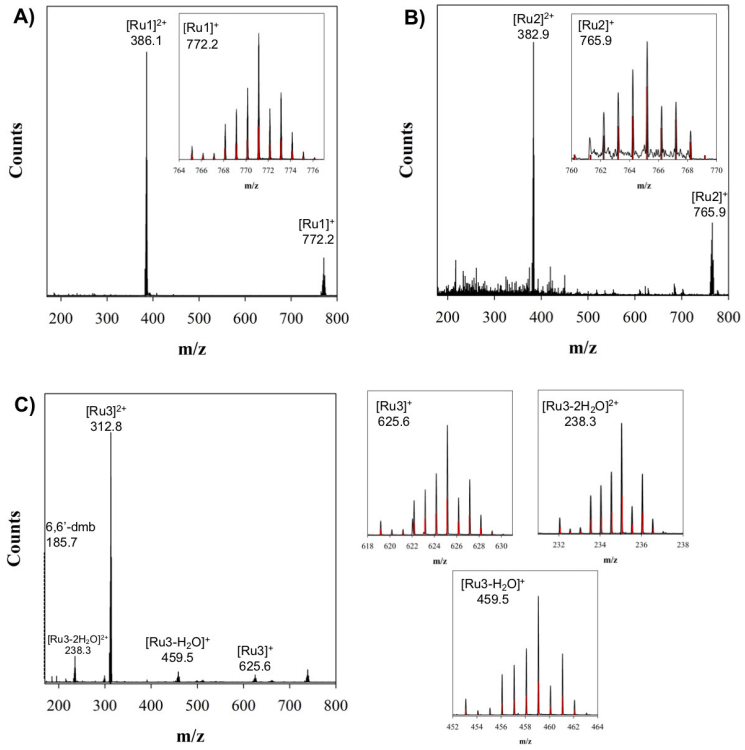

Figure 2.3 ESI-MS of unactivated **Ru1** (A), **Ru2** (B), and **Ru3** (C) in NH_4CO_3 buffer (20 mM, pH 9.0) showing the stability of **Ru1-2** when kept in the dark and ligand exchange for **Ru3**. Zoomed in regions show the isotope pattern for Ru complexes, red shows the theoretical isotope pattern expected for the complexes.

The Ru(II) complexes (**Ru1-3**) undergo photochemical ligand dissociation upon exposure to visible light.[143,241] The activation time for **Ru1-3** was determined by monitoring the changes in the UV-Vis absorbance spectrum as described in the literature.[143,149,243] The data analysis showed that the photochemical reaction for **Ru1**, **Ru2**, and **Ru3** was complete at 10 min., 12 min., and 25 min, respectively (Figure 2.4), after initial exposure to a cold white light (5500 – 6000 K), which affords maximum intensity in the energy range 450 – 560 nm.[244]

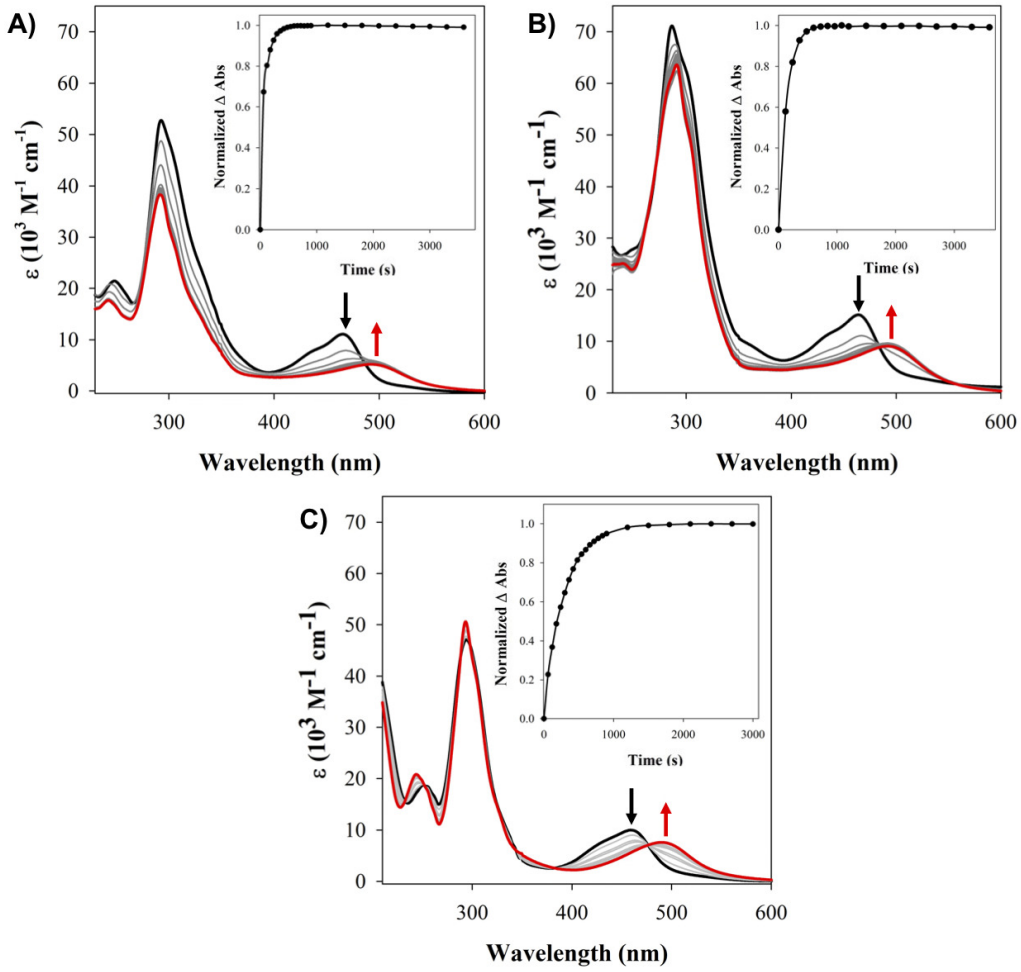

Figure 2.4 Photochemical ligand dissociation of **Ru1** (A), **Ru2** (B), and **Ru3** (C) (10 µM) in PBS buffer (0.01 M, pH 7.4) monitored by UV-Vis absorption spectroscopy. Data were collected first for unactivated samples (black spectra). Photoactivation was followed at 1 minute intervals up to 15 min., and then every 5 min. (grey spectra) until completion of experiment at 60 min. (red spectra). Insets show the change in absorption at 486 nm (**Ru1**), 483 nm (**Ru2**), and 477 nm (**Ru3**), with complete release of the ligand in 10 min., 12 min., and 25 min. for **Ru1**, **Ru2**, and **Ru3** respectively.

The photoejection was shown to be selective for the dissociation of the 6,6'-dmb ligand for **Ru1-3**, as demonstrated by ^{1}H NMR (Figure 2.5). The same was observed *via* ESI-MS (Figure 2.6), with mass peaks associated with different ligands (H_2O, DMSO, Cl^-), (where DMSO = dimethyl sulfoxide) occupying the vacant coordination sites. The greater degree of distortion induced by the 2,2'-bipyridine (bpy) ligands containing methyl substituents pointing towards the metal centre is an important factor for photoejection.[143,245] ^{1}H NMR results for the photoactivated samples exhibit a decrease in Ru(II) complex signals, and we hypothesize that this occurs due to the different products formed upon photoactivation, and in addition, precipitation. We observed the precipitation of photoactivated **Ru1-3** in the NMR tubes over time, which indicates the decreased solubility of photoactivated products, leading to a decrease in ^{1}H NMR signals. The PBS buffer concentration used in the assays has a chloride concentration that is meant to mimic those found in the cerebrospinal fluid (CSF) and serum, and the neutral dichloro complex that can be formed upon the 6,6'-dmb dissociation exhibits low water solubility compared to other Ru(II) polypyridyl complexes.[246,247] At lower concentrations (50-60 µM), no precipitate was observed, even after 24 h of incubation, however, at these lower concentrations the ^{1}H NMR signals were not discernible from the baseline noise.

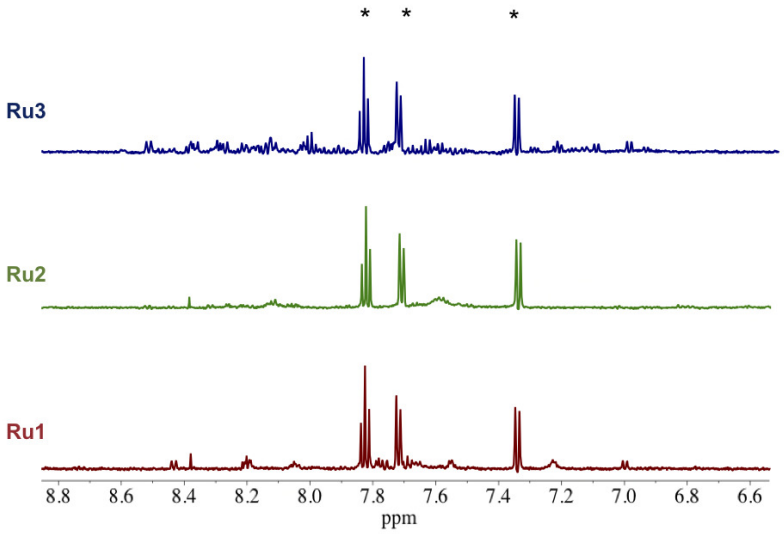

Figure 2.5 ^{1}H NMR spectra showing the presence of free 6,6'-dmb ligand immediately after activation of **Ru1** (red), **Ru2** (green), and **Ru3** (blue) (200 µM) in PBS buffer (0.01 M, pH 7.4). * 6,6'-dmb ligand.

Photoactivation of **Ru1-3** leads to ligand dissociation, however, **Ru3** exhibited an activation time *ca.* two times longer than that of **Ru1** and **Ru2** and we hypothesize that the difference in the kinetics of the ligand dissociation could be related to the enhanced ability of **Ru3** to decay *via* generation of $^{1}O_2$ as opposed to ligand dissociation. The quantum yield for $^{1}O_2$ is 0.03 for **Ru1**[143] and 0.01 for **Ru2**,[241] which are low compared to the quantum

yield of $[Ru(bpy)_3]^{2+}$ (0.22),[239,240] a complex that upon photoactivation leads to the formation of $^1O_2$ as a main relaxation pathway. The low values for quantum yield for $^1O_2$ indicate that the release of the 6,6'-dmb ligand is a major relaxation pathway upon light exposure for **Ru1-2**. The $^1O_2$ yield for **Ru3** still needs to be measured. Interestingly, the McFarland group observed no correlation between the size of the extended aromatic ligand and the time for ligand photoejection of similar Ru(II) polypyridyl complexes, which reinforces the hypothesis that the aryl group does not play a role in the photolysis, indicating that a competition among the decay pathways (Figure 1.10 B) is likely the main reason for the different ligand photoejection times.[241,248] The results for the photoactivated samples show the availability of exchangeable coordination sites on **Ru1-3** for interaction with the Aβ peptide upon photoejection of the 6,6-dmb ligand. The nature of the interaction between Aβ and **Ru1-3** will be further discussed in the following sections.

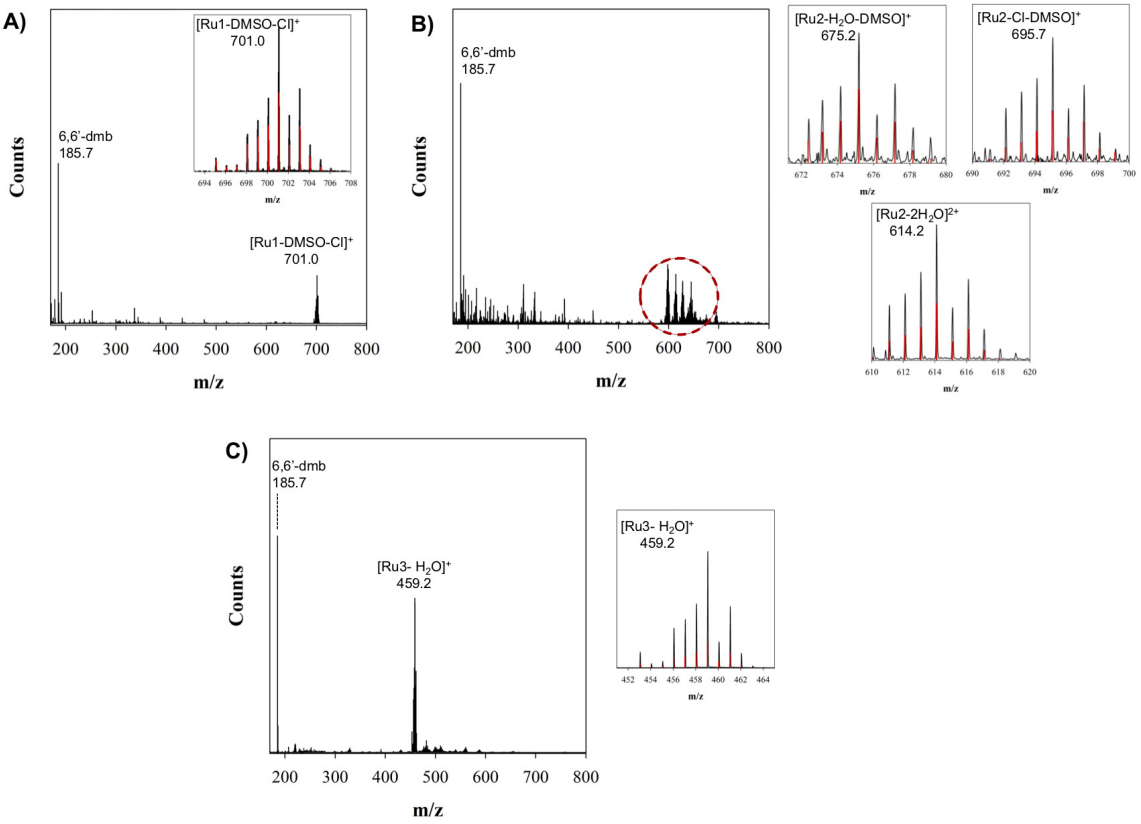

Figure 2.6 ESI-MS of activated **Ru1** (A), **Ru2** (B), and **Ru3** (C) in NH_4CO_3 buffer (20 mM, pH 9.0) showing the release of the 6,6'-dmb ligand and new ligands occupying the vacant sites of the complexes. Zoomed in regions show the isotope pattern for Ru complexes, red shows the theoretical isotope pattern expected for the complexes.

2.2.2 Binding of Aβ to Ru1-3

We evaluated the nature of the interactions between **Ru1-3** and the Aβ peptide by ^{1}H NMR and ESI-MS. The N-terminal region of the Aβ peptide is hydrophilic (1-16 fragment) and includes most of the amino acids associated with metal binding, while the C-terminus is hydrophobic (17-42 fragment) and responsible for peptide aggregation. To investigate the interaction of **Ru1-3** with the Aβ peptide, the non-aggregating $A\beta_{1\text{-}16}$ fragment, containing the three His residues (in positions 6, 13 and 14) involved in metal binding, was employed. The $His^{13/14}$ residues are located near the hydrophobic core of the peptide (17-21) responsible for the aggregation of Aβ, and thus binding of a metal complex in this region could cause an alteration in the aggregation pattern of the full-length peptide.[70]

As expected, the unactivated samples of Aβ and **Ru1** exhibited all NMR features for **Ru1** and Aβ, with no change in the peptide signals when **Ru1** was present in solution (Figure 2.7 A). Upon addition of 1.0 eq. of **Ru1** to $A\beta_{1\text{-}16}$ and photoactivation for 10 min., we observed the presence of free 6,6'-dmb signals in the ^{1}H NMR, indicating the release of this ligand, a shift for some peptide residues, and the loss of signals of the Ru(II) complex (Figure 2.7 B) likely due to multiple species bound to the peptide that are formed upon photoactivation, and precipitation of the activated complexes. Interestingly, while the majority of the peptide residues do not shift upon photoactivation, the His residues shift upfield immediately after light exposure. The His resonances at 7.78 ppm, 6.94 ppm, and 6.89 ppm shift to 7.71 ppm, 6.93 ppm, and 6.85 ppm respectively (Figure 2.7 B). The His signal at 7.78 ppm shifts upfield and was determined to be at the same shift value as a peptide signal at 7.71 ppm, based on the increase in integration. Exposure of $A\beta_{1\text{-}16}$ alone to the photolysis conditions did not shift any ^{1}H NMR signals in comparison to $A\beta_{1\text{-}16}$ in the absence of photolysis.

For samples containing 1.0 eq. of **Ru2** and $A\beta_{1\text{-}16}$ we observed similar results as described for **Ru1**-$A\beta_{1\text{-}16}$. The unactivated samples did not exhibit any changes in peptide signals even after 24 h of incubation (Figure 2.8 A), while photoactivated samples exhibited His shifts immediately after photoactivation (Figure 2.8 B). However, the upfield shift for the His residues of **Ru2**-$A\beta_{1\text{-}16}$ are not as large as those observed for **Ru1**-$A\beta_{1\text{-}16}$. We observed shifts from 7.86 ppm, 7.01 ppm, and 6.96 ppm to 7.83 ppm, 7.00 ppm, and 6.93 ppm, respectively (Figure 2.8 B). Overall, the activated **Ru1-2** samples exhibited an upfield shift for the His residues of the $A\beta_{1\text{-}16}$ peptide, similar to what was observed by our group in a previous study involving Ru(III) complexes,[194] and by Guo *et al.*[249] and Hureau *et al.*[161] for Pt (II) complexes, indicating that these residues are involved in the interaction of **Ru1-2** with Aβ.

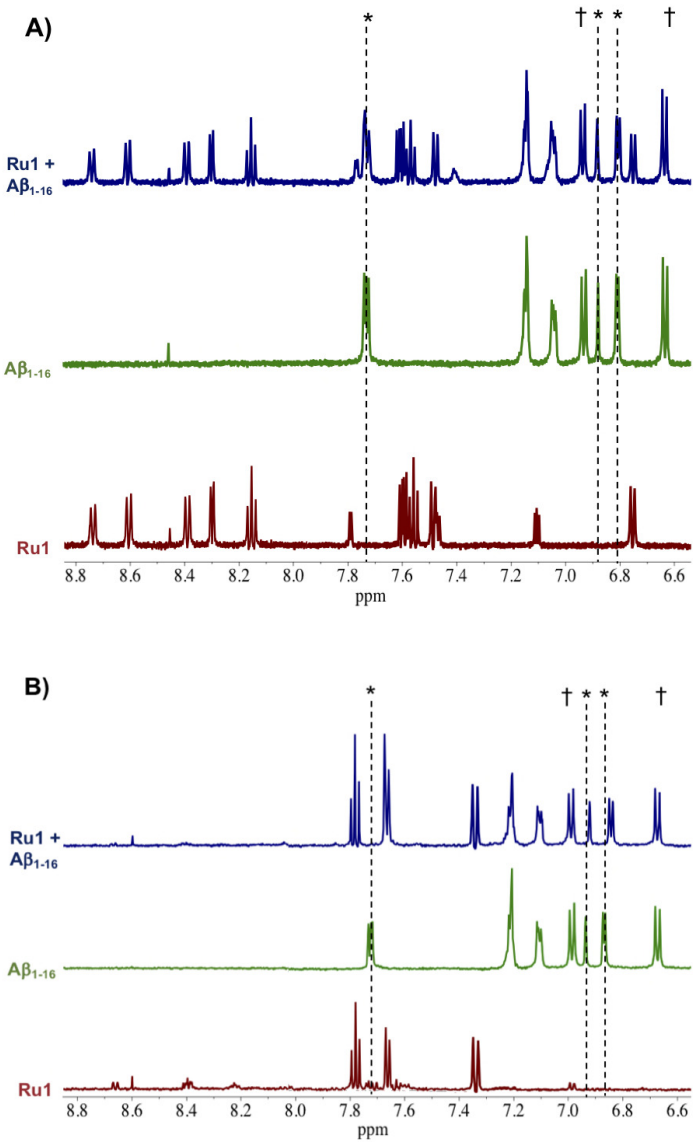

Figure 2.7 (A) ^{1}H NMR spectra of A$\beta_{1\text{-}16}$ (200 µM) in the presence of 1.0 eq. unactivated **Ru1** showing no changes of peptide residue signals after 24 h of incubation. (B) ^{1}H NMR spectra of photoactivated **Ru1**-A$\beta_{1\text{-}16}$ (200 µM) showing His shifts immediately after photoactivation (10 min.). Samples were prepared in PBS buffer (0.01 M, pH 7.4) at 37 °C. * His^{6}, His^{13} and His^{14}. † Tyr^{10}.

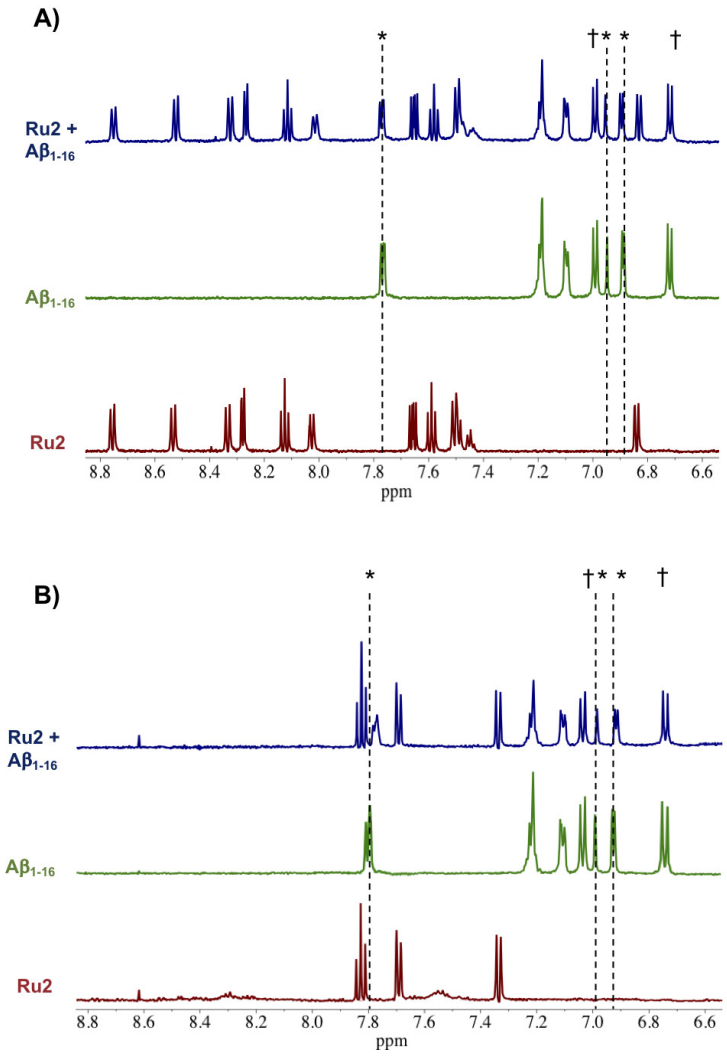

Figure 2.8 (A) ^{1}H NMR spectra of A$\beta_{1\text{-}16}$ (200 µM) in the presence of 1.0 eq. unactivated **Ru2** showing no changes of peptide residues after 24 h of incubation. (B) ^{1}H NMR spectra of photoactivated **Ru2**-A$\beta_{1\text{-}16}$ (200 µM) showing His shifts immediately after photoactivation time (12 min.). Samples were prepared in PBS buffer (0.01 M, pH 7.4) at 37 °C. * His^{6}, His^{13} and His^{14}. † Tyr^{10}.

Unactivated samples containing 1.0 eq. of **Ru3** and A$\beta_{1\text{-}16}$ did not exhibit any changes in peptide residue shifts (Figure 2.9 A). Interestingly, photoactivated **Ru3**-A$\beta_{1\text{-}16}$ samples exhibited free 6,6'-dmb ligand, however, no shifts of any peptide residues were observed (Figure 2.9 B), even after 24 h of incubation (Appendix A, Figure A.1). Overall, these results suggest that the release of the 6,6'-dmb ligand by photoactivation is necessary for binding of the Ru(II) complexes to Aβ to occur, however, differences in binding are observed for the three complexes.

The signals for the His residues were shifted upfield in the presence of **Ru1** and **Ru2**, suggesting the involvement of these residues in metal binding (Figures 2.7 B and 2.8 B).[161,194,249,250] For other residues, no shifts were observed even after 24 h of incubation (Appendix A, Figure A.1). Interestingly, despite the loss of the 6,6'-dmb ligand for **Ru3**, no shifts were observed (Figure 2.9 B), even after 24 h of incubation (Appendix A, Figure A.1) or upon addition of 2.0 eq. of **Ru3** to the peptide solution (Appendix A, Figure A.2). These results suggest that while His binding to Aβ is occurring for complexes **Ru1** and **Ru2**, **Ru3** does not interact with the peptide in the same manner.

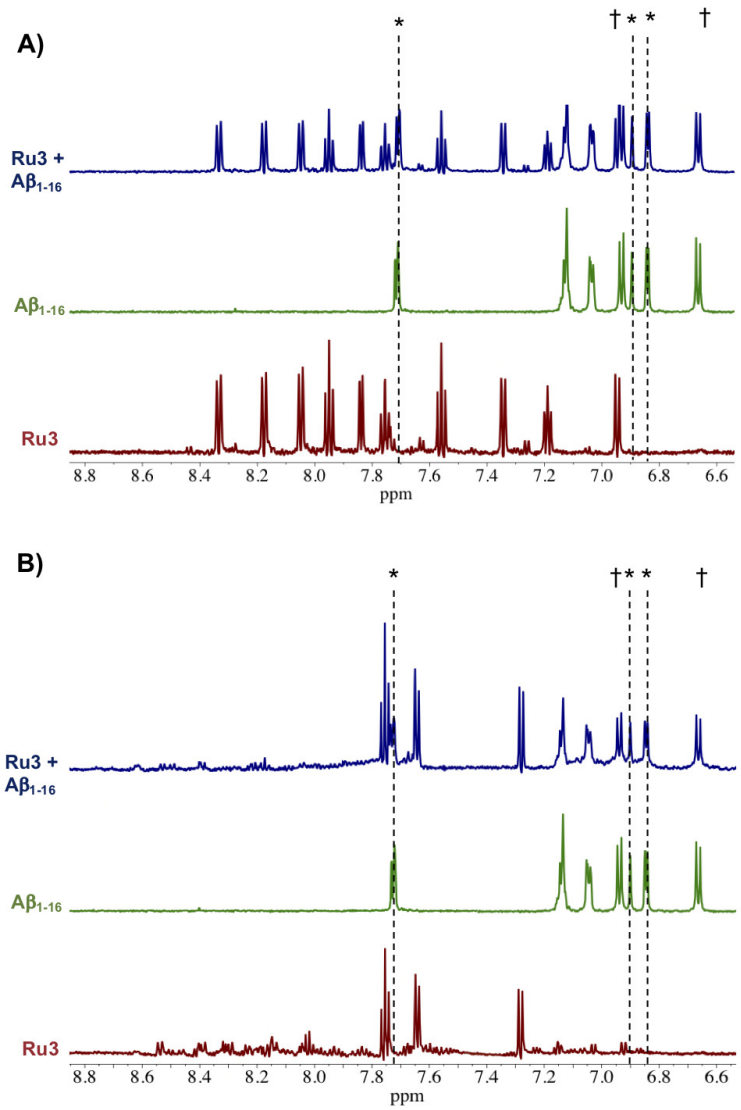

Figure 2.9 (A) ^{1}H NMR spectra of $A\beta_{1\text{-}16}$ (200 µM) in the presence of 1.0 eq. unactivated **Ru3** showing no changes of peptide residues after 24 h of incubation. (B) ^{1}H NMR spectra of photoactivated **Ru3**-$A\beta_{1\text{-}16}$ (200 µM) showing His shifts immediately after photoactivation time (25 min.). Samples were prepared in PBS buffer (0.01 M, pH 7.4) at 37 °C. * His^{6}, His^{13} and His^{14}. † Tyr^{10}.

To further investigate the interaction between the complexes and Aβ, ESI-MS was performed on solutions of $A\beta_{1\text{-}16}$ incubated with either **Ru1**, **Ru2**, or **Ru3** with and without photoactivation. The mass spectrum of **Ru1** and $A\beta_{1\text{-}16}$ in the absence of photoactivation shows peaks for the intact Ru complex ($[\mathbf{Ru1}]^{+}$ and $[\mathbf{Ru1}]^{2+}$), and for the Aβ peptide ($[A\beta_{1\text{-}16}]^{2+}$ and $[A\beta_{1\text{-}16}]^{3+}$), and no evidence of adduct formation (Figure 2.10 A). However, upon photoactivation, the ESI-MS data indicates the formation of the adducts [**Ru1**-DMSO-$A\beta_{1\text{-}16}$)]$^{4+}$ (m/z = 653.6) and [**Ru1**-$A\beta_{1\text{-}16}$]$^{3+}$ (m/z = 849.3) for **Ru1** (Figure 2.10 B). The isotopic distribution confirms the presence of Ru in the adduct peaks (Figure 2.10 B). The DMSO in the 653.6 m/z adduct is likely derived from the DMSO used to solubilize the Ru(II) complexes (2.5% in the final solution), and the masses of the adducts are consistent with loss of the 6-6'-dmb ligand and coordination to the peptide.

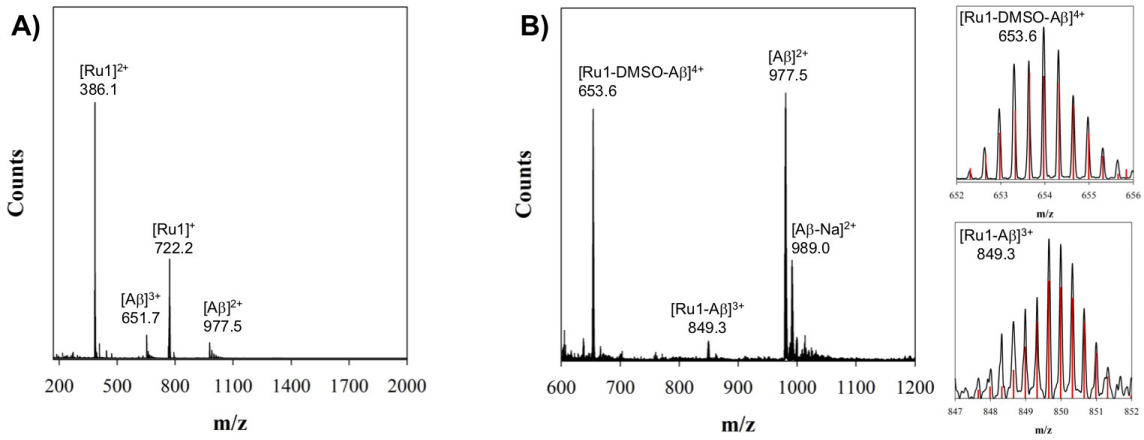

Figure 2.10 (A) ESI-MS of unactivated **Ru1** + $A\beta_{1\text{-}16}$ showing no evidence of adduct formation. (B) ESI-MS of photoactivated **Ru1** + $A\beta_{1\text{-}16}$ showing evidence of adduct formation. Zoomed regions exhibit the isotopic pattern of the adducts detected, and in red the theoretical isotopic pattern for the corresponding adduct. Samples were prepared in NH_4CO_3 buffer (20 mM, pH 9.0) and data was collected after 10 min. of activativation.

The data for **Ru2** in the absence of photoactivation is similar to that for **Ru1**, with peaks for $[\mathbf{Ru2}]^{+}$ and $[\mathbf{Ru2}]^{2+}$, and $[A\beta_{1\text{-}16}]^{2+}$ (Figure 2.11 A). Photoactivation shows adduct peaks [**Ru2**-$A\beta_{1\text{-}16}$]$^{3+}$ (m/z = 845.1), [**Ru2**-H_2O-$A\beta_{1\text{-}16}$]$^{3+}$ (m/z = 851.1), [**Ru2**-CO_3-$A\beta_{1\text{-}16}$]$^{3+}$ (m/z = 858.6), and [**Ru2**-DMSO-$A\beta_{1\text{-}16}$]$^{3+}$ (m/z = 871.1) for **Ru2**, with isotopic distributions confirming the presence of Ru (Figure 2.11 B). Interestingly, **Ru3** exhibits peaks consistent with 6-6'-dmb ligand loss and Aβ peptide binding ([**Ru3**-$A\beta_{1\text{-}16}$]$^{2+}$ (m/z = 1197.7), even in the absence of photoactivation (Figure 2.12 A). This result is consistent with *ca.* 6% 6-6'-dmb ligand loss in the ^{1}H NMR experiment (Figure 2.2). Upon photoactivation of **Ru3** in the presence of $A\beta_{1\text{-}16}$, adduct peaks [**Ru3**-$A\beta_{1\text{-}16}$]$^{3+}$ (m/z =

798.5), [**Ru3**-Cl-A$\beta_{1\text{-}16}$]$^{3+}$ (m/z = 812.4), and [**Ru3**-A$\beta_{1\text{-}16}$]$^{2+}$ (m/z = 1197.7) are observed (Figure 2.12 B).

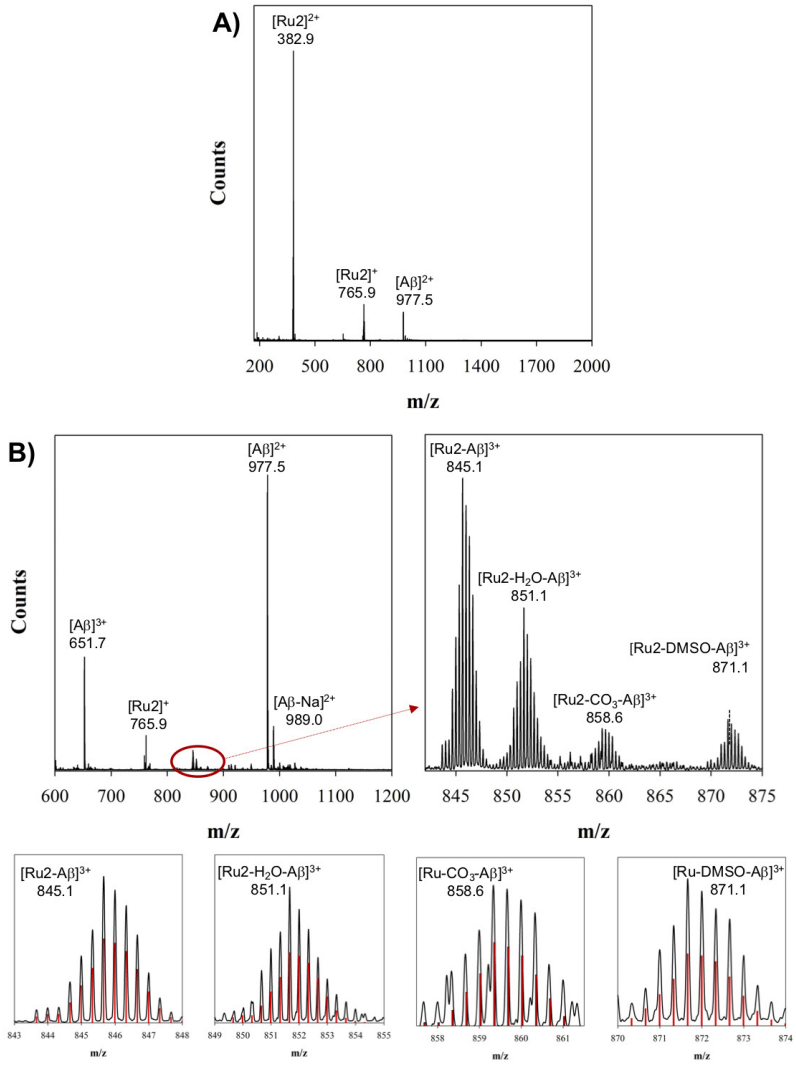

Figure 2.11 (A) ESI-MS of unactivated **Ru2** + A$\beta_{1\text{-}16}$ showing no evidence of adduct formation. (B) ESI-MS of photoactivated **Ru2** + A$\beta_{1\text{-}16}$ showing evidence of adduct formation. Zoomed regions exhibit the isotopic pattern of the adducts detected, and in red the theoretical isotopic pattern for the corresponding adduct. Samples were prepared in NH_4CO_3 buffer (20 mM, pH 9.0) and data was collected after 12 min. of activation.

Overall, the ESI-MS results show a lack of interaction between either **Ru1** or **Ru2** and the A$\beta_{1\text{-}16}$ peptide in the absence of photoactivation, however the *ca.* 6% 6-6'-dmb ligand loss for **Ru3** leads to the presence of peptide adduct peaks even in the dark. Upon photoactivation, all three Ru complexes exhibit adduct peaks in the ESI-MS consistent

with 6-6'-dmb ligand loss and peptide binding. MS/MS fragmentation experiments were not successful in indicating the residue(s) responsible for peptide binding.

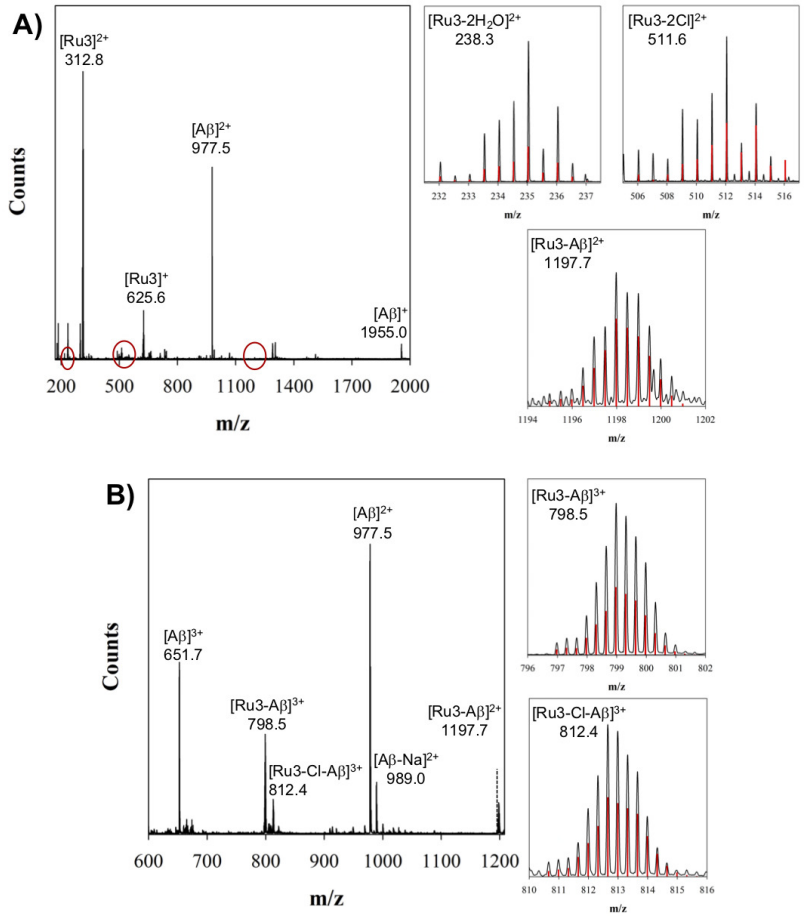

Figure 2.12 (A) ESI-MS of unactivated **Ru3** + $A\beta_{1\text{-}16}$ showing evidence of adduct formation. (B) ESI-MS of photoactivated **Ru3** + $A\beta_{1\text{-}16}$ also showing evidence of adduct formation.Zoomed regions exhibit the isotopic pattern of the adducts detected, and in red the theoretical isotopic pattern for the corresponding adduct. Samples were prepared in NH_4CO_3 buffer (20 mM, pH 9.0) and data was collected after 25 min. of activativation.

It is interesting to note that while **Ru3** exhibits adduct formation in the ESI-MS spectrum, no significant His residue shifts (or any other peptide residue) were observed in the ^{1}H NMR experiment. Based on the ^{1}H NMR and ESI-MS experiments we speculate that while a significant amount of adduct forms in the photoactivation experiment for **Ru1** and **Ru2**, comparatively less adduct forms for **Ru3**. We suggest a potential pre-organizing effect of the extended planar aromatic ligands for **Ru1** and **Ru2**, which facilitates covalent binding upon photoactivation. The enhanced interaction of the Aβ peptide with Ru(II) polypyridyl complexes incorporating extended planar aromatic ligands has been reported,[198,200] and in

addition, planar aromatic ligands enhance covalent adduct formation for Pt(II) complexes with both the Aβ peptide[159,165,251,252] and DNA.[253] We also performed ESI-MS experiments with the longer length aggregation-prone $A\beta_{1\text{-}40}$ peptide. The ESI-MS studies with the $A\beta_{1\text{-}40}$ peptide afforded similar results to those described with $A\beta_{1\text{-}16}$ above, showing that covalent adduct formation upon photoactivation occurs for the longer length peptide (Appendix A, Figure A.3).

2.2.3 Influence of Ru1-3 on the aggregation of Aβ

Metal complexes have been shown to modulate the aggregation pattern of the Aβ peptide through covalent and non-covalent interactions.[183,192,194] We were interested to investigate the impact of photoactivation of **Ru1-3** on Aβ aggregation, as previous reports have shown that Ru(II) polypyridyl complexes can influence Aβ aggregation *via* non-covalent interactions,[198,200] and $^1O_2$ generation upon photoactivation.[197] To investigate if the intact **Ru1-3** complexes and their photoactivated forms alter the size distribution and morphology of Aβ species, gel electrophoresis/Western blotting, TEM, and a Bicinchoninic acid assay (BCA assay) were employed. Due to the higher propensity for aggregation and toxicity, the $A\beta_{1\text{-}42}$ peptide was used in these studies.[206,254]

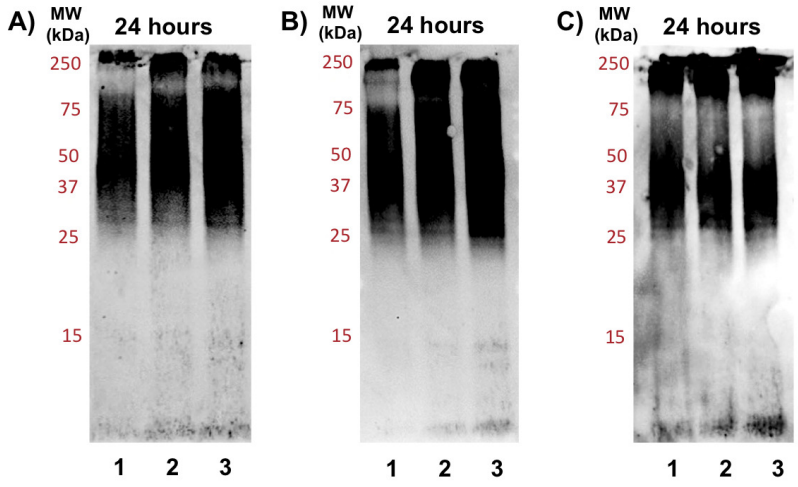

Figure 2.13 Gel electrophoresis/Western blot of $A\beta_{1\text{-}42}$ (25 μM) and different concentrations of unactivated **Ru1** (A), **Ru2** (B), and **Ru3** (C) in PBS buffer (0.01 M, pH 7.4) after 24 h of incubation at 37 °C. Lane 1: $A\beta_{1\text{-}42}$; lane 2: $A\beta_{1\text{-}42}$ + 1.0 eq. Ru(II) complex; lane 3: $A\beta_{1\text{-}42}$ + 2.0 eq. Ru(II) complex.

We initially investigated incubation of the $A\beta_{1\text{-}42}$ peptide (25 μM) with and without different concentrations (1.0 eq. and 2.0 eq.) of unactivated **Ru1-3**. Gel electrophoresis/ Western blotting after 24 h incubation showed that the intact complexes do not alter the aggregation pattern relative to peptide alone (Figure 2.13). Even though a number of Ru(II)

polypyridyl complexes have been reported to interact in a non-covalent manner with the Aβ peptide,[198,200] and in some cases alter the aggregation process,[201] unactivated **Ru1-3** did not exhibit an effect on the $A\beta_{1\text{-}42}$ peptide aggregation profile based on the gel electrophoresis experiment. We next investigated the incubation of the $A\beta_{1\text{-}42}$ peptide (25 µM) with and without different concentrations of photoactivated **Ru1-3** (0.1 to 2.0 eq.) over 24 h. At 1.0 eq. of **Ru1** and **Ru2**, peptide aggregation is significantly affected, resulting in the formation of higher molecular weight (MW) aggregates (Figure 2.14 A, B), while **Ru3** only shows a similar effect at 2.0 eq. (Figure 2.14 C).

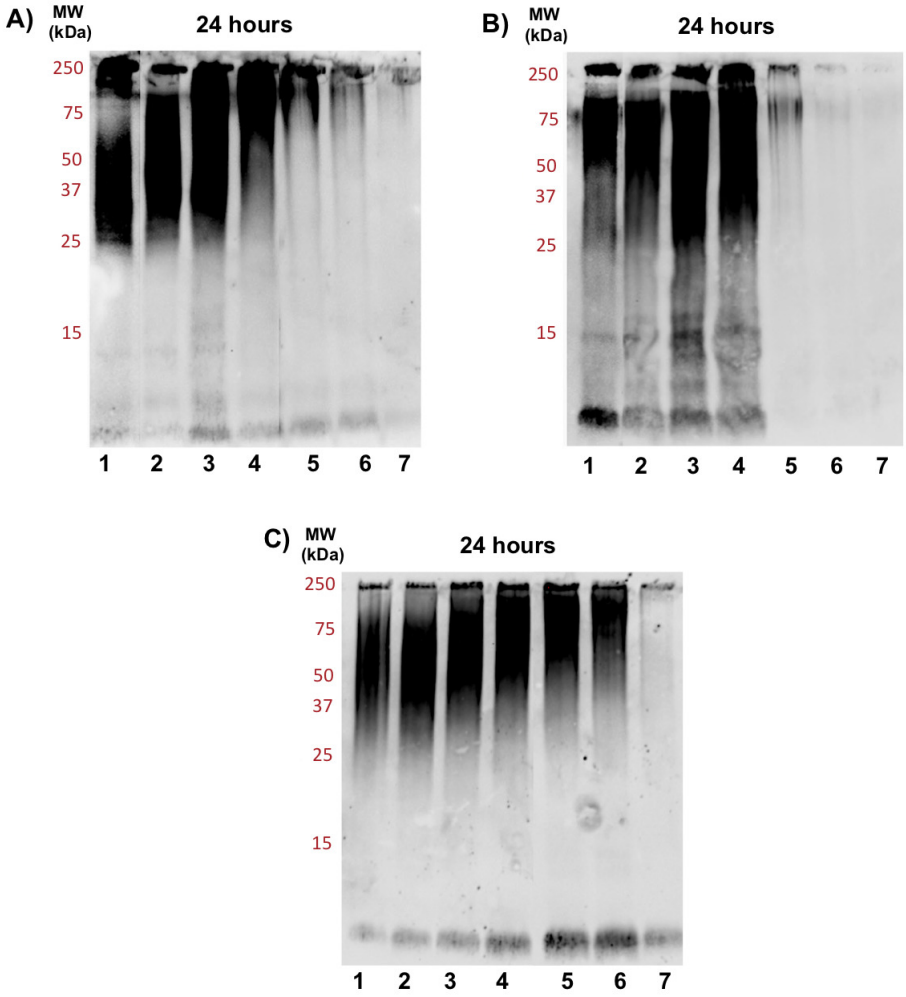

Figure 2.14 Gel Electrophoresis/Western blot of 25 µM $A\beta_{1\text{-}42}$ and different concentrations of **Ru1** (A), **Ru2** (B), and **Ru3** (C) in PBS buffer (0.01 M, pH 7.4) at 24 h incubation with agitation at 37 ℃, using anti-Aβ antibody 6E10. Lane 1: $A\beta_{1\text{-}42}$; lane 2: $A\beta_{1\text{-}42}$ + 0.10 eq. Ru complex; lane 3 $A\beta_{1\text{-}42}$ + 0.25 eq. Ru complex; lane 4: $A\beta_{1\text{-}42}$ + 0.50 eq. Ru complex; lane 5: $A\beta_{1\text{-}42}$ + 1.0 eq. Ru complex; lane 6: $A\beta_{1\text{-}42}$ + 1.5 eq. Ru complex; lane 7: $A\beta_{1\text{-}42}$ + 2.0 eq. Ru complex.

We were interested to explore the differences between **Ru1-3** in terms of peptide aggregation, and based on the initial results that showed a significant change in aggregation pattern at 24 h in the presence of 1.0 eq. of **Ru1** and **Ru2**, in comparison to the limited change observed for **Ru3** under the same conditions (Figure 2.14), we further investigated the aggregation of $A\beta_{1\text{-}42}$ in the presence of 1.0 eq. of **Ru1-3** over time. Figure 2.15 shows the aggregation results after photoactivation at 0 h, and after 24 h of incubation. At 0 h, peptide in the absence of activated Ru complex is primarily present in solution in monomeric and dimeric forms (low MW species), and after 24 h of incubation, higher MW species are predominant as previously reported.[183,255–257] Photoactivation of **Ru1** and **Ru2** induced the formation of large MW aggregates immediately after photoactivation (t = 0 h) (Figure 2.15 A, B), however, **Ru3** did not exhibit induction of high MW species on the gel at the initial timepoint (Figure 2.15 C). The immediate formation of high MW aggregates for photoactivated **Ru1-2**, as opposed to **Ru3**, suggests that the greater degree of covalent binding observed by ^{1}H NMR results in increased peptide aggregation. Interestingly, this immediate change from monomer/dimer to high MW aggregates for **Ru1-2** limits the formation of oligomers in the *ca.* 15-30 kDa range, which are reported to exhibit significant toxicity.[258–263]

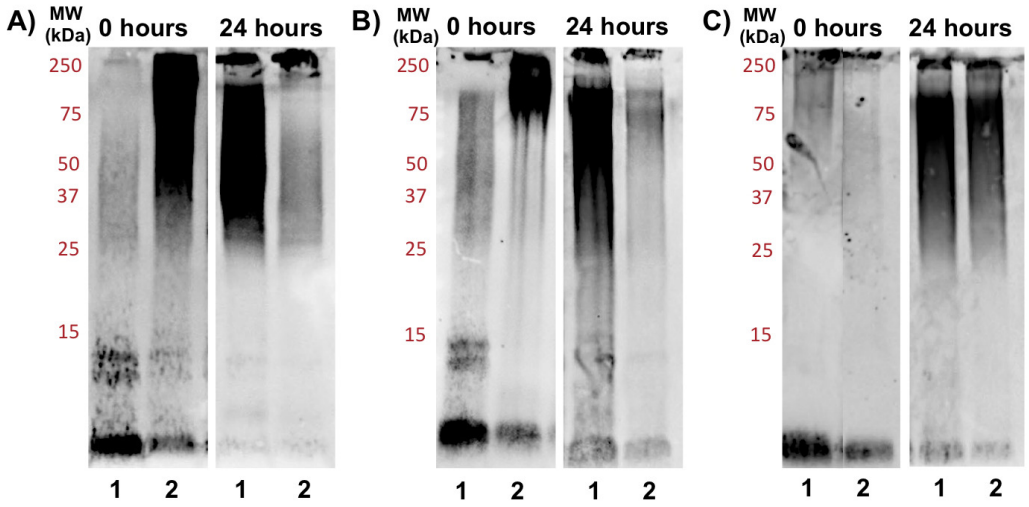

Figure 2.15 Influence of photoactivated **Ru1** (A), **Ru2** (B), and **Ru3** (C) on the aggregation profile of $A\beta_{1\text{-}42}$. Gel electrophoresis/Western blot of 25 µM $A\beta_{1\text{-}42}$ and 1.0 eq. of **Ru1-3** in PBS buffer (0.01 M, pH 7.4) at incubation time points 0 h and 24 h, with agitation at 37 ℃, using anti-Aβ antibody 6E10. Lane 1: $A\beta_{1\text{-}42}$; lane 2: $A\beta_{1\text{-}42}$ + 1.0 eq. Ru(II) complex.

After 24 h of incubation, photoactivated **Ru1-2** afforded only high MW species (MW higher than 250 kDa) as observed on the gel (Figure 2.15 A, B). However, the aggregation pattern for **Ru3** at 24 h appears qualitatively similar to peptide alone (Figure 2.15 C), again showing a significant difference in comparison to the results for **Ru1-2**. Overall, these results indicate that photoactivation, and covalent binding of **Ru1-2** to the $A\beta_{1\text{-}42}$ peptide, are necessary to observe substantial changes in the aggregation pattern, thus highlighting the role of the extended planar aromatic ligands of **Ru1-2** in modulating $A\beta_{1\text{-}42}$ peptide aggregation. To confirm that the integrity of the peptide was not compromised by the presence of the photoactivated Ru complexes (*via* oxidation and/or cleavage), a dot blot experiment was performed on the bulk sample (Figure 2.16). The peptide is recognized by the specific antibody 6E10 at the 24 h timepoint in all cases, showing that the high MW species formed in the presence of activated **Ru1-2** samples do not penetrate the gel.

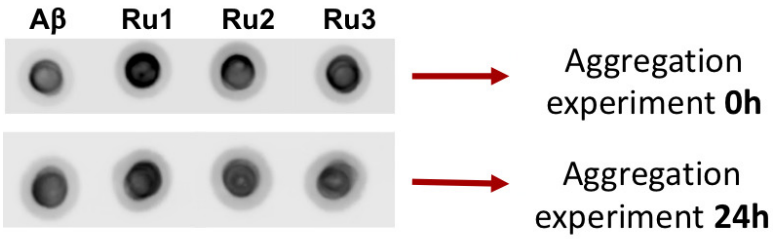

Figure 2.16 Dot blot of 25 µM $A\beta_{1\text{-}42}$ alone, and 25 µM $A\beta_{1\text{-}42}$ in the presence of 1.0 eq. of photoactivated **Ru1-3** at 0 h and 24 h of incubation showing that even after interaction with Ru complexes, the peptide is recognized by the 6E10 antibody.

While gel electrophoresis combined with Western blotting revealed the presence of higher MW $A\beta_{1\text{-}42}$ species and their size distribution, TEM analysis allowed us to characterize larger, insoluble $A\beta_{1\text{-}42}$ aggregates that cannot be analyzed by gel electrophoresis. Thus, the combination of these two methods provides a more complete picture of the $A\beta_{1\text{-}42}$ aggregation pathway under different conditions. As expected, the TEM images did not show large insoluble aggregates for the $A\beta_{1\text{-}42}$ sample at 0 h (Figure 2.17), however, immediately after light activation, samples containing **Ru1** and **Ru2** showed large insoluble amorphous aggregates, while the sample containing **Ru3** showed the presence of smaller amorphous aggregates (Figure 2.17). Incubation of $A\beta_{1\text{-}42}$ alone at 37 ℃ for 24 h led to the formation of both insoluble amorphous aggregates and fibrillar species (Figure 2.17), which agrees with previous reports.[170,264] Incubation of $A\beta_{1\text{-}42}$ for 24 h in the presence of activated **Ru1-3** affords similar sized amorphous aggregates (Figure 2.17), indicating that the Ru(II) complexes inhibit peptide fibrillization at 24 h.

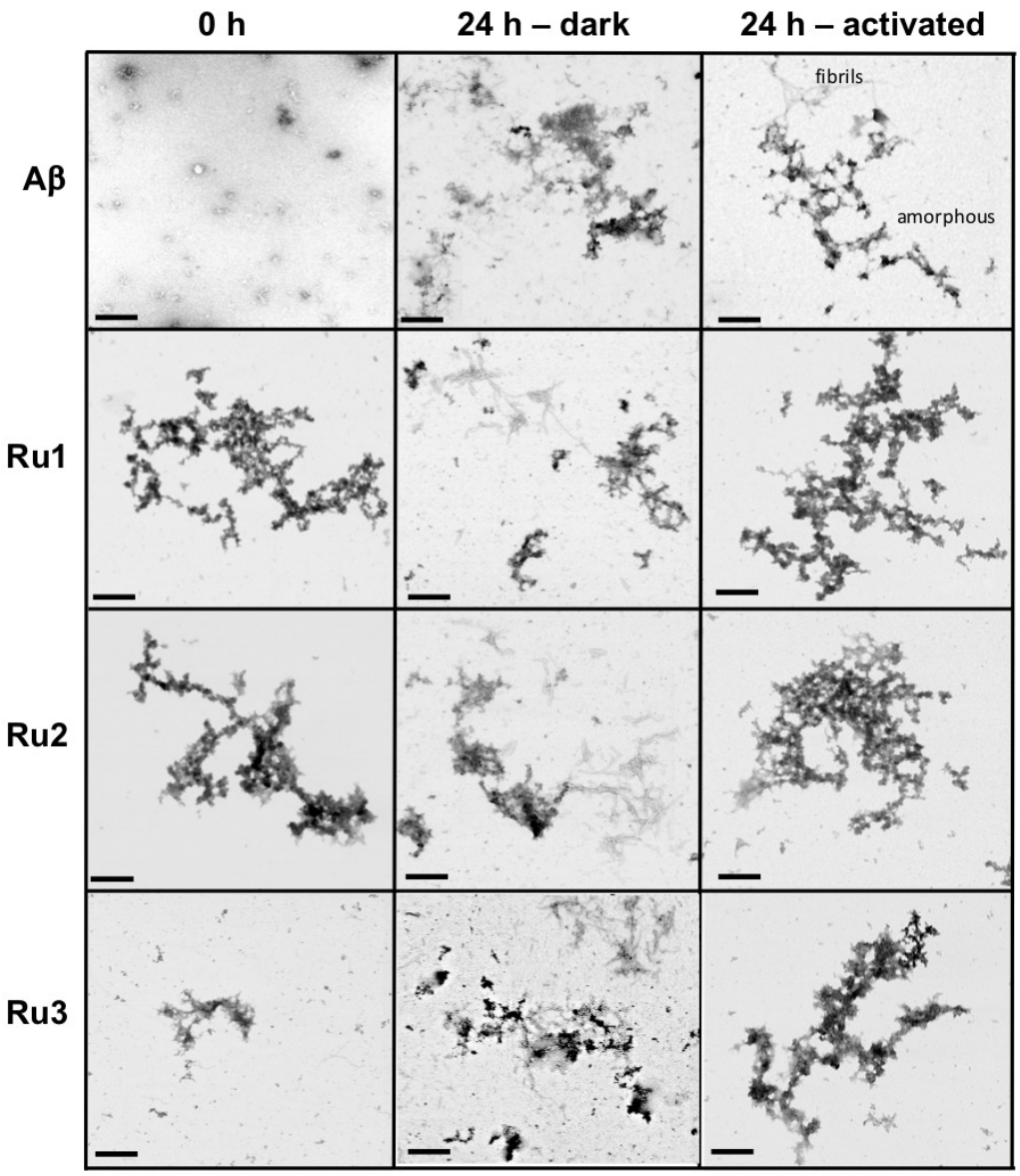

Figure 2.17 TEM images to monitor the influence of 1.0 eq. of **Ru1-3** on the morphology of $A\beta_{1\text{-}42}$ (25 µM) at 0 h (photoactivated samples) and 24 h (for unactivated and photoactivated samples) (scale bar = 200 nm).

Our results suggest that upon photoactivation, **Ru1** and **Ru2** immediately promote changes in peptide aggregation *via* the formation of soluble high MW species and large insoluble amorphous aggregates. In contrast to photoactivated **Ru1-2**, photoactivated **Ru3** does not promote the formation of large insoluble amorphous aggregates immediately, however, similar sized aggregates are observed by TEM after 24 h (Figure 2.17). $A\beta_{1\text{-}42}$ in the presence of unactivated **Ru1-3** showed similar aggregation morphology by TEM as $A\beta_{1\text{-}42}$

alone (Figure 2.17). The TEM images are consistent with the gel electrophoresis results, suggesting that photoactivation is essential for modulation of peptide aggregation.

To further analyze the change in peptide aggregation in the presence of the Ru(II) complexes, a BCA assay was used to determine the total concentration of protein in solution.[265] Before measurement, the samples were centrifuged to remove insoluble aggregates using an established protocol.[266,267] As expected, the results show a *ca.* 50% reduction in soluble peptide after 24 h for peptide alone, which is similar to the change in peptide concentration in the presence of unactivated **Ru1-3** after 24 h (Figure 2.18). It is interesting to note that even the peptide samples in the presence of the unactivated **Ru1-3** complexes exhibited a small but statistically-relevant reduction in peptide solubility, however, as we demonstrated previously, this interaction is not strong enough to change the overall size distribution or the morphology of Aβ.

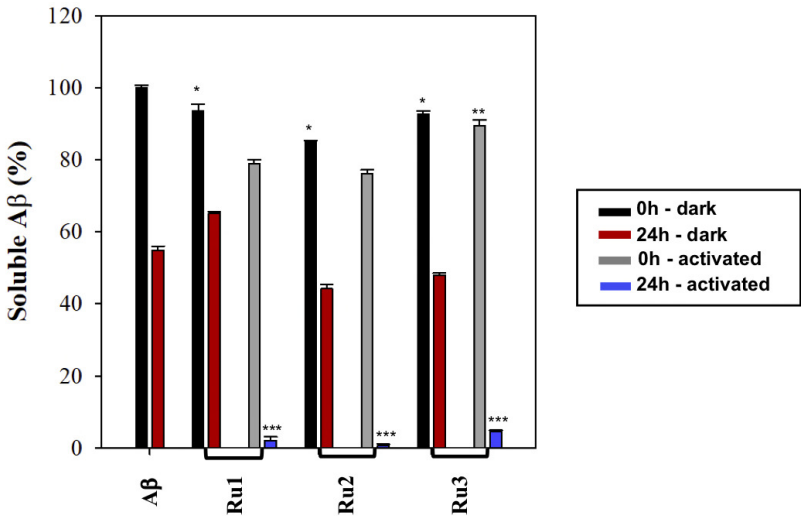

Figure 2.18 BCA assay of 60 µM $A\beta_{1\text{-}42}$ in the presence of 1.0 eq. of **Ru1-3** in PBS buffer (0.01 M, pH 7.4) at 0 h and 24 h with and without photoactivation. Samples were centrifuged at 14,000 g for 5 min. prior to absorbance measurement. Statistically significant difference between: *$A\beta_{1\text{-}42}$ 0 h and all three complexes at 0 h in the dark (**Ru1**, $p = 0.02$; **Ru2**, $p < 0.0001$; **Ru3**, $p = 0.0002$); ** photoactivated **Ru1-2** 0 h compared to photoactivated **Ru3** 0 h (**Ru3**, $p = 0.0003$) (no statistical difference between photoactivated **Ru1** and **Ru2** at 0 h); and *** $A\beta_{1\text{-}42}$ (24 h) and photoactivated **Ru1-3** (24 h) ($p < 0.0001$). Calculated using 2-way ANOVA.

Immediately after photoactivation, the concentration of soluble peptide is less than peptide alone for samples containing all three complexes, however, **Ru1** and **Ru2** display a slightly larger reduction in Aβ solubility in comparison to **Ru3**, which is consistent with the results obtained for gel electrophoresis and TEM studies (see above). Strikingly, in the pres-

ence of all three activated Ru(II) complexes, the peptide is almost completely precipitated at 24 h (Figure 2.18), which is consistent with the large insoluble amorphous aggregates observed in the TEM studies for **Ru1-3** (Figure 2.17), and gel electrophoresis of **Ru1-2**, where we observe that the species formed after 24 h of incubation are not able to penetrate the gel (Figure 2.15). Interestingly, the BCA results show that after 24 h, photoactivated **Ru3** also significantly decreases the solubility of the peptide, even though gel electrophoresis still displays soluble high MW species. The morphology of the aggregates formed for **Ru1-3** were similar as indicated by TEM, however we hypothesize that **Ru3** leads to the formation of less stable insoluble amorphous aggregates when compared to **Ru1-2**. It is known that sodium dodecyl sulfate (SDS) can promote the dissociation of protein aggregates,[268,269] and we hypothesize that the electrophoresis running buffer (containing 0.1% SDS) could promote the disassembly of the less stable amorphous aggregates of **Ru3**.

The BCA results show that unactivated **Ru1-3** induce only a small decrease in the solubility of $A\beta_{1\text{-}42}$, which is consistent with the lack of changes in peptide morphology or overall size distribution by TEM and gel electrophoresis. Immediately after photoactivation, **Ru1-2** lead to a significant change in the aggregation pattern of $A\beta_{1\text{-}42}$, as shown by the TEM and gel electrophoresis data. These results highlight the importance of photoactivation for modulation of the peptide aggregation pathway. It interesting to note that for **Ru3**, upon photoactivation, there was very little change in the aggregation pattern at 0 h compared to **Ru1-2**, however, at 24 h the change in aggregation for **Ru3** was similar to that observed for the other two complexes, resulting in large amorphous aggregates and significant precipitation of the peptide from solution.

2.2.4 Binding Constants and Docking Studies

Based on previous work showing the interaction of octahedral Ru(II) polypyridyl complexes with amyloid fibrils,[270–272] we investigated the binding of unactivated **Ru1-3** with $A\beta_{1\text{-}42}$ fibrils. $A\beta_{1\text{-}42}$ contains a Tyr^{10} residue, an intrinsic fluorophore that allows the determination of the slightest changes in the fluorophore surroundings due to the interaction of its phenol ring and micro-environment.[251,273–275] In addition, the use of Tyr^{10} fluorescence to measure small molecule binding interactions removes the potential for interference when using extrinsic probes that may compete for fibril binding sites.[276,277] To form $A\beta_{1\text{-}42}$ fibrils, the monomeric peptide was incubated, and TEM was used to monitor aggregate morphology over time (Figure 2.19). By 96 h, only fibrils were evident by TEM analysis, and thus samples at 96 h incubation were used for binding studies with unactivated **Ru1-3**.

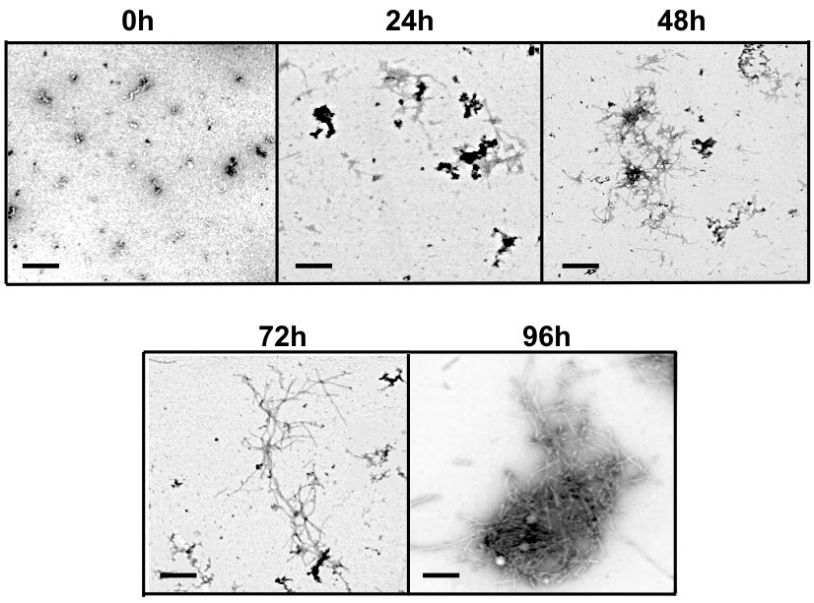

Figure 2.19 Change in morphology of $A\beta_{1\text{-}42}$ over time leading to the formation of mature fibrils after 96 h of incubation (scale bar = 200nm).

Binding of the Ru complexes was measured using tyrosine fluorescence, in comparison to ThT as a positive control (Figure 2.20 and Appendix A, Figure A.4 for titration data), a common fluorescent dye used to detect fibrillar Aβ structures.[278,279] The binding constant (K_d) of ThT to the synthesized $A\beta_{1\text{-}42}$ fibrils under our conditions was determined to be 9.5 ± 1.1 µM, which is in agreement to published values ranging from 5 µM[280] to 11 µM.[281] Using the same protocol, the binding constants for **Ru1** (1.8 ± 1.1 µM), **Ru2** (6.1 ± 0.5 µM), and **Ru3** (640 ± 22 µM) were obtained for unactivated complexes (Figure 2.20 and Appendix A, Figure A.4 for spectra). The values for **Ru1** and **Ru2** compare well to the K_d of $[Ru(bpy)_2(dppz)]^{2+}$ (~2.1 µM)[198] (Figure 1.12), while **Ru3** displays considerably weaker binding to $A\beta_{1\text{-}42}$ fibrils. This data provides further support that the extended planar aromatic ligands 2-(thiophen-2-yl)-1H-imidazo[4,5-f][1,10]phenanthroline) for **Ru1**, and 2-phenyl-1H-imidazo[4,5-f][1,10]phenanthroline) for **Ru2** are required for enhanced interaction with $A\beta_{1\text{-}42}$ fibrils, likely *via* hydrophobic interactions. While the fibril structure is obviously different in comparison to monomeric peptide in solution, the increased potential for hydrophobic interactions between **Ru1-2** and the $A\beta_{1\text{-}42}$ peptide may also pre-organize the complexes so that covalent binding occurs more readily upon photoactivation (see NMR section).

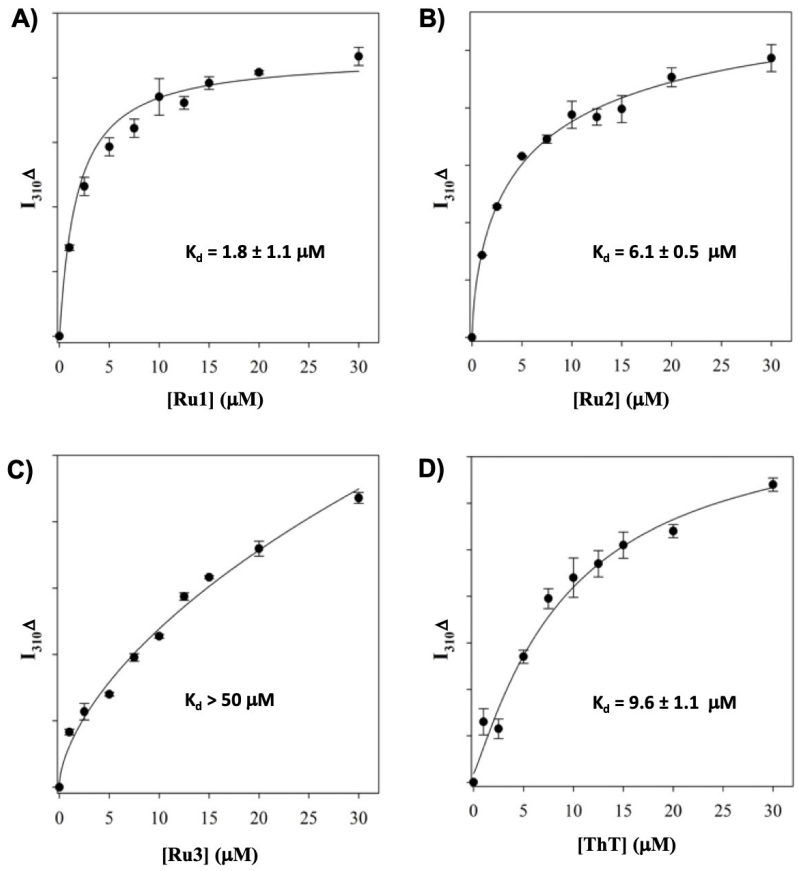

Figure 2.20 Binding constants of **Ru1** (A), **Ru2** (B) and **Ru3** (C), and ThT (D) with $A\beta_{1\text{-}42}$ fibrils (10 µM in PBS 0.01 M, pH 7.4) measured from the change in Tyrosine fluorescence ($\lambda_{ex}/\lambda_{em}$ = 275/310 nm).

We subsequently used molecular docking to visualize potential interactions between **Ru1-3** and $A\beta_{1\text{-}42}$ fibrils. There are a number of reported experimental structures of Aβ fibrils,[45,282,283] and we have chosen to perform docking using the protein data bank (PDB) 2MXU structure.[283] This structure contains 12 β-strand filaments, which is significantly more than many other structures found in the PDB at the time of investigation and provides sufficient surface area for modelling the interactions with our Ru complexes. Further, it contains a well-defined hydrophobic cleft for positioning of the ligand during docking, as docking results are most reliable when they are not mediated by significant bulk solvent interactions that can add further confounding degrees of freedom to the docking simulation.[284–286] As such, these docking results will best describe the binding of these ligands to single-symmetry $A\beta_{1\text{-}42}$ fibrils.

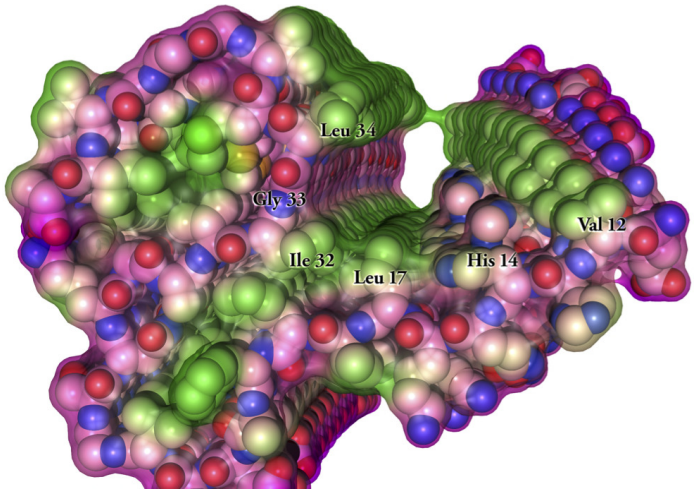

Figure 2.21 View down the hydrophobic cleft present in PDB 2MXU. Atoms are shown as space filling models (Grey: carbon, red: oxygen, blue: nitrogen, yellow: sulfur. Hydrogens are omitted) inside of a water-accessible Van der Waals surface shaded to show lipophilic (green) and hydrophilic (pink) regions.

The 2MXU structure contains a hydrophobic cleft composed of Val^{12}, His^{14}, Leu^{17}, Ile^{32}, Gly^{33}, and Leu^{34}, with Gly and His polar surface areas providing the only potential for electrostatic interactions (Figure 2.21). Also present is a twist in the His^{14}/Val^{12} side of the cleft, meaning that the width of the channel decreases as it travels further away from the viewer's perspective. We would expect the hydrophobicity of this cleft to be a large driving factor for binding these compounds prior to photoactivation.

The docking results showed that the highest scored binding poses are placed further towards the narrower end of the channel, likely driven by a desire to exclude as much of the bulk solvent from the pose as possible (Figure 2.22). Further, the larger **Ru1** and **Ru2** complexes bear a striking resemblance to a ship's anchor, with pyridinyl rings wedging between the grooves created by the Val sidechains, while the His ring and Gly backbone atoms provide electrostatic interactions with aromatic rings of the ligands. The docking results provide further insight into the importance of the extended hydrophobic ligands of unactivated **Ru1-2** over **Ru3** in the interaction with the peptide, which can facilitate the formation of the covalent bond once the complexes are photoactivated.

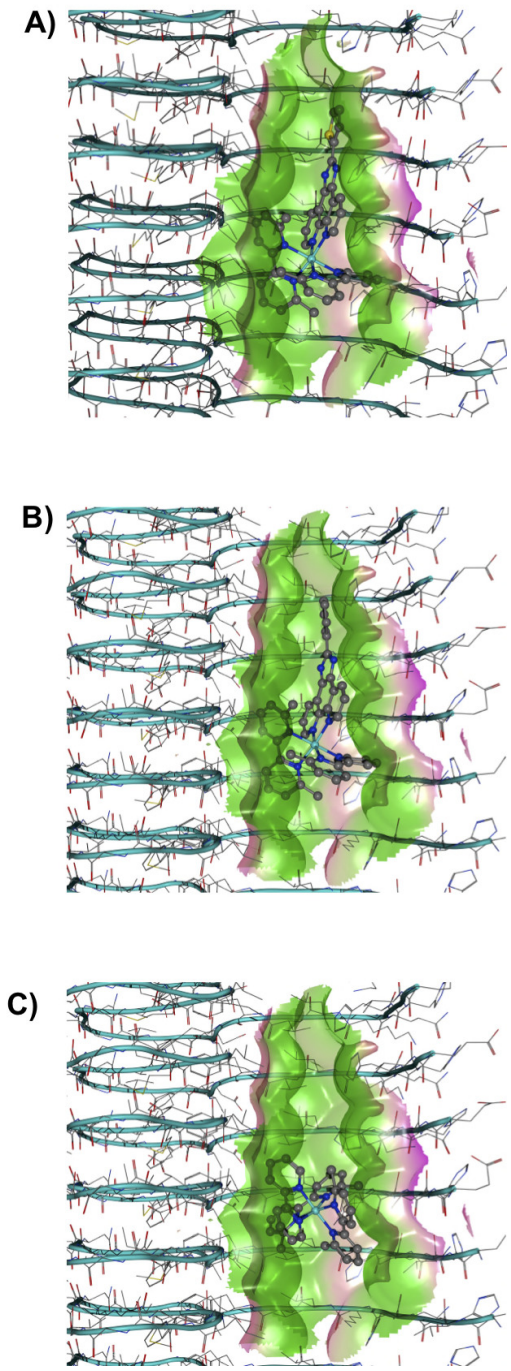

Figure 2.22 Docking results for **Ru1** (A), **Ru2** (B), and **Ru3** (C) showing the highest scored pose, indicating the interaction of side chains and ligands. For all three complexes, the Λ isomers were used.

2.2.5 Influence of Ru1-3 on the morphology of pre-formed $A\beta_{1\text{-}42}$ Fibrils

In order to investigate if the Ru(II) complexes could change the morphology of insoluble $A\beta_{1\text{-}42}$ fibrils, we incubated the unactivated and activated complexes with pre-formed fibrils and monitored for a change in morphology *via* TEM. Our binding studies show that the intact **Ru1-2** complexes have a much stronger affinity for $A\beta_{1\text{-}42}$ fibrils in comparison to **Ru3** (see above), and thus we hypothesized that photoactivation of the **Ru1-2** complexes (and possibly even **Ru3**) may lead to alteration of aggregate morphology.

As expected, incubation of $A\beta_{1\text{-}42}$ for 96 h exclusively produced mature fibrillar structures (Figure 2.23). Remarkably, we observed that after the addition of the Ru(II) complexes and photoactivation, an immediate morphology change from fibrillar to amorphous species is observed for **Ru1** and **Ru2**, yet a more gradual change is observed for **Ru3** (Figure 2.23). No further changes were observed over an additional 24 h incubation for **Ru1-2**, while for **Ru3** the mixture of amorphous and fibrillar aggregates observed by TEM immediately after photoactivation changes to amorphous at 24 h (Figure 2.23). Photoactivation is necessary for morphology changes, as there was no difference between pre-incubated $A\beta_{1\text{-}42}$ alone and $A\beta_{1\text{-}42}$ incubated for additional 24 h in the presence of unactivated **Ru1-3** (Figure 2.23). Even though the intact complexes display a high affinity for $A\beta_{1\text{-}42}$ fibrils, especially for **Ru1-2** (Figure 2.20), the non-covalent interaction does not in itself lead to a change in aggregate morphology. Upon photoactivation, immediate changes to peptide aggregate morphology are observed, with **Ru1-2** exhibiting the most significant change in comparison to **Ru3**, in line with the measured binding affinities. However, all three photoactivated complexes exclusively afford amorphous aggregates at the 24 h timepoint.

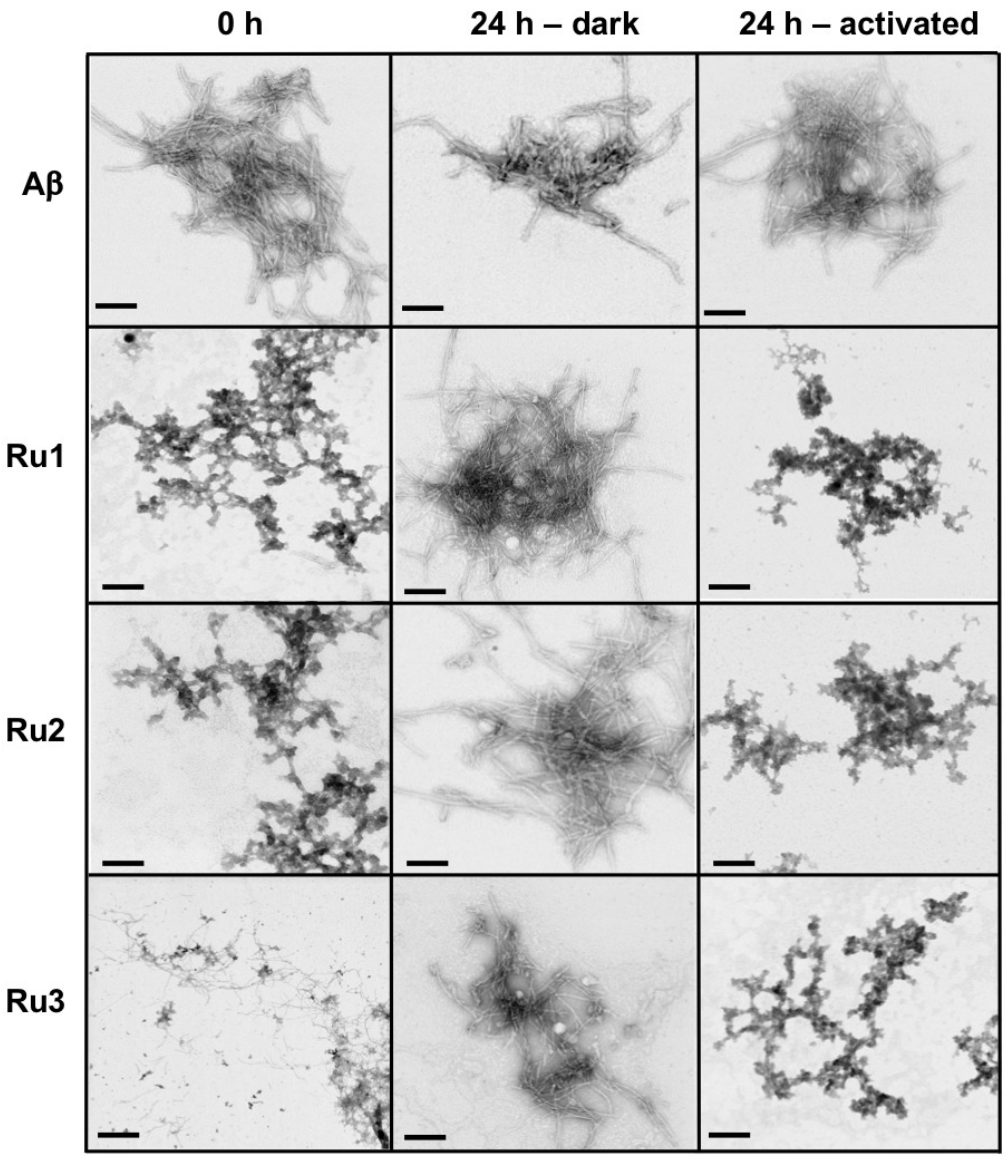

Figure 2.23 Influence of 1.0 eq. of **Ru1-3** on the morphology of fibrillar $A\beta_{1\text{-}42}$ (25 µM) at 0 h (photoactivated samples) and 24 h (for unactivated and photoactivated samples) (scale bar = 200 nm).

2.3 Effect of the Extended Aromatic Ligand

In order to further investigate the importance of photoactivation and the extended planar aromatic ligand, $Ru(bpy)_2CO_3$ (Figure 2.24) was synthetized following a published procedure,[287] and the complex was tested as a control. Metal complexes with labile ligands have been successfully used for the labeling of cytochrome c,[288] copper protein mutants,[289] and glucose oxidase,[290] in many cases by ligand-exchange reactions and binding to His residues.

$Ru(bpy)_2CO_3$ is an example of a complex that undergoes facile ligand-exchange of the bidentate carbonato ligand ,[291] and studies have demonstrated the ability of $Ru(bpy)_2CO_3$ to bind to imidazole (Im), a model compound of His,[292,293] and also to His-containing peptide.[294] $Ru(bpy)_2CO_3$ first exchanges the carbonato ligand for two H_2O molecules, similar to cisplatin hydrolysis, and when in the presence of Im (or His), the bis-aqua complex readily replaces one H_2O molecule for one Im (or His).

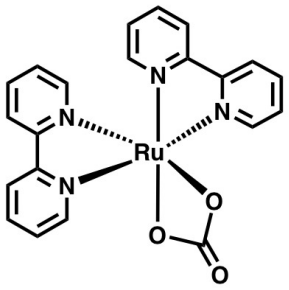

Figure 2.24 Structure of $[Ru(bpy)_2CO_3]$ complex.

We chose to use $Ru(bpy)_2CO_3$ as a control complex to further evaluate the role of photoactivation and the extended planar aromatic ligands in mediating the interaction between the Ru(II) polypyridyl complexes and Aβ. Facile ligand exchange of the carbonato ligand provides a Ru(II) complex with two cis-exchangeable coordination sites, similarly to photoactivated **Ru1-3**. Thus, we expected photoactivated **Ru3** and $Ru(bpy)_2CO_3$ to perform similarly in the peptide aggregation experiments. ^{1}H NMR of $Ru(bpy)_2CO_3$ in the presence of $A\beta_{1\text{-}16}$ did not show a His residue shift (or any other shift) (Appendix A, Figure A.5), and precipitation was observed over time, which could be related to the broadening of NMR signals. Even though ^{1}H NMR did not show any shifts for Aβ residues, ESI-MS data showed the formation of a peptide adduct indicating that the complex is able to interact covalently with $A\beta_{1\text{-}16}$ similarly to **Ru3** (Appendix A, Figure A.6). The gel electrophoresis/Western blot experiment exhibited no difference in peptide aggregation pathway for samples containing different concentrations of the $Ru(bpy)_2CO_3$ complex (Appendix A, Figure A.7), which is similar to the results observed for **Ru3**. Overall, the results for $Ru(bpy)_2CO_3$ are similar to that for photoactivated **Ru3**, which provide further support for the importance of the extended hydrophobic ligands in **Ru1-2** in providing a better environment for Ru(II)-peptide binding.

2.4 Summary

This study underlines the ability of photoactivated **Ru1-3** to target and modulate the aggregation pathway of $A\beta_{1\text{-}42}$, one of the hallmarks of AD. **Ru1-3** were demonstrated to bind covalently to the peptide upon photoactivation and loss of the 6,6'-dmb ligand. ^{1}H NMR showed release of the 6,6'-dmb ligand and His residue shifts for **Ru1** and **Ru2**, indicating that these residues are involved in the binding process. ESI-MS confirmed the release of the 6,6'-dmb ligand upon photoactivation, and also showed the presence of complex-peptide adducts for **Ru1-3**.

Ru1-2, and to a lesser extent **Ru3**, significantly alter the $A\beta_{1\text{-}42}$ aggregation process, with **Ru1-2** promoting the formation of soluble high MW weight aggregates immediately after photoactivation. TEM analysis also shows the formation of large amorphous aggregates for **Ru1-2**, while the aggregates observed for **Ru3** are considerably smaller. This immediate change for **Ru1-2** upon photoactivation, bypasses the formation of low MW peptide oligomers, suggesting that these complexes could prevent the formation of toxic oligomeric species.[258–263] However, we have not investigated cellular toxicity at this time. After 24 h incubation, photoactivated **Ru1-2** afford very little soluble $A\beta_{1\text{-}42}$ as observed in the gel electrophoresis and BCA experiments, and TEM shows formation of large insoluble amorphous aggregates, in comparison to the presence of both fibrils and amorphous aggregates for peptide alone. Photoactivated **Ru3** displays soluble aggregates in the 30-250 kDa size range at 24 h, however the majority of the peptide has precipitated as indicated by the BCA assay, and large amorphous aggregates are observed by TEM, similarly for **Ru1-2**.

Binding constant analysis of fibrillar $A\beta_{1\text{-}42}$ in the presence of non-activated **Ru1** (K_d = 1.8 ± 1.1 µM) and **Ru2** (K_d = 6.1 ± 0.5 µM) showed similar binding constants to ThT (K_d = 9.5 ± 1.1 µM), which indicates that these complexes will be in close proximity to the peptide once the 6,6'-dmb ligand has been photoejected, likely favoring the formation of a covalent bond between the complexes and peptide. The docking experiments indicate that the extended hydrophobic ligands of **Ru1** and **Ru2** fit into a cleft in the $A\beta_{1\text{-}42}$ fibril structure and provides an indication as to why **Ru3** displays a significantly weaker binding constant (K_d = 640 ± 22 µM). Extrapolating from the data obtained from **Ru1-3** with fibrillar $A\beta_{1\text{-}42}$ and the differences in structures of the complexes, we expect an enhanced interaction of **Ru1-2** with the monomeric peptide in comparison to **Ru3**. Indeed, a number of similar Ru(II) complexes have been shown to interact with oligomeric species and not just fibrils.[200,202] TEM images also demonstrated that the complexes are able to modify the morphology of mature fibrils after photoactivation, generating insoluble amorphous aggregates, even though **Ru1-2** are able to induce this change much more quickly in comparison to **Ru3**.

Overall, this study shows that photoactivation of **Ru1-3** is a critical process that allows the interaction of the Ru(II) complexes with the Aβ peptide. Photoactivated **Ru1-3** are able to modulate size distribution and peptide morphology. The formation of amorphous aggregates in the presence of the photoactivated Ru(II) complexes is a common endpoint herein, either starting with monomeric peptide or fibrils. Our results also show that the extended hydrophobic ligands present in **Ru1** and **Ru2** enhance the peptide interaction, especially at early time points, facilitating the formation of a covalent adduct between the Ru(II) complexes and Aβ when samples are photoactivated.

2.5 Experimental

All common reagents were purchased from commercial suppliers and used without further purification. All Ru(II) complexes, **Ru1**, **Ru2**, and, **Ru3** were synthesized by the McFarland group,[143,241] and $Ru(bpy)_2CO_3$ were synthesized following a standard procedure.[287] The $A\beta_{1\text{-}16}$ peptide was purchased from Genscript (Piscataway, NJ, USA), and $A\beta_{1\text{-}42}$ and $A\beta_{1\text{-}40}$ from 21st Century Biochemicals (Malborough, MA, USA) and they were all monomerized before use according to a reported procedure.[295,296] $A\beta_{1\text{-}16}$ was dissolved in double distilled water (ddH_2O), while $A\beta_{1\text{-}40/1\text{-}42}$ was dissolved in DMSO and ddH_2O in a 1:1 mixture, unless stated otherwise. The stock peptide solution concentration was determined by absorbance with the use of a Thermo Nicolet UV nanodrop of Tyr^{10} considered as free tyrosine (extinction coefficient of 1410 M^{-1} cm^{-1} at 280 nm).[297] UV-Vis spectra were obtained on a Cary 5000 spectrophotometer. ^1H NMR spectra were recorded on a Bruker AV-600 instrument. TEM images were obtained using an OSIRIS FEI scanning TEM (STEM) operating at 200 kV. ESI-MS experiments were performed on an Agilent 6130 mass spectrometer connected to an Agilent 1260 HPLC system. The determination of the binding affinities was performed on a Fluorolog-3®fluorimeter. Default parameters were used for all computational procedures unless stated otherwise. All molecular mechanics methods were performed in the Molecular Operating Environment version 2015 (MOE, Chemical Computing Group, Montreal, Canada) using the Born solvation model. All DFT calculations were performed in Gaussian 16 (G16RevC.01) using the polarizable continuum model (PCM, water) for solvation. Images were generated in POV-ray engine v3.7.0 (www.povray.org).

2.5.1 Photoejection of 6,6'-dimethyl-2,2 Bipyridine (6,6'-dmb) Ligand

Ru(II) complexes were dissolved in DMSO and added to a phosphate buffered saline solution (PBS, 0.01 M Na_2HPO_4, 0.001 M KH_2PO_4, 0.14 M NaCl, 0.003 M KCl, pH 7.4). Photoejection experiments were carried out *via* UV-Vis using a visible light source with cool

white colour (5500 – 6000 K) (SOLLA 30W LED), which is past the cutoff radiation of a black body (4000 K), indicating that the black body emission does not affect the activation of the complexes. Data were collected from 200-900 nm, and irradiation intervals were as short as 1 min. at early times and after 15 min., data were collected every 5 min. until 60 min. of experiment. The photoejection time was determined when no further spectral changes were observed. Photoejection kinetics were analyzed by plotting the normalized change in absorption at two wavelengths against irradiation time using a published method.[141,149,243,245] The wavelength selected were those within 50 nm of the longest wavelength isosbestic point and exhibited the greatest change in the course of the experiment.

2.5.2 ^{1}H NMR Binding Assay of A$\beta_{1\text{-}16}$ Peptide to Ru(II) Complexes

Deuterated PBS (0.01 M, pH 7.4) buffer was prepared by removal of water by vacuum drying of PBS buffer and dissolving the powder in D_2O. A$\beta_{1\text{-}16}$ and Ru(II) stock solutions in DMSO (1 mM) were dissolved in deuterated PBS (0.01 M, pH 7.4) buffer, and the ^{1}H NMR spectra of A$\beta_{1\text{-}16}$ alone, Ru(II) complexes (200 µM - kept in the dark or light activated), and A$\beta_{1\text{-}16}$ plus Ru(II) complexes (1:1 eq. dark or light activated) were collected after solubilization at 0 h and 24 h.

2.5.3 Mass Spectrometry of Binding of Aβ Peptide to Ru(II) Complexes

Samples were analyzed by direct infusion (1 – 4 µL) of analyte into a mobile phase of 1:1 water:acetonitrile containing 5 mM ammonium acetate (pH unmodified), flowing at 0.3 mL/min and maintained at 30 ℃. All components of the mobile phase were MS grade and water was ultra-pure grade from MilliQ A-10 system. Nitrogen drying gas was heated to 250 ℃ and run at 5 L/min with a nebulizing pressure of 15 psig. Voltages were: capillary 3 kV, fragmentor 175 V, slimmer 30 V, octupole 250 V. Samples were prepared as ~1 mg/mL of total protein (A$\beta_{1\text{-}16/1\text{-}40}$) in ammonium carbonate (0.02 M, pH 9) buffer with 0 or 1 eq. of Ru(II) complexes (dark and activated).

2.5.4 Gel Electrophoresis and Western Blotting

Lyophilized A$\beta_{1\text{-}42}$ was dissolved in 1:1 DMSO/ddH_2O to obtain a stock solution with a concentration of approximately 250 µM. The A$\beta_{1\text{-}42}$ stock solution was diluted to 25 µM in PBS (0.01 M, pH 7.4) then incubated at 37 ℃ with continuous agitation at 200 rpm to form aggregates in the presence of activated and non-activated Ru(II) complexes. For the first set of experiments the peptide was incubated for a total of 24 h, in the presence of different concentrations of Ru(II) complexes (0.10, 0.25, 0.50, 1.0, 1.5, and 2.0 eq.). For the second

set of experiments, 1.0 eq. of Ru(II) complexes was also incubated for a total of 24 h, but aliquots were collect at different time points (0 h and 24 h). Electrophoresis separation of peptide aggregates was completed using 8-16% Mini-PROTEAN®TGX Precast Gels from Bio-Rad, at 100 V for 100 min in running buffer (25 mM Tris, 192 mM glycine, 0.1% SDS). The gels were then transferred to a nitrocellulose membrane for 1 h at 100 V at 4 ℃, followed by blocking of the membrane in a 3% BSA solution in Tris-buffered saline (TBS) (0.02 M Tris, 0.15 M NaCl, 0.003 M KCl) for 1 h. The membrane was incubated in a solution (1:2000 dilution) with a primary antibody that recognizes Aβ, 6E10, (Biolegends) overnight. After washing 5 x 5 min with TBS, the membrane was incubated in a solution containing the secondary antibody (Horseradish peroxidase, Caymen Chemicals) for 3 h. A Thermo Scientific SuperSignal®West Pico Chemiluminescent Substrate kit was used to visualize the Aβ species using a Bio-Rad ChemiDoc™MP imaging system.

2.5.5 Transmission Electron Microscopy (TEM)

TEM grids were prepared from the 1:1 Ru(II)/Aβ samples from the Western blot assay after 0 h and 24 h incubation for the monomeric form of $A\beta_{1\text{-}42}$ and 0 h and 24 h incubation at 37 ℃ after 96 hours of peptide incubation for the fibrillar form of $A\beta_{1\text{-}42}$. TEM grids were prepared following previously reported methods.[192,298] In order to increase hydrophilicity of the Ultrathin Carbon Film 400-mesh grids (Ted Pella), the grids were glow discharged in a vacuum for 10 seconds. Drops of samples (10 µL) were placed onto a sheet of parafilm and the TEM grid was placed on the drop for 5 min. The grid was then placed on top of syringe-filtered 5% uranyl acetate for 1 min. Excess uranyl acetate was removed using a tissue between drops. The grid was allowed to air-dry for at least 15 min. Bright field images were obtained on a FEI Tecnai Osiris STEM at 200 kV.

2.5.6 Binding Constant (K_d)

$A\beta_{1\text{-}42}$ film was dissolved in 1:1 DMSO/ddH_2O, and the stock solution was diluted to a final concentration of 10 µM in PBS (0.01 M, pH 7.4) buffered solution and incubated for a period of 96 h at 200 rpm at 37 ℃. The Aβ solution was titrated with the Ru(II) complexes (0.10, 0.25, 0.50, 0.75, 1.0, 1.25, 1.5, and 2.0 eq.) and the fluorescence intensity was measured ($\lambda_{ex}/\lambda_{em} = 275/310$ nm). The plot was obtained using the Sigma Plot software and dissociation constants were determined using a reported method.[251]

2.5.7 BCA Assay

$A\beta_{1\text{-}42}$ (60 µM) was incubated in PBS buffer (0.01 M, pH 7.4) with and without the Ru(II) complexes (1 eq.) for a period of 24 h for the BCA assay. The samples were centrifuged at 14,000 g for 5 min., and aliquots were taken at 0 h and kept in the freezer. In a 96 well plate, 20 µL of solution were added in triplicate for each time point, and 200 µL of working reagent from the Thermo Fisher BCA Protein Assay® kit was added to each well. The plate was then incubated for 30 min. at 37 ℃, and the concentration of peptide in the supernatant was analyzed by measuring the absorbance at 562 nm.

2.5.8 Docking

For the docking analysis, the protein was protonated using the Protonate3D algorithm in the Born solvation model, using the Lennard-Jones 12-6 potential, and dielectric constants of 78.6 and 4 for bulk solvent and the protein, respectively. The entirety of the cleft was sampled during docking using MOE's Site Finder panel. For each ligand, 10,000 initial binding poses were generated, with grid-based energy minimization (GRIDMIN). The London_dG scoring function was used to select the best 300 poses for MMFF94x minimization (RMSG=0.001, 9 angstrom cutoff, no tethering, backbone atoms held fixed). Results were ranked based on the London_dG scoring function. For the docking analysis of all three complexes, the Λ isomers were used.

2.5.9 Synthesis of $Ru(bpy)_2CO_3$

$Ru(bpy)_2CO_3$ was prepared flowing a synthetic route described in the literature.[287] The commercially available $[Ru(bpy)_2Cl_2]$ complex was used as a precursor. $[Ru(bpy)_2Cl_2]$ (0.5 g) was suspended in 37.5 mL of ultra-pure water at heated at reflux for 15 min under N_2 atmosphere. Sodium carbonate (1.65 g) was added to the solution and heated under the previous conditions for 2 h. The solution was filtered, yielding purple, needle-shaped crystals, which were washed 3 times with water and air-dried.

Chapter 3

Ongoing and Future Directions

3.1 Thesis Summary

Alzheimer's Disease (AD) is a progressive neurodegenerative disorder that accounts for approximately two-thirds of dementia cases worldwide.[299] Despite the great effort to develop an effective treatment, currently available therapeutics are only capable of minimizing the effects of the disease.[21,22] AD is characterized by the presence of extracellular deposits of amyloid beta (Aβ) plaques in the brain and targeting the aggregation pathway of Aβ could lead to new therapeutics for this disease.[35] Many research groups have investigated metal complexes that interact with Aβ and are able to modify its aggregation process.[44,228] This thesis outlines the interaction of three Ru(II) polypyridyl complexes (**Ru1-3**) with the Aβ peptide, and demonstrates that photoactivation of **Ru1-3** with visible light enables the Ru(II) complexes to covalently bind to Aβ, promoting changes in peptide aggregation. Unactivated samples did not exhibit any indication of Ru(II) – Aβ adduct formation, or modification in the size distribution and morphology of peptide aggregates. Interestingly, ^{1}H NMR for the photoactivated samples indicated the involvement of His residues in the adducts formed for **Ru1-2**, while no His residue shifts were observed for **Ru3**, even though ESI-MS detected adducts for all three photoactivated samples. While **Ru1-2** were able to promote changes in monomeric and fibrillar peptide immediately after photoactivation, **Ru3** needed longer incubation periods to promote similar changes. We hypothesize that the interaction between photoactivated **Ru1-2** and Aβ is enhanced by the extended phenanthroline ligand, which is not present in **Ru3**. While performing this study, new ideas and directions have emerged, and the proposed experiments in this chapter will provide further insight into the interaction of **Ru1-3** with the Aβ peptide.

3.2 Quantification of Ru(II) polypyridyl complexes by ICP-MS

The interaction of **Ru1-3** with the Aβ peptide were investigated in Chapter 2 and it was shown that the photoactivated complexes are able to covalently bind to Aβ and lead to the formation of large amorphous aggregates, either by interacting with monomeric peptide or mature fibrils. In 1990, Tothill *et al.* first described the use of inductively coupled plasma mass spectrometry (ICP-MS) for the analysis of Pt(II) anticancer agents in the blood and urine of rats.[300] Since this publication, ICP-MS has become a popular method for the analysis of metal-based anticancer drugs, and it has been applied for the analysis of Pt and Ru complexes, resulting in an increasing number of publications related to the quantitative analysis of these complexes in the past 20 years.[301] ICP-MS is a highly sensitive technique that can be applied in a wide range of areas, including biological and environmental samples, allowing for the determination of metal concentration in biological fluids, cells, and DNA- and protein adducts.[302,303]

Additional studies with **Ru1-3** could include the quantification of the Ru-Aβ adducts upon photoactivation by ICP-MS. Since photoactivation results in the formation of insoluble amorphous aggregates, it is possible to isolate the aggregates through centrifugation,[266,267] perform acid digestion[304] of the samples, and determine the percentage of Ru(II) that is present in the pellet and supernatant. Comparison of the percentages of Ru in the photoactivated and unactivated samples in the presence of monomeric (0 h and 24 h) and mature fibrils (0 h and 24 h) will lead to be a better understanding of the interaction of the Ru(II) complexes and Aβ, and changes upon light exposure. For the photoactivated samples, the majority of Ru is expected to be present in the pellet, since the photoactivated complexes promote the formation of large insoluble aggregates immediately after activation for **Ru1-2**, and over time for **Ru3**.

3.3 Cytotoxicity and Cell viability

The neurotoxicity of Aβ, especially $A\beta_{1\text{-}42}$, has been reported in several studies,[305–307] and the peptide has been linked to disruption of synapses,[308,309] oxidative stress,[71,310,311] and dysregulation of metal ion homeostasis.[312,313] Differentiated SH-SY5Y cells can be used to determine if **Ru1-3** are able to limit the cytotoxicity caused by $A\beta_{1\text{-}42}$. SH-SY5Y was subcloned three times from the human cell line SK-N-NK and expresses neuron-like characteristics.[314,315] Cell studies could be performed in triplicate in 96-well flat bottom plates, and differentiated cells would first be treated with varying concentrations of **Ru1-3** to determine the half maximal lethal dose (LD_{50}) of the Ru(II) complexes. The samples

will be submitted to dark and light (photoactivation) treatments, and cell viability will be determined after 24 h of incubation at 37 ℃. LD_{50} for the cytotoxicity (dark) and photocytotoxicity (light) will be calculated from the dose-response curves.[143] These results will provide information on the dark / light metal complex cytotoxicity, and provide the range of concentrations to be used in the presence of peptide.

It is reported that pre-formed $A\beta_{1\text{-}42}$ oligomers, or those formed in situ, show concentration dependent toxicity to SH-SY5Y cells,[316] and that exposure of these cells to $A\beta_{1\text{-}42}$ results in a significant decrease in cell viability.[317,318] Unactivated and photoactivated samples with different concentrations of **Ru1-3** and monomeric $A\beta_{1\text{-}42}$ will be added to wells containing differentiated SH-SY5Y cells. As a control, $A\beta_{1\text{-}42}$ with the same volume of DMSO used to prepare the stock solution of Ru(II) complexes will also be added to these samples. Samples will be exposed to dark and light treatments prior to incubation at 37 ℃. The cell viability results will show if the presence of activated **Ru1-3** complexes restores cell viability in comparison to unactivated complexes or samples containing only $A\beta_{1\text{-}42}$.

3.4 Ru-Peptide interactions *via* 2-D ^{1}H-^{15}N SOFAST-HMQC NMR

Interactions of proteins with other molecules is essentially what defines protein function.[319] Such interactions are not only involved in biological processes but are the key events of external modulation of proteins.[320,321] NMR spectroscopy is a very efficient technique used to obtain information about the interaction of proteins and other molecules at atomic resolution.[322,323] In this scenario, ^{1}H-^{15}N correlation spectra serve as a tool to elucidate the effects of a molecule on the protein structure. Since this technique provides one correlation peak per amino acid, it is often used to resolve most of the signals corresponding to individual residues along the peptide chain.[324] Therefore, ^{1}H-^{15}N correlation spectra can be used to follow spectral changes in the peptide chain upon interaction with other molecules. However, 2-D NMR studies on peptides and proteins is time consuming and can take hours, which exclude many phenomena in solution that may occur on a short time-scale.[325] In order to overcome this issue, 2-D band-selective optimized flip-angle short transient heteronuclear multiple quantum correlation (SOFAST-HMQC) NMR spectroscopy can be used.[264,326] A decrease in the time period between each scan is achieved by limiting the relaxation time of the system, which results in a decrease of inter-scan delays, allowing for data collection in a matter of minutes.[322] I propose that 2-D ^{1}H-^{15}N SOFAST-HMQC NMR spectroscopy could be used to obtain information about the interaction of **Ru1-3** with monomeric Aβ. This technique has been previously used by the Storr group,[264] and others,[327] to investigate small molecule-Aβ peptide interactions. $A\beta_{1\text{-}40}$, the peptide length that is the least prone to aggregation (in comparison to $A\beta_{1\text{-}42}$),[328] will be used in order to

limit aggregation during data collection and ensure that all shifts result from the interaction between peptide and Ru(II) complexes instead of peptide aggregation. The ^{15}N-labeled A$\beta_{1\text{-}40}$ samples will be treated with **Ru1-3** and the samples will be exposed to light and dark treatments. It is expected that the unactivated samples will show some chemical shift perturbations (CSPs) compared to the peptide alone, and we hypothesize that these CSPs will occur in the self-recognition site (Leu^{17}-Ala^{21}) responsible for the initiation of peptide aggregation. The results are also expected to support the 1-D ^{1}H NMR data that showed the involvement of His residues in the binding of photoactivated **Ru1-2** to Aβ and elucidate if any other residues are involved in the binding to photoactivated **Ru3**.

Bibliography

[1] D. J. Bonda, H. G. Lee, J. A. Blair, X. Zhu, G. Perry and M. A. Smith, *Metallomics*, 2011, **3**, 267–70.

[2] M. H. Baig, K. Ahmad, G. Rabbani and I. Choi, *Front. Aging Neurosci.*, 2018, **10**, 21–27.

[3] R. U. Haque and A. I. Levey, *Proc. Natl. Acad. Sci. USA*, 2019, **116**, 26224–26229.

[4] A. D. International, *Dementia statistics*, `https://www.alz.co.uk/research/statistics`, 2017, [Online; accessed March 24th, 2020].

[5] C. Patterson, *Aust. Prescr.*, 2018, **41**, 176–177.

[6] V. H. Finder, *J. Alzheimers Dis.*, 2010, **22**, 5–19.

[7] L. E. Hebert, J. Weuve, P. A. Scherr and D. A. Evans, *Neurology*, 2013, **80**, 1778–83.

[8] D. J. Selkoe, *Nat. Med.*, 2011, **17**, 1060–5.

[9] H. Hippius and G. Neundorfer, *Dialogues Clin. Neurosci.*, 2003, **5**, 101–8.

[10] N. S. Ryan, M. N. Rossor and N. C. Fox, *Brain*, 2015, **138**, 3816–3821.

[11] A. Atri, *Semin. Neurol.*, 2019, **39**, 227–240.

[12] K. G. Yiannopoulou and S. G. Papageorgiou, *Ther. Adv. Neurol. Disord.*, 2013, **6**, 19–33.

[13] M. A. DeTure and D. W. Dickson, *Mol. Neurodegener.*, 2019, **14**, 32–50.

[14] F. M. Elahi and B. L. Miller, *Nat. Rev. Neurol.*, 2017, **13**, 457–476.

[15] L. V. Fulton, D. Dolezel, J. Harrop, Y. Yan and C. P. Fulton, *Brain Sci.*, 2019, **9**, 212–228.

[16] H. W. Querfurth and F. M. LaFerla, *New Engl. J. Med.*, 2010, **362**, 329–44.

[17] D. J. Selkoe, *Neuron*, 1991, **6**, 487–98.

[18] G. Liu, M. R. Garrett, P. Men, X. Zhu, G. Perry and M. A. Smith, *Biochim. Biophys. Acta*, 2005, **1741**, 246–52.

[19] M. Pohanka, *Curr. Med. Chem.*, 2014, **21**, 356–64.

[20] J. Y. Szeto and S. J. Lewis, *Curr. Neuropharmacol.*, 2016, **14**, 326–38.

[21] S. Agatonovic-Kustrin, C. Kettle and D. W. Morton, *Biomed. Pharmacother.*, 2018, **106**, 553–565.

[22] S. Habtemariam, *Molecules*, 2019, **24**, 1519–1536.

[23] J. Cummings, G. Lee, A. Ritter, M. Sabbagh and K. Zhong, *Alzheimers Dement. (NY)*, 2019, **5**, 272–293.

[24] M. N. Sabbagh, S. Hendrix and J. E. Harrison, *Alzheimers Dement. (NY)*, 2019, **5**, 13–19.

[25] J. Cummings, P. S. Aisen, B. DuBois, L. Frolich, J. Jack, C. R., R. W. Jones, J. C. Morris, J. Raskin, S. A. Dowsett and P. Scheltens, *Alzheimers Res. Ther.*, 2016, **8**, 39.

[26] K. Gadhave, B. R. Gehi, P. Kumar, B. Xue, V. N. Uversky and R. Giri, *Cell. Mol. Life Sci.*, 2020, 1–46.

[27] E. Mezeiova, K. Chalupova, E. Nepovimova, L. Gorecki, L. Prchal, D. Malinak, K. Kuca, O. Soukup and J. Korabecny, *Curr. Alzheimer Res.*, 2019, **16**, 772–800.

[28] D. J. Selkoe and J. Hardy, *EMBO Mol. Med.*, 2016, **8**, 595–608.

[29] A. Abbott, *Nature*, 2008, **456**, 161–4.

[30] R. J. O'Brien and P. C. Wong, *Annu. Rev. Neurosci.*, 2011, **34**, 185–204.

[31] M. Korte, *Science*, 2019, **363**, 123–124.

[32] C. A. McLean, R. A. Cherny, F. W. Fraser, S. J. Fuller, M. J. Smith, K. Beyreuther, A. I. Bush and C. L. Masters, *Ann. Neurol.*, 1999, **46**, 860–6.

[33] M. P. Murphy and r. LeVine, H., *J. Alzheimers Dis.*, 2010, **19**, 311–23.

[34] S. Sadigh-Eteghad, B. Sabermarouf, A. Majdi, M. Talebi, M. Farhoudi and J. Mahmoudi, *Med. Princ. Pract.*, 2015, **24**, 1–10.

[35] G. F. Chen, T. H. Xu, Y. Yan, Y. R. Zhou, Y. Jiang, K. Melcher and H. E. Xu, *Acta Pharmacol. Sin.*, 2017, **38**, 1205–1235.

[36] K. Pauwels, T. L. Williams, K. L. Morris, W. Jonckheere, A. Vandersteen, G. Kelly, J. Schymkowitz, F. Rousseau, A. Pastore, L. C. Serpell and K. Broersen, *J. Biol. Chem.*, 2012, **287**, 5650–60.

[37] D. M. Vadukul, O. Gbajumo, K. E. Marshall and L. C. Serpell, *FEBS Lett.*, 2017, **591**, 822–830.

[38] F. Kametani and M. Hasegawa, *Front. Neurosci.*, 2018, **12**, 25–36.

[39] H. M. Lanoiselee, G. Nicolas, D. Wallon, A. Rovelet-Lecrux, M. Lacour, S. Rousseau, A. C. Richard, F. Pasquier, A. Rollin-Sillaire, O. Martinaud, M. Quillard-Muraine, V. de la Sayette, C. Boutoleau-Bretonniere, F. Etcharry-Bouyx, V. Chauvire, M. Sarazin, I. le Ber, S. Epelbaum, T. Jonveaux, O. Rouaud, M. Ceccaldi, O. Felician, O. Godefroy, M. Formaglio, B. Croisile, S. Auriacombe, L. Chamard, J. L. Vincent, M. Sauvee, C. Marelli-Tosi, A. Gabelle, C. Ozsancak, J. Pariente, C. Paquet, D. Hannequin, D. Campion and C. J. p. collaborators of the, *PLoS Med.*, 2017, **14**, e1002270.

[40] S. Thordardottir, A. Kinhult Stahlbom, O. Almkvist, H. Thonberg, M. Eriksdotter, H. Zetterberg, K. Blennow and C. Graff, *Alzheimers Res. Ther.*, 2017, **9**, 9–19.

[41] H. M. Brothers, M. L. Gosztyla and S. R. Robinson, *Front. Aging Neurosci.*, 2018, **10**, 118–134.

[42] M. T. Colvin, R. Silvers, Q. Z. Ni, T. V. Can, I. Sergeyev, M. Rosay, K. J. Donovan, B. Michael, J. Wall, S. Linse and R. G. Griffin, *J. Am. Chem. Soc.*, 2016, **138**, 9663–74.

[43] R. Roychaudhuri, M. Yang, M. M. Hoshi and D. B. Teplow, *J. Biol. Chem.*, 2009, **284**, 4749–53.

[44] J. M. Suh, G. Kim, J. Kang and M. H. Lim, *Inorg. Chem.*, 2019, **58**, 8–17.

[45] M. A. Wälti, F. Ravotti, H. Arai, C. G. Glabe, J. S. Wall, A. Böckmann, P. Güntert, B. H. Meier and R. Riek, *Proc. Natl. Acad. Sci. U. S. A.*, 2016, **113**, 4976–4984.

[46] M. Yang and D. B. Teplow, *J. Mol. Biol.*, 2008, **384**, 450–64.

[47] S. Lesne, M. T. Koh, L. Kotilinek, R. Kayed, C. G. Glabe, A. Yang, M. Gallagher and K. H. Ashe, *Nature*, 2006, **440**, 352–7.

[48] A. R. Upadhaya, I. Lungrin, H. Yamaguchi, M. Fandrich and D. R. Thal, *J. Cell. Mol. Med.*, 2012, **16**, 287–95.

[49] M. Sakono and T. Zako, *FEBS J.*, 2010, **277**, 1348–58.

[50] U. Sengupta, A. N. Nilson and R. Kayed, *EBioMedicine*, 2016, **6**, 42–49.

[51] A. D. Watt, V. L. Villemagne and K. J. Barnham, *J. Alzheimers Dis.*, 2013, **33**, 283–93.

[52] R. Squitti, *Front. Biosci.*, 2012, **17**, 451–72.

[53] S. Arbor, *Neural. Regen. Res.*, 2017, **12**, 207–209.

[54] C. Overk and E. Masliah, *Brain*, 2019, **142**, 1853–1855.

[55] S.-K. Park, S. D. Pegan, A. D. Mesecar, L. M. Jungbauer, M. J. LaDu and S. W. Liebman, *Dis. Model. Mech.*, 2011, **4**, 822–831.

[56] M. Gold, *Alzheimers Dement. (NY)*, 2017, **3**, 402–409.

[57] L. K. Huang, S. P. Chao and C. J. Hu, *J. Biomed. Sci.*, 2020, **27**, 18–31.

[58] K. Ritchie, C. W. Ritchie, K. Yaffe, I. Skoog and N. Scarmeas, *Alzheimers Dement. (NY)*, 2015, **1**, 122–130.

[59] R. Gonzalez-Dominguez, T. Garcia-Barrera and J. L. Gomez-Ariza, *Biometals*, 2014, **27**, 539–49.

[60] S. K. T. S. Wärmländer, N. Österlund, C. Wallin, J. Wu, J. Luo, A. Tiiman, J. Jarvet and A. Gräslund, *J. Biol. Inorg. Chem.*, 2019, **24**, 1189–1196.

[61] A. C. Kim, S. Lim and Y. K. Kim, *Int. J. Mol. Sci.*, 2018, **19**, 128–143.

[62] P. Faller and C. Hureau, *Dalton Trans.*, 2009, **41**, 1080–94.

[63] K. P. Kepp, *Chem. Rev.*, 2012, **112**, 5193–239.

[64] M. A. Lovell, J. D. Robertson, W. J. Teesdale, J. L. Campbell and W. R. Markesbery, *J. Neurol. Sci.*, 1998, **158**, 47–52.

[65] L. M. Miller, Q. Wang, T. P. Telivala, R. J. Smith, A. Lanzirotti and J. Miklossy, *J. Struct. Biol.*, 2006, **155**, 30–7.

[66] A. S. Pithadia, A. Kochi, M. T. Soper, M. W. Beck, Y. Liu, S. Lee, A. S. DeToma, B. T. Ruotolo and M. H. Lim, *Inorg. Chem.*, 2012, **51**, 12959–67.

[67] M. G. Savelieff, A. S. DeToma, J. S. Derrick and M. H. Lim, *Acc. Chem. Res.*, 2014, **47**, 2475–82.

[68] R. Squitti, *Front. Biosci.*, 2012, **17**, 451–72.

[69] Y. Li, Q. Jiao, H. Xu, X. Du, L. Shi, F. Jia and H. Jiang, *Front. Mol. Neurosci.*, 2017, **10**, 339–357.

[70] B. Alies, A. Conte-Daban, S. Sayen, F. Collin, I. Kieffer, E. Guillon, P. Faller and C. Hureau, *Inorg. Chem.*, 2016, **55**, 10499–10509.

[71] C. Cheignon, M. Tomas, D. Bonnefont-Rousselot, P. Faller, C. Hureau and F. Collin, *Redox. Biol.*, 2018, **14**, 450–464.

[72] F. Hane and Z. Leonenko, *Biomolecules*, 2014, **4**, 101–16.

[73] L. Q. Hatcher, L. Hong, W. D. Bush, T. Carducci and J. D. Simon, *J. Phys. Chem. B*, 2008, **112**, 8160–4.

[74] M. C. Heffern, P. T. Velasco, L. M. Matosziuk, J. L. Coomes, C. Karras, M. A. Ratner, W. L. Klein, A. L. Eckermann and T. J. Meade, *Chembiochem*, 2014, **15**, 1584–9.

[75] K. P. Kepp, *J. Alzheimers Dis.*, 2017, **55**, 447–457.

[76] V. Wineman-Fisher and Y. Miller, *Phys. Chem. Chem. Phys.*, 2016, **18**, 21590–9.

[77] Y. Miller, B. Ma, C. J. Tsai and R. Nussinov, *Proc. Natl. Acad. Sci. U. S. A.*, 2010, **107**, 14128–33.

[78] Y. Miller, B. Ma and R. Nussinov, *Coord. Chem. Rev.*, 2012, **256**, 2245–2252.

[79] S. Parthasarathy, F. Long, Y. Miller, Y. Xiao, D. McElheny, K. Thurber, B. Ma, R. Nussinov and Y. Ishii, *J. Am. Chem. Soc.*, 2011, **133**, 3390–400.

[80] V. Wineman-Fisher, D. N. Bloch and Y. Miller, *Coord. Chem. Rev.*, 2016, **327-328**, 20–26.

[81] P. Faller, C. Hureau and O. Berthoumieu, *Inorg. Chem.*, 2013, **52**, 12193–206.

[82] Y. Liu, M. Nguyen, A. Robert and B. Meunier, *Acc. Chem. Res.*, 2019, **52**, 2026–2035.

[83] J. S. Cristovao, R. Santos and C. M. Gomes, *Oxid. Med. Cell. Longev.*, 2016, **2016**, 9812178–9812178.

[84] M. A. Greenough, J. Camakaris and A. I. Bush, *Neurochem. Int.*, 2013, **62**, 540–55.

[85] W. J. Huang, X. Zhang and W. W. Chen, *Biomed. Rep.*, 2016, **4**, 519–522.

[86] E. L. Sampson, L. Jenagaratnam and R. McShane, *Cochrane Database Syst. Rev.*, 2012, **5**, 5380–5403.

[87] D. R. McLachlan, W. L. Smith and T. P. Kruck, *Ther. Drug Monit.*, 1993, **15**, 602–7.

[88] D. R. Crapper McLachlan, A. J. Dalton, T. P. Kruck, M. Y. Bell, W. L. Smith, W. Kalow and D. F. Andrews, *Lancet*, 1991, **337**, 1304–8.

[89] C. Treiber, A. Simons, M. Strauss, M. Hafner, R. Cappai, T. A. Bayer and G. Multhaup, *J. Biol. Chem.*, 2004, **279**, 51958–64.

[90] V. Moret, Y. Laras, N. Pietrancosta, C. Garino, G. Quelever, A. Rolland, B. Mallet, J. C. Norreel and J. L. Kraus, *Bioorg. Med. Chem. Lett.*, 2006, **16**, 3298–301.

[91] P. A. Adlard, R. A. Cherny, D. I. Finkelstein, E. Gautier, E. Robb, M. Cortes, I. Volitakis, X. Liu, J. P. Smith, K. Perez, K. Laughton, Q.-X. Li, S. A. Charman, J. A. Nicolazzo, S. Wilkins, K. Deleva, T. Lynch, G. Kok, C. W. Ritchie, R. E. Tanzi, R. Cappai, C. L. Masters, K. J. Barnham and A. I. Bush, *Neuron*, 2008, **59**, 43–55.

[92] S. C. Drew, *Front. Neurosci.*, 2017, **11**, 317–328.

[93] V. L. Villemagne, C. C. Rowe, K. J. Barnham, R. Cherny, M. Woodward, S. Bozinosvski, O. Salvado, P. Bourgeat, K. Perez, C. Fowler, A. Rembach, P. Maruff, C. Ritchie, R. Tanzi and C. L. Masters, *Alzheimers Dement. (NY)*, 2017, **3**, 622–635.

[94] Z. Chen and C. Zhong, *Neurosci. Bull.*, 2014, **30**, 271–81.

[95] E. Shohami, E. Beit-Yannai, M. Horowitz and R. Kohen, *J. Cerebr. Blood F. Met.*, 1997, **17**, 1007–19.

[96] D. A. Butterfield, A. M. Swomley and R. Sultana, *Antioxid. Redox Sign.*, 2013, **19**, 823–35.

[97] L. Zuo, B. T. Hemmelgarn, C. C. Chuang and T. M. Best, *Oxid. Med. Cell. Longev.*, 2015, **2015**, 604658–604671.

[98] X. Du, X. Wang and M. Geng, *Transl. Neurodegener.*, 2018, **7**, 2–9.

[99] P.-P. Liu, Y. Xie, X.-Y. Meng and J.-S. Kang, *Signal Transduct. Tar.*, 2019, **4**, 29–51.

[100] N. Robinson, P. Grabowski and I. Rehman, *Mech. Ageing Dev.*, 2018, **174**, 86–94.

[101] H. Li, C.-C. Liu, H. Zheng and T. Y. Huang, *Transl. Neurodegener.*, 2018, **7**, 34–50.

[102] R. B. Maccioni, G. Farias, I. Morales and L. Navarrete, *Arch. Med. Res.*, 2010, **41**, 226–31.

[103] S. H. Barage and K. D. Sonawane, *Neuropeptides*, 2015, **52**, 1–18.

[104] S. Ahmadi, S. Zhu, R. Sharma, D. J. Wilson and H. B. Kraatz, *J. Inorg. Biochem.*, 2019, **194**, 44–51.

[105] S. Ahmadi, S. Zhu, R. Sharma, B. Wu, R. Soong, R. Dutta Majumdar, D. J. Wilson, A. J. Simpson and H. B. Kraatz, *ACS Omega*, 2019, **4**, 5356–5366.

[106] M. Llorens-Marítin, J. Jurado, F. Hernández and J. Ávila, *Front. Mol. Neurosci.*, 2014, **7**, 46–57.

[107] J. Maja, B. Mirjana, P. Nela, H. Patrick and S. Goran, *Transl. Neurosci.*, 2013, **4**, 466–476.

[108] D. X. Medina, A. Caccamo and S. Oddo, *Brain Pathol.*, 2011, **21**, 140–9.

[109] C. M. Wischik, P. C. Edwards, R. Y. Lai, M. Roth and C. R. Harrington, *Proc. Natl. Acad. Sci. USA*, 1996, **93**, 11213–8.

[110] M. Petukh and E. Alexov, *Asian J .Phys.*, 2014, **23**, 735–744.

[111] D. Gaynor and D. M. Griffith, *Dalton Trans.*, 2012, **41**, 13239–57.

[112] C. Orvig and M. J. Abrams, *Chem. Rev.*, 1999, **99**, 2201–4.

[113] F. Bosch and L. Rosich, *Pharmacology*, 2008, **82**, 171–9.

[114] R. S. Schwartz, *New Engl. J. Med.*, 2004, **350**, 1079–80.

[115] B. Rosenberg, L. Vancamp and T. Krigas, *Nature*, 1965, **205**, 698–9.

[116] K. J. Franz and N. Metzler-Nolte, *Chem. Rev.*, 2019, **119**, 727–729.

[117] M. Varol, *J. Appl. Pharm.*, 2016, **8**, 1–2.

[118] G. Eperon, M. Balasegaram, J. Potet, C. Mowbray, O. Valverde and F. Chappuis, *Expert Rev. Anti Infect. Ther.*, 2014, **12**, 1407–17.

[119] B. Bertrand and A. Casini, *Dalton Trans.*, 2014, **43**, 4209–19.

[120] S. Medici, M. Peana, V. Nurchi, J. Lachowicz, G. Crisponi and M. Zoroddu, *Coord. Chem. Rev.*, 2014, **284**, 329–350.

[121] K. D. Mjos and C. Orvig, *Chem. Rev.*, 2014, **114**, 4540–63.

[122] C. C. Society, *C. C. Society, Cancer Statistics at a Glance*, `https://www.cancer.ca/en/cancer-information/cancer-101/cancer-statistics-at-a-glance`, 2020, [Online; accessed January 30th, 2020].

[123] D. R. Brenner, H. K. Weir, A. A. Demers, L. F. Ellison, C. Louzado, A. Shaw, D. Turner, R. R. Woods, L. M. Smith and C. Canadian Cancer Statistics Advisory, *Can. Med. Assoc. J.*, 2020, **192**, 199–205.

[124] L. Zeng, P. Gupta, Y. Chen, E. Wang, L. Ji, H. Chao and Z. S. Chen, *Chem. Soc. Rev.*, 2017, **46**, 5771–5804.

[125] J. Spencer and B. Walden, *Future Med. Chem.*, 2018, **10**, 607–609.

[126] V. Volarevic, B. Djokovic, M. G. Jankovic, C. R. Harrell, C. Fellabaum, V. Djonov and N. Arsenijevic, *J. Biomed. Sci.*, 2019, **26**, 25–39.

[127] U. Ndagi, N. Mhlongo and M. E. Soliman, *Drug Des. Devel. Ther.*, 2017, **11**, 599–616.

[128] K. Lin, Z. Z. Zhao, H. B. Bo, X. J. Hao and J. Q. Wang, *Front. Pharmacol.*, 2018, **9**, 1323–1333.

[129] E. Alessio and L. Messori, *Molecules*, 2019, **24**, 1549–1560.

[130] W. Cao, W. Zheng and T. Chen, *Sci. Rep.*, 2015, **5**, 9157–9168.

[131] M. Debidda, B. Sanna, A. Cossu, A. M. Posadino, B. Tadolini, C. Ventura and G. Pintus, *Int. J. Oncol.*, 2003, **23**, 477–82.

[132] S. W. Chang, A. R. Lewis, K. E. Prosser, J. R. Thompson, M. Gladkikh, M. B. Bally, J. J. Warren and C. J. Walsby, *Inorg. Chem.*, 2016, **55**, 4850–63.

[133] M. I. Webb, B. Wu, T. Jang, R. A. Chard, E. W. Wong, M. Q. Wong, D. T. Yapp and C. J. Walsby, *Chemistry*, 2013, **19**, 17031–42.

[134] C. G. Hartinger, M. Groessl, S. M. Meier, A. Casini and P. J. Dyson, *Chem. Soc. Rev.*, 2013, **42**, 6186–99.

[135] C. G. Hartinger, M. A. Jakupec, S. Zorbas-Seifried, M. Groessl, A. Egger, W. Berger, H. Zorbas, P. J. Dyson and B. K. Keppler, *Chem. Biodivers.*, 2008, **5**, 2140–55.

[136] D. Wernitznig, K. Kiakos, G. Del Favero, N. Harrer, H. Machat, A. Osswald, M. A. Jakupec, A. Wernitznig, W. Sommergruber and B. K. Keppler, *Metallomics*, 2019, **11**, 1044–1048.

[137] D. A. Smithen, H. Yin, M. H. Beh, M. Hetu, T. S. Cameron, S. A. McFarland and A. Thompson, *Inorg. Chem.*, 2017, **56**, 4121–4132.

[138] T. Mede, M. Jager and U. S. Schubert, *Chem. Soc. Rev.*, 2018, **47**, 7577–7627.

[139] F. E. Poynton, S. A. Bright, S. Blasco, D. C. Williams, J. M. Kelly and T. Gunnlaugsson, *Chem. Soc. Rev.*, 2017, **46**, 7706–7756.

[140] F. Heinemann, J. Karges and G. Gasser, *Acc. Chem. Res.*, 2017, **50**, 2727–2736.

[141] B. S. Howerton, D. K. Heidary and E. C. Glazer, *J. Am. Chem. Soc.*, 2012, **134**, 8324–7.

[142] M. Vonlanthen, A. Cevallos, E. Aguilar-Ortíz, A. Ruiu, P. Porcu and E. Rivera, *Polymer*, 2016, **99**, 13–20.

[143] T. Sainuddin, M. Pinto, H. Yin, M. Hetu, J. Colpitts and S. A. McFarland, *J. Inorg. Biochem.*, 2016, **158**, 45–54.

[144] F. D. Abreu, T. F. Paulo, M. H. Gehlen, R. A. Ando, L. G. F. Lopes, A. C. S. Gondim, M. A. Vasconcelos, E. H. Teixeira, E. H. S. Sousa and I. M. M. de Carvalho, *Inorg. Chem.*, 2017, **56**, 9084–9096.

[145] H. Guo, L. Zhu, C. Dang, J. Zhao and B. Dick, *Phys. Chem. Chem. Phys.*, 2018, **20**, 17504–17516.

[146] E. Baranoff, J. P. Collin, J. Furusho, Y. Furusho, A. C. Laemmel and J. P. Sauvage, *Inorg. Chem.*, 2002, **41**, 1215–22.

[147] L. Kohler, L. Nease, P. Vo, J. Garofolo, D. K. Heidary, R. P. Thummel and E. C. Glazer, *Inorg. Chem.*, 2017, **56**, 12214–12223.

[148] P. Mobian, J. M. Kern and J. P. Sauvage, *Angew. Chem. Int. Ed.*, 2004, **43**, 2392–5.

[149] E. Wachter, D. K. Heidary, B. S. Howerton, S. Parkin and E. C. Glazer, *Chem. Commun.*, 2012, **48**, 9649–51.

[150] Y. A. Fouad and C. Aanei, *Am. J. Cancer Res.*, 2017, **7**, 1016–1036.

[151] M. R. Gill and J. A. Thomas, *Chem. Soc. Rev.*, 2012, **41**, 3179–92.

[152] M. B. Kastan and J. Bartek, *Nature*, 2004, **432**, 316–23.

[153] Y. Yang, Z. Liu, C. P. Selby and A. Sancar, *J. Biol. Chem.*, 2019, **294**, 11960–11968.

[154] C. R. R. Rocha, M. M. Silva, A. Quinet, J. B. Cabral-Neto and C. F. M. Menck, *Clinics (Sao Paulo)*, 2018, **73**, e478s.

[155] A. Mihailovic, I. Vladescu, M. McCauley, E. Ly, M. C. Williams, E. M. Spain and M. E. Nuñez, *Langmuir*, 2006, **22**, 4699–4709.

[156] A. E. Friedman, J. C. Chambron, J. P. Sauvage, N. J. Turro and J. K. Barton, *J. Am. Chem. Soc.*, 1990, **112**, 4960–4962.

[157] J. P. Hall, P. M. Keane, H. Beer, K. Buchner, G. Winter, T. L. Sorensen, D. J. Cardin, J. A. Brazier and C. J. Cardin, *Nucleic Acids Res.*, 2016, **44**, 9472–9482.

[158] A. Mihailovic, I. Vladescu, M. McCauley, E. Ly, M. C. Williams, E. M. Spain and M. E. Nunez, *Langmuir*, 2006, **22**, 4699–709.

[159] K. J. Barnham, V. B. Kenche, G. D. Ciccotosto, D. P. Smith, D. J. Tew, X. Liu, K. Perez, G. A. Cranston, T. J. Johanssen, I. Volitakis, A. I. Bush, C. L. Masters, A. R. White, J. P. Smith, R. A. Cherny and R. Cappai, *Proc. Natl. Acad. Sci. USA*, 2008, **105**, 6813–8.

[160] F. Collin, I. Sasaki, H. Eury, P. Faller and C. Hureau, *Chem. Commun.*, 2013, **49**, 2130–2.

[161] I. Sasaki, C. Bijani, S. Ladeira, V. Bourdon, P. Faller and C. Hureau, *Dalton Trans.*, 2012, **41**, 6404–6407.

[162] D. Florio, A. M. Malfitano, S. Di Somma, C. Mugge, W. Weigand, G. Ferraro, I. Iacobucci, M. Monti, G. Morelli, A. Merlino and D. Marasco, *Int. J. Mol. Sci.*, 2019, **20**, 829–842.

[163] V. B. Kenche, L. W. Hung, K. Perez, I. Volitakes, G. Ciccotosto, J. Kwok, N. Critch, N. Sherratt, M. Cortes, V. Lal, C. L. Masters, K. Murakami, R. Cappai, P. A. Adlard and K. J. Barnham, *Angew. Chem. Int. Ed.*, 2013, **52**, 3374–8.

[164] H. Liu, Y. Qu and X. Wang, *Future Med. Chem.*, 2018, **10**, 679–701.

[165] V. A. Streltsov, V. Chandana Epa, S. A. James, Q. I. Churches, J. M. Caine, V. B. Kenche and K. J. Barnham, *Chem. Commun.*, 2013, **49**, 11364–6.

[166] S. Yao, R. A. Cherny, A. I. Bush, C. L. Masters and K. J. Barnham, *J. Pept. Sci.*, 2004, **10**, 210–7.

[167] B. Y.-W. Man, H.-M. Chan, C.-H. Leung, D. S.-H. Chan, L.-P. Bai, Z.-H. Jiang, H.-W. Li and D.-L. Ma, *Chem. Sci.*, 2011, **2**, 917–921.

[168] L. Lu, H. J. Zhong, M. Wang, S. L. Ho, H. W. Li, C. H. Leung and D. L. Ma, *Sci. Rep.*, 2015, **5**, 14619–14628.

[169] J. Kang, J. S. Nam, H. J. Lee, G. Nam, H. W. Rhee, T. H. Kwon and M. H. Lim, *Chem. Sci.*, 2019, **10**, 6855–6862.

[170] J. S. Derrick, J. Lee, S. J. Lee, Y. Kim, E. Nam, H. Tak, J. Kang, M. Lee, S. H. Kim, K. Park, J. Cho and M. H. Lim, *J. Am. Chem. Soc.*, 2017, **139**, 2234–2244.

[171] J. Suh, S. H. Yoo, M. G. Kim, K. Jeong, J. Y. Ahn, M.-s. Kim, P. S. Chae, T. Y. Lee, J. Lee, J. Lee, Y. A. Jang and E. H. Ko, *Angew. Chem. Int. Ed.*, 2007, **46**, 7064–7067.

[172] A. Aliyan, B. Kirby, C. Pennington and A. A. Marti, *J. Am. Chem. Soc.*, 2016, **138**, 8686–9.

[173] A. Aliyan, T. J. Paul, B. Jiang, C. Pennington, G. Sharma, R. Prabhakar and A. A. Martí, *Chem. Biodivers.*, 2017, **3**, 898–912.

[174] D. Pramanik and S. G. Dey, *J. Am. Chem. Soc.*, 2011, **133**, 81–87.

[175] C. Yuan and Z. Gao, *Chem. Res. Toxicol.*, 2013, **26**, 262–9.

[176] H. Atamna and K. Boyle, *Proc. Natl. Acad. Sci. USA*, 2006, **103**, 3381–6.

[177] H. Atamna and n. Frey, W. H., *Proc. Natl. Acad. Sci. USA*, 2004, **101**, 11153–8.

[178] D. Pramanik, C. Ghosh and S. G. Dey, *J. Am. Chem. Soc.*, 2011, **133**, 15545–52.

[179] V. Borghesani, B. Alies and C. Hureau, *Eur. J. Inorg. Chem.*, 2018, **2018**, 7–15.

[180] A. Henriksen, A. T. Smith and M. Gajhede, *J. Biol. Chem.*, 1999, **274**, 35005–11.

[181] J. N. Rodriguez-Lopez, A. T. Smith and R. N. Thorneley, *J. Biol. Chem.*, 1996, **271**, 4023–30.

[182] I. Pal, A. K. Nath, M. Roy, M. Seal, C. Ghosh, A. Dey and S. G. Dey, *Chem. Sci.*, 2019, **10**, 8405–8410.

[183] L. M. F. Gomes, A. Mahammed, K. E. Prosser, J. R. Smith, M. A. Silverman, C. J. Walsby, Z. Gross and T. Storr, *Chem. Sci.*, 2019, **10**, 1634–1643.

[184] M. Eckshtain, I. Zilbermann, A. Mahammed, I. Saltsman, Z. Okun, E. Maimon, H. Cohen, D. Meyerstein and Z. Gross, *Dalton Trans.*, 2009, **38**, 7879–82.

[185] A. Mahammed and Z. Gross, *J. Am. Chem. Soc.*, 2005, **127**, 2883–7.

[186] C. E. Alves de Souza, H. d. M. Alves de Souza, M. C. Stipp, C. R. Corso, C. M. Galindo, C. R. Cardoso, R. L. Dittrich, E. A. de Souza Ramos, G. Klassen, R. M. Carlos, S. M. S. Correia Cadena and A. Acco, *Free Rad. Biol. Med.*, 2017, **110**, 228–239.

[187] V. Brabec and O. Nováková, *Drug Resist. Updat.*, 2006, **9**, 111–122.

[188] M. Galanski, V. B. Arion, M. A. Jakupec and B. K. Keppler, *Curr. Pharm. Des.*, 2003, **9**, 2078–89.

[189] I. Kostova, *Curr. Med. Chem.*, 2006, **13**, 1085–107.

[190] D. Valensin, P. Anzini, E. Gaggelli, N. Gaggelli, G. Tamasi, R. Cini, C. Gabbiani, E. Michelucci, L. Messori, H. Kozlowski and G. Valensin, *Inorg. Chem.*, 2010, **49**, 4720–2.

[191] L. Messori, M. Camarri, T. Ferraro, C. Gabbiani and D. Franceschini, *ACS Med. Chem. Lett.*, 2013, **4**, 329–32.

[192] M. R. Jones, C. Mu, M. C. Wang, M. I. Webb, C. J. Walsby and T. Storr, *Metallomics*, 2015, **7**, 129–35.

[193] M. I. Webb, R. A. Chard, Y. M. Al-Jobory, M. R. Jones, E. W. Wong and C. J. Walsby, *Inorg. Chem.*, 2012, **51**, 954–66.

[194] L. M. F. Gomes, J. C. Bataglioli, A. J. Jussila, J. R. Smith, C. J. Walsby and T. Storr, *Front. Chem.*, 2019, **7**, 838–851.

[195] S. E. Huffman, G. K. Yawson, S. S. Fisher, P. J. Bothwell, D. C. Platt, M. A. Jones, C. G. Hamaker and M. I. Webb, *Metallomics*, 2020, **12**, 491–503.

[196] G. Li, L. Sun, L. Ji and H. Chao, *Dalton Trans.*, 2016, **45**, 13261–76.

[197] G. Son, B. I. Lee, Y. J. Chung and C. B. Park, *Acta Biomater.*, 2018, **67**, 147–155.

[198] N. P. Cook, M. Ozbil, C. Katsampes, R. Prabhakar and A. A. Marti, *J. Am. Chem. Soc.*, 2013, **135**, 10810–6.

[199] A. Aliyan, N. P. Cook and A. A. Martí, *Chem. Rev.*, 2019, **119**, 11819–11856.

[200] B. Jiang, A. Aliyan, N. P. Cook, A. Augustine, G. Bhak, R. Maldonado, A. D. Smith McWilliams, E. M. Flores, N. Mendez, M. Shahnawaz, F. J. Godoy, J. Montenegro, I. Moreno-Gonzalez and A. A. Marti, *J. Am. Chem. Soc.*, 2019, **141**, 15605–15610.

[201] N. A. Vyas, S. S. Bhat, A. S. Kumbhar, U. B. Sonawane, V. Jani, R. R. Joshi, S. N. Ramteke, P. P. Kulkarni and B. Joshi, *Eur. J. Med. Chem.*, 2014, **75**, 375–81.

[202] D. E. S. Silva, M. P. Cali, W. M. Pazin, E. Carlos-Lima, M. T. Salles Trevisan, T. Venâncio, M. Arcisio-Miranda, A. S. Ito and R. M. Carlos, *J. Med. Chem.*, 2016, **59**, 9215–9227.

[203] G. Karthivashan, P. Ganesan, S. Y. Park, J. S. Kim and D. K. Choi, *Drug Deliv.*, 2018, **25**, 307–320.

[204] A. Kumar, A. Singh and Ekavali, *Pharmacol. Rep.*, 2015, **67**, 195–203.

[205] M. Prince, A. Wimo, M. Guerchet, G.-C. Ali, Y.-T. Wu and M. Prina, *World Alzheimer Report 2015. The Global Impact on Dementia. An Analysis of Prevalence, Incidence, Cost and Trends*, web, 2015.

[206] R. Nortley, N. Korte, P. Izquierdo, C. Hirunpattarasilp, A. Mishra, Z. Jaunmuktane, V. Kyrargyri, T. Pfeiffer, L. Khennouf, C. Madry, H. Gong, A. Richard-Loendt, W. Huang, T. Saito, T. C. Saido, S. Brandner, H. Sethi and D. Attwell, *Science*, 2019, **365**, 250–263.

[207] I. Espuny-Camacho, A. M. Arranz, M. Fiers, A. Snellinx, K. Ando, S. Munck, J. Bonnefont, L. Lambot, N. Corthout, L. Omodho, E. Vanden Eynden, E. Radaelli, I. Tesseur, S. Wray, A. Ebneth, J. Hardy, K. Leroy, J.-P. Brion, P. Vanderhaeghen and B. De Strooper, *Neuron*, 2017, **93**, 1066–1081.

[208] A. Tanghe, A. Termont, P. Merchiers, S. Schilling, H.-U. Demuth, L. Scrocchi, F. Van Leuven, G. Griffioen and T. Van Dooren, *Int. J. Alzheimers Dis.*, 2010, **2010**, 417314–417323.

[209] V. W. Chow, M. P. Mattson, P. C. Wong and M. Gleichmann, *Neuromol. Med.*, 2010, **12**, 1–12.

[210] R. P. Friedrich, K. Tepper, R. Ronicke, M. Soom, M. Westermann, K. Reymann, C. Kaether and M. Fandrich, *Proc. Natl. Acad. Sci. USA*, 2010, **107**, 1942–7.

[211] A. M. Klein, N. W. Kowall and R. J. Ferrante, *Ann. N. Y. Acad. Sci.*, 1999, **893**, 314–20.

[212] B. Barz, Q. Liao and B. Strodel, *J. Am. Chem. Soc.*, 2018, **140**, 319–327.

[213] W. S. Shin, J. Di, Q. Cao, B. Li, P. M. Seidler, K. A. Murray, G. Bitan and L. Jiang, *Alzheimers Res. Ther.*, 2019, **11**, 86–99.

[214] I. C. Stancu, B. Vasconcelos, D. Terwel and I. Dewachter, *Mol. Neurodegener.*, 2014, **9**, 51–65.

[215] W. H. Zheng, S. Bastianetto, F. Mennicken, W. Ma and S. Kar, *Neuroscience*, 2002, **115**, 201–11.

[216] Y. P. Ginotra, S. N. Ramteke, G. R. Walke, S. Rapole and P. P. Kulkarni, *Free Radic. Res.*, 2016, **50**, 405–13.

[217] H. Kadowaki, H. Nishitoh, F. Urano, C. Sadamitsu, A. Matsuzawa, K. Takeda, H. Masutani, J. Yodoi, Y. Urano, T. Nagano and H. Ichijo, *Cell. Death Differ.*, 2005, **12**, 19–24.

[218] M. Nakamura, N. Shishido, A. Nunomura, M. A. Smith, G. Perry, Y. Hayashi, K. Nakayama and T. Hayashi, *Biochemistry*, 2007, **46**, 12737–43.

[219] S. Parthasarathy, B. Yoo, D. McElheny, W. Tay and Y. Ishii, *J. Biol. Chem.*, 2014, **289**, 9998–10010.

[220] D. G. Smith, R. Cappai and K. J. Barnham, *Biochim. Biophys. Acta*, 2007, **1768**, 1976–90.

[221] L. He, X. Wang, D. Zhu, C. Zhao and W. Du, *Metallomics*, 2015, **7**, 1562–72.

[222] J. Martins, A. C., P. Morcillo, O. M. Ijomone, V. Venkataramani, F. E. Harrison, E. Lee, A. B. Bowman and M. Aschner, *Int. J. Environ. Res. Public Health*, 2019, **16**, 3546–3562.

[223] R. Alberto, K. Ortner, N. Wheatley, R. Schibli and A. P. Schubiger, *J. Am. Chem. Soc.*, 2001, **123**, 3135–6.

[224] C. Y. Chan, A. Noor, C. A. McLean, P. S. Donnelly and P. J. Barnard, *Chem. Commun.*, 2017, **53**, 2311–2314.

[225] Y. Cheng, M. Ono, H. Kimura, M. Ueda and H. Saji, *J. Med. Chem.*, 2012, **55**, 2279–86.

[226] C. Kiritsis, B. Mavroidi, A. Shegani, L. Palamaris, G. Loudos, M. Sagnou, I. Pirmettis, M. Papadopoulos and M. Pelecanou, *ACS Med. Chem. Lett.*, 2017, **8**, 1089–1092.

[227] M. Li, S. E. Howson, K. Dong, N. Gao, J. Ren, P. Scott and X. Qu, *J. Am. Chem. Soc.*, 2014, **136**, 11655–63.

[228] L. M. F. Gomes, J. C. Bataglioli and T. Storr, *Coord. Chem. Rev.*, 2020, **412**, 213255–213292.

[229] A. Spinello, R. Bonsignore, G. Barone, B. K. Keppler and A. Terenzi, *Curr. Pharm. Des.*, 2016, **22**, 3996–4010.

[230] A. O. Adeloye and P. A. Ajibade, *Molecules*, 2014, **19**, 12421–60.

[231] G. Leem, Z. A. Morseth, K. R. Wee, J. Jiang, M. K. Brennaman, J. M. Papanikolas and K. S. Schanze, *Chem. Asian J.*, 2016, **11**, 1257–67.

[232] M. Schwalbe, M. Karnahl, H. Gorls, D. Chartrand, F. Laverdiere, G. S. Hanan, S. Tschierlei, B. Dietzek, M. Schmitt, J. Popp, J. G. Vos and S. Rau, *Dalton Trans.*, 2009, **20**, 4012–22.

[233] J. P. Barolli, R. S. Corrêa, F. S. Miranda, J. U. Ribeiro, C. Bloch Jr., J. Ellena, V. Moreno, M. R. Cominetti and A. A. Batista, *J. Brazil Chem. Soc.*, 2017, **28**, 1879–1889.

[234] M. R. Gill, S. N. Harun, S. Halder, R. A. Boghozian, K. Ramadan, H. Ahmad and K. A. Vallis, *Sci. Rep.*, 2016, **6**, 31973.

[235] L. Perdisatt, S. Moqadasi, L. O'Neill, G. Hessman, A. Ghion, M. Q. M. Warraich, A. Casey and C. O'Connor, *J. Inorg. Biochem.*, 2018, **182**, 71–82.

[236] P. Canovic, A. R. Simovic, S. Radisavljevic, I. Bratsos, N. Demitri, M. Mitrovic, I. Zelen and Z. D. Bugarcic, *J. Biol. Inorg. Chem.*, 2017, **22**, 1007–1028.

[237] S. H. Lai, W. Li, J. H. Yao, B. J. Han, G. B. Jiang, C. Zhang, C. C. Zeng and Y. J. Liu, *J. Photochem. Photobiol. B*, 2016, **158**, 39–48.

[238] F. Li, M. Feterl, J. M. Warner, A. I. Day, F. R. Keene and J. G. Collins, *Dalton Trans.*, 2013, **42**, 8868–8877.

[239] A. A. Abdel-Shafi, H. A. Hassanin and S. S. Al-Shihry, *Photochem. Photobiol. Sci.*, 2014, **13**, 1330–7.

[240] M. I. Gutiérrez, C. G. Martínez, D. García-Fresnadillo, A. M. Castro, G. Orellana, A. M. Braun and E. Oliveros, *J. Phys. Chem. A*, 2003, **107**, 3397–3403.

[241] J. Roque III, D. Havrylyuk, P. Barrett, T. Sainuddin, J. McCain, K. Colón, W. Sparks, E. Bradner, S. Monro, K. Heidary, C. Cameron, E. Glazer and S. McFarland, *Photochem. Photobiol.*, 2019, **96**, 327–339.

[242] K. Lin, Z.-Z. Zhao, H.-B. Bo, X.-J. Hao and J.-Q. Wang, *Front. Pharmacol.*, 2018, **9**, 1323–1333.

[243] E. Wachter, B. S. Howerton, E. C. Hall, S. Parkin and E. C. Glazer, *Chem. Commun.*, 2014, **50**, 311–3.

[244] R. P. C. GmbH, *Article on Color Temperature in the RP Photonics Encyclopedia*, `https://www.rp-photonics.com/color_temperature.html`, 2020, [Online; accessed August 06th, 2020].

[245] A. N. Hidayatullah, E. Wachter, D. K. Heidary, S. Parkin and E. C. Glazer, *Inorg. Chem.*, 2014, **53**, 10030–2.

[246] A. D. Chapp, S. Schum, J. E. Behnke, T. Hahka, M. J. Huber, E. Jiang, R. A. Larson, Z. Shan and Q.-H. Chen, *Physiol. rep.*, 2018, **6**, 13666–13666.

[247] W. M. Motswainyana and P. A. Ajibade, *Adv. Chem.*, 2015, **2015**, 859730.

[248] E. Wachter and E. C. Glazer, *J. Phys. Chem. A*, 2014, **118**, 10474–86.

[249] X. Wang, X. Wang, C. Zhang, Y. Jiao and Z. Guo, *Chem. Sci.*, 2012, **3**, 1304–1312.

[250] J. Danielsson, R. Pierattelli, L. Banci and A. Graslund, *FEBS J.*, 2007, **274**, 46–59.

[251] G. Ma, F. Huang, X. Pu, L. Jia, T. Jiang, L. Li and Y. Liu, *Chem. Eur. J.*, 2011, **17**, 11657–11666.

[252] M. Turner, J. A. Platts and R. J. Deeth, *J. Chem. Theory Comput.*, 2016, **12**, 1385–1392.

[253] A. A. Almaqwashi, W. Zhou, M. N. Naufer, I. A. Riddell, O. H. Yilmaz, S. J. Lippard and M. C. Williams, *J. Am. Chem. Soc.*, 2019, **141**, 1537–1545.

[254] B. Zott, M. M. Simon, W. Hong, F. Unger, H. J. Chen-Engerer, M. P. Frosch, B. Sakmann, D. M. Walsh and A. Konnerth, *Science*, 2019, **365**, 559–565.

[255] F. Hane, G. Tran, S. J. Attwood and Z. Leonenko, *PLoS One*, 2013, **8**, 59005–59013.

[256] K. E. Marshall, D. M. Vadukul, L. Dahal, A. Theisen, M. W. Fowler, Y. Al-Hilaly, L. Ford, G. Kemenes, I. J. Day, K. Staras and L. C. Serpell, *Sci. Rep.*, 2016, **6**, 30182.

[257] H. M. Sanders, R. Lust and J. K. Teller, *Peptides*, 2009, **30**, 849–54.

[258] F. G. De Felice, P. T. Velasco, M. P. Lambert, K. Viola, S. J. Fernandez, S. T. Ferreira and W. L. Klein, *J. Biol. Chem.*, 2007, **282**, 11590–601.

[259] E. Y. Hayden and D. B. Teplow, *Alzheimers Res. Ther.*, 2013, **5**, 60–71.

[260] W. L. Klein, *J. Alzheimers Dis.*, 2013, **33**, 49–65.

[261] S. E. Lesne, *Swiss Med. Wkly*, 2014, **144**, 14021–14031.

[262] r. LeVine, H., Q. Ding, J. A. Walker, R. S. Voss and C. E. Augelli-Szafran, *Neurosci. Lett.*, 2009, **465**, 99–103.

[263] M. Verma, A. Vats and V. Taneja, *Ann. Indian Acad. Neurol.*, 2015, **18**, 138–45.

[264] M. R. Jones, E. Mathieu, C. Dyrager, S. Faissner, Z. Vaillancourt, K. J. Korshavn, M. H. Lim, A. Ramamoorthy, V. Wee Yong, S. Tsutsui, P. K. Stys and T. Storr, *Chem. Sci.*, 2017, **8**, 5636–5643.

[265] M. Merezhko, P. Muggalla, N. P. Nykanen, X. Yan, P. Sakha and H. J. Huttunen, *PLoS One*, 2014, **9**, 98619–98628.

[266] Y. F. Mok and G. J. Howlett, *Methods Enzymol.*, 2006, **413**, 199–217.

[267] H. W. Wang, J. F. Pasternak, H. Kuo, H. Ristic, M. P. Lambert, B. Chromy, K. L. Viola, W. L. Klein, W. B. Stine, G. A. Krafft and B. L. Trommer, *Brain Res.*, 2002, **924**, 133–40.

[268] N. E. Pryor, M. A. Moss and C. N. Hestekin, *Int. J. Mol. Sci.*, 2012, **13**, 3038–3072.

[269] N. Rezaei-Ghaleh, M. Amininasab, S. Kumar, J. Walter and M. Zweckstetter, *Nature Commun.*, 2016, **7**, 11359–11359.

[270] G. Gong, J. Xu, X. Huang and W. Du, *J. Biol. Inorg. Chem.*, 2019, **24**, 179–189.

[271] D. J. Hayne, S. Lim and P. S. Donnelly, *Chem. Soc. Rev.*, 2014, **43**, 6701–15.

[272] D. Zhu, G. Gong, W. Wang and W. Du, *J. Inorg. Biochem.*, 2017, **170**, 109–116.

[273] A. Alghamdi, V. Vyshemirsky, D. J. S. Birch and O. J. Rolinski, *Methods Appl. Fluoresc.*, 2018, **6**, 024002–024008.

[274] M. Amaro, D. J. Birch and O. J. Rolinski, *Phys. Chem. Chem. Phys.*, 2011, **13**, 6434–41.

[275] O. J. Rolinski, T. Wellbrock, D. J. Birch and V. Vyshemirsky, *J. Phys. Chem. Lett.*, 2015, **6**, 3116–20.

[276] M. Biancalana, K. Makabe, A. Koide and S. Koide, *J. Mol. Biol.*, 2009, **385**, 1052–1063.

[277] F. Peccati, S. Pantaleone, V. Riffet, X. Solans-Monfort, J. Contreras-García, V. Guallar and M. Sodupe, *J. Phys. Chem. B*, 2017, **121**, 8926–8934.

[278] K. Gade Malmos, L. M. Blancas-Mejia, B. Weber, J. Buchner, M. Ramirez-Alvarado, H. Naiki and D. Otzen, *Amyloid*, 2017, **24**, 1–16.

[279] C. Xue, T. Y. Lin, D. Chang and Z. Guo, *R. Soc. Open Sci.*, 2017, **4**, 160696–160708.

[280] r. LeVine, H., *Amyloid*, 2005, **12**, 5–14.

[281] M. Groenning, *J. Chem. Biol.*, 2010, **3**, 1–18.

[282] A. T. Petkova, Y. Ishii, J. J. Balbach, O. N. Antzutkin, R. D. Leapman, F. Delaglio and R. Tycko, *Proc. Natl. Acad. Sci. USA*, 2002, **99**, 16742–16747.

[283] Y. Xiao, B. Ma, D. McElheny, S. Parthasarathy, F. Long, M. Hoshi, R. Nussinov and Y. Ishii, *Nat. Struct. Mol. Biol.*, 2015, **22**, 499–505.

[284] S. Barelier, S. E. Boyce, I. Fish, M. Fischer, D. B. Goodin and B. K. Shoichet, *PLoS One*, 2013, **8**, 69153–69164.

[285] G. Lemmon and J. Meiler, *PLoS One*, 2013, **8**, 67536–67548.

[286] H. Zhong, Z. Wang, X. Wang, H. Liu, D. Li, H. Liu, X. Yao and T. Hou, *Phys. Chem. Chem. Phys.*, 2019, **21**, 25276–25289.

[287] E. C. Johnson, B. P. Sullivan, D. J. Salmon, S. A. Adeyemi and T. J. Meyer, *Inorg. Chem.*, 1978, **17**, 2211–2215.

[288] D. S. Wuttke, M. J. Bjerrum, I. J. Chang, J. R. Winkler and H. B. Gray, *BBA - Bioenergetics*, 1992, **1101**, 168–170.

[289] K. Sigfridsson, M. Sundahl, M. J. Bjerrum and O. Hansson, *J. Biol. Inorg. Chem.*, 1996, **1**, 405–414.

[290] E. S. Ryabova, V. N. Goral, E. Csöregi, B. Mattiasson and A. D. Ryabov, *Angew. Chem. Int. Ed.*, 1999, **38**, 804–807.

[291] S. Mondal, S. Ray, A. Chattopadhyay, D. Nandi and A. Ghosh, *Prog. React. Kinet. Mec.*, 2014, **39**, 311–327.

[292] T. B. Karpishin, M. W. Grinstaff, S. Komar-Panicucci, G. McLendon and H. B. Gray, *Structure*, 1994, **2**, 415–22.

[293] S. Reiter, K. Eckhard, A. Blöchl and W. Schuhmann, *Analyst*, 2001, **126**, 1912–8.

[294] J. Hong, Y. Miao, R. Miao, G. Yang, H. Tang, Z. Guo and L. Zhu, *J. Mass Spectrom.*, 2005, **40**, 91–9.

[295] S. K. Pachahara, N. Chaudhary, C. Subbalakshmi and R. Nagaraj, *J. Pept. Sci.*, 2012, **18**, 233–41.

[296] R. Sabate, M. Gallardo and J. Estelrich, *Biopolymers*, 2003, **71**, 190–5.

[297] C. Cheignon, M. Jones, E. Atrian-Blasco, I. Kieffer, P. Faller, F. Collin and C. Hureau, *Chem. Sci.*, 2017, **8**, 5107–5118.

[298] L. Chiang, L. E. Allan, J. Alcantara, M. C. Wang, T. Storr and M. P. Shaver, *Dalton Trans.*, 2014, **43**, 4295–304.

[299] J. K. Kasim, I. Kavianinia, P. W. R. Harris and M. A. Brimble, *Front. Chem.*, 2019, **7**, 472–497.

[300] P. Tothill, L. M. Matheson, J. F. Smyth and K. McKay, *J. Anal. At. Spectrom.*, 1990, **5**, 619–622.

[301] E. E. Brouwers, M. Tibben, H. Rosing, J. H. Schellens and J. H. Beijnen, *Mass Spectrom. Rev.*, 2008, **27**, 67–100.

[302] J. Gong, M. J. Solivio, E. J. Merino, J. A. Caruso and J. A. Landero-Figueroa, *Anal. Bioanal. Chem.*, 2015, **407**, 2433–7.

[303] R. Larios, M. E. Del Castillo Busto, D. Garcia-Sar, C. Ward-Deitrich and H. Goenaga-Infante, *J. Anal. At. Spectrom.*, 2019, **34**, 729–740.

[304] M. H. M. Klose, S. Theiner, C. Kornauth, S. M. Meier-Menches, P. Heffeter, W. Berger, G. Koellensperger and B. K. Keppler, *Metallomics*, 2018, **10**, 388–396.

[305] N. Baruch-Eliyahu, V. Rud, A. Braiman and E. Priel, *Sci. Rep.*, 2019, **9**, 18118.

[306] R. Rajmohan and P. H. Reddy, *J. Alzheimers Dis.*, 2017, **57**, 975–999.

[307] M. Sardar Sinha, A. Ansell-Schultz, L. Civitelli, C. Hildesjö, M. Larsson, L. Lannfelt, M. Ingelsson and M. Hallbeck, *Acta Neuropathol.*, 2018, **136**, 41–56.

[308] S. Forner, D. Baglietto-Vargas, A. C. Martini, L. Trujillo-Estrada and F. M. LaFerla, *Trends in Neurosci.*, 2017, **40**, 347–357.

[309] L. Mucke and D. J. Selkoe, *CSH Perspect. Med.*, 2012, **2**, 6338–6356.

[310] H. Hu and M. Li, *Biochem. Biophys. Res. Commun.*, 2016, **478**, 174–180.

[311] A. K. Singh, A. Bissoyi, M. P. Kashyap, P. K. Patra and S. I. Rizvi, *Neurotox. Res.*, 2017, **32**, 351–361.

[312] C. Garza-Lombo, Y. Posadas, L. Quintanar, M. E. Gonsebatt and R. Franco, *Antioxid. Redox. Sign.*, 2018, **28**, 1669–1703.

[313] P. Su, M. Aschner, J. Chen and W. Luo, in *Chapter 19 - Metals and Autophagy in Neurotoxicity*, Academic Press, 2017, book section 19, pp. 377–398.

[314] J. Kovalevich and D. Langford, *Methods Mol. Biol.*, 2013, **1078**, 9–21.

[315] H. Xicoy, B. Wieringa and G. J. M. Martens, *Mol. Neurodegener.*, 2017, **12**, 10–21.

[316] J. Bieschke, M. Herbst, T. Wiglenda, R. P. Friedrich, A. Boeddrich, F. Schiele, D. Kleckers, J. M. Lopez del Amo, B. A. Gruning, Q. Wang, M. R. Schmidt, R. Lurz, R. Anwyl, S. Schnoegl, M. Fandrich, R. F. Frank, B. Reif, S. Gunther, D. M. Walsh and E. E. Wanker, *Nat. Chem. Biol.*, 2011, **8**, 93–101.

[317] S. C. Drew and K. J. Barnham, *Acc. Chem. Res.*, 2011, **44**, 1146–1155.

[318] R. Liu, H. Barkhordarian, S. Emadi, C. B. Park and M. R. Sierks, *Neurobiol. Dis.*, 2005, **20**, 74–81.

[319] K. K. Frederick, M. S. Marlow, K. G. Valentine and A. J. Wand, *Nature*, 2007, **448**, 325–9.

[320] A. D. Gossert and W. Jahnke, *Prog. Nucl. Magn. Reson. Spectrosc.*, 2016, **97**, 82–125.

[321] U. Holzgrabe, *Prog. Nucl. Magn. Reson. Spectrosc.*, 2010, **57**, 229–40.

[322] P. Rossi, Y. Xia, N. Khanra, G. Veglia and C. G. Kalodimos, *J. Biomol. NMR*, 2016, **66**, 259–271.

[323] P. Schanda, V. Forge and B. Brutscher, *Proc. Natl. Acad. Sci. USA*, 2007, **104**, 11257–62.

[324] P. Schanda, E. Kupce and B. Brutscher, *J. Biomol. NMR*, 2005, **33**, 199–211.

[325] B. R. Sahoo, S. J. Cox and A. Ramamoorthy, *Chem. Commun.*, 2020, **56**, 4627–4639.

[326] P. Schanda and B. Brutscher, *J. Magn. Reson.*, 2006, **178**, 334–9.

[327] J. Kang, S. J. Lee, J. S. Nam, H. J. Lee, M. G. Kang, K. J. Korshavn, H. T. Kim, J. Cho, A. Ramamoorthy, H. W. Rhee, T. H. Kwon and M. H. Lim, *Chemistry*, 2017, **23**, 1645–1653.

[328] T. Qiu, Q. Liu, Y. X. Chen, Y. F. Zhao and Y. M. Li, *J. Pept. Sci.*, 2015, **21**, 522–9.

Appendix A

Supplementary Information for Chapter 2

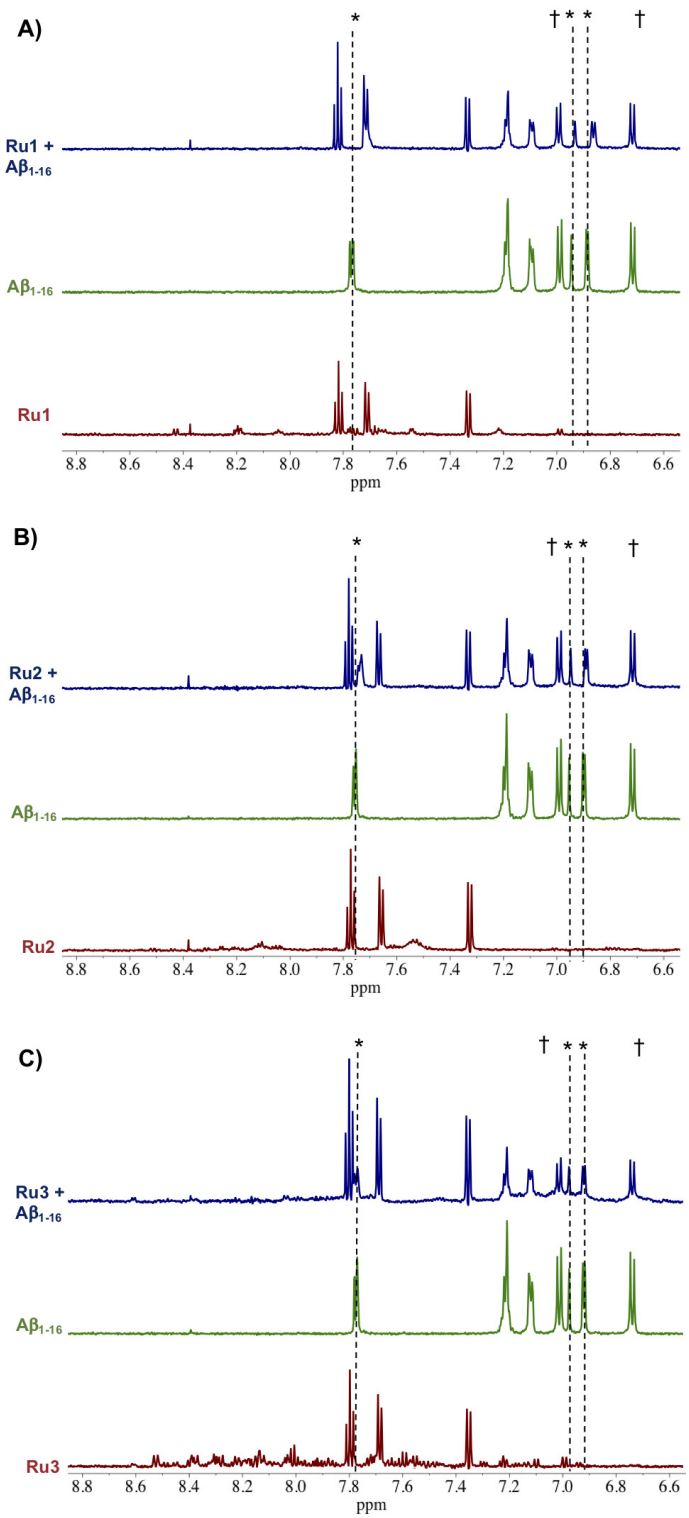

Figure A.1 Changes in ^{1}H NMR spectra in the presence of Ru(II) complexes. Shown are spectra obtained at 200 µM of A$\beta_{1\text{-}16}$ and **Ru1** (A), **Ru2** (B), and **Ru3** (C) prepared in PBS buffer (0.01 M, pH 7.4) at 37 ℃ and 24 h after photoactivation. * His^{6}, His^{13} and His^{14}. † Tyr^{10}.

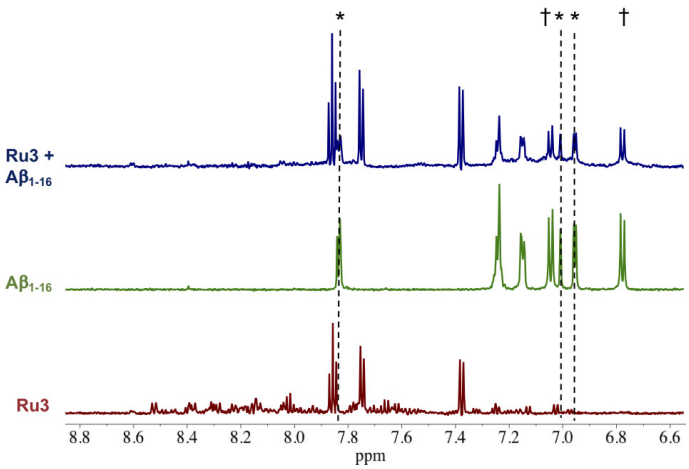

Figure A.2 Shown are spectra obtained at 200 µM of $A\beta_{1\text{-}16}$ and 2.0 eq. of **Ru3** prepared in PBS buffer (0.01 M, pH 7.4) at 37 ℃ and 24 h after photoactivation. * His^{6}, His^{13} and His^{14}. † Tyr^{10}.

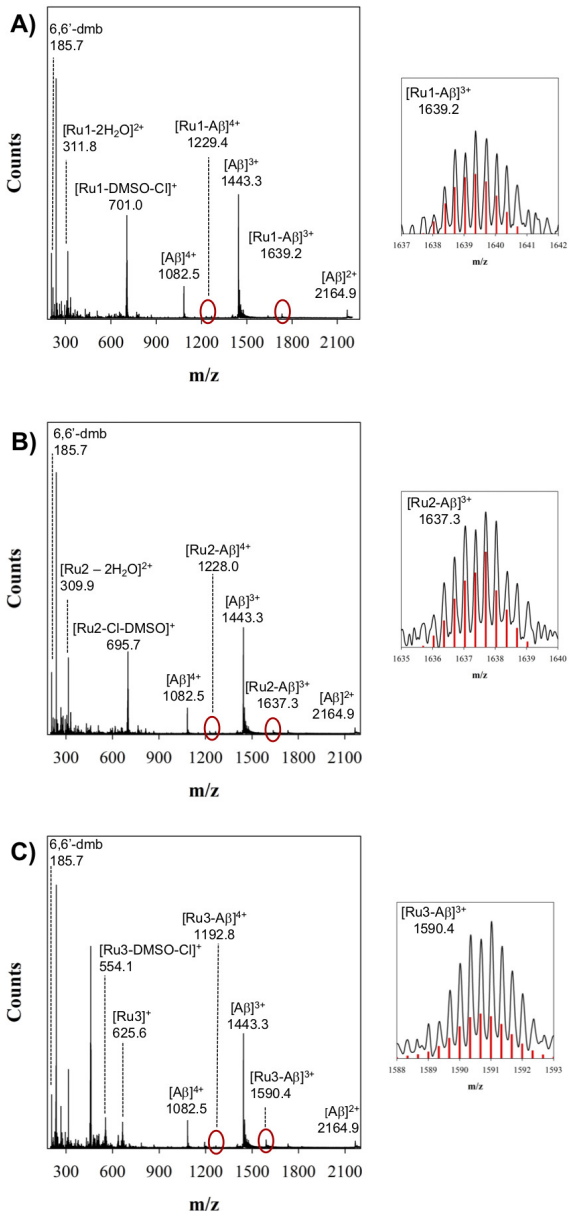

Figure A.3 ESI-MS of **Ru1** (A), **Ru2** (B), and **Ru3** (C) and $A\beta_{1\text{-}40}$ indicating the adduct formation in the zoomed in regions. In red the theoretical isotopic pattern. Samples were prepared in NH_4CO_3 buffer (20 mM, pH 9.0) and data was collected after the respective times for activation.

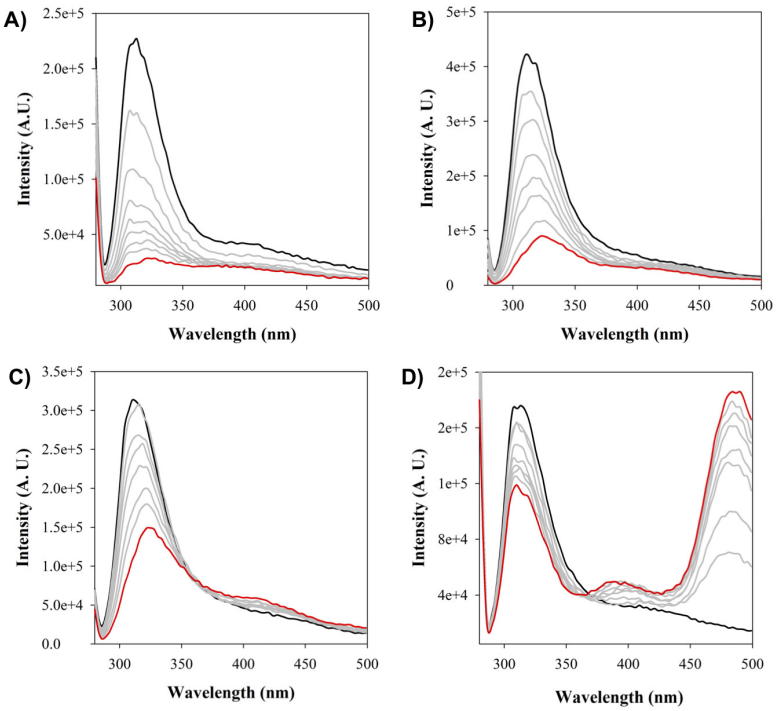

Figure A.4 Tyrosine fluorescence titration of 10 µM $A\beta_{1\text{-}42}$ upon titration with **Ru1** (A), **Ru2** (B), **Ru3** (C), and ThT (D) in PBS 0.01 M, pH 7.4 ($\lambda_{ex}/\lambda_{em}$ = 275/310 nm).

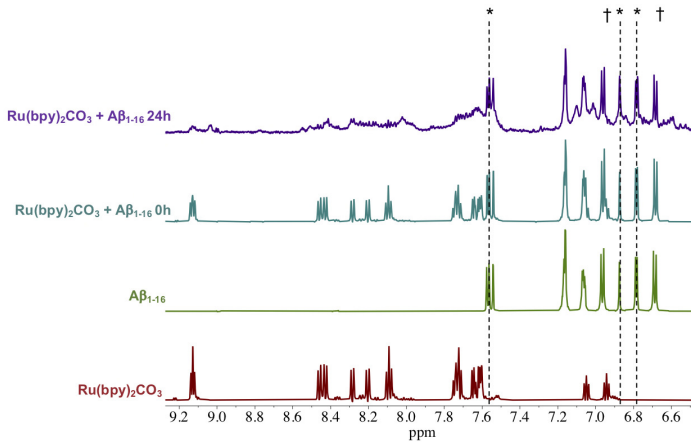

Figure A.5 Changes in ^{1}H NMR spectra in the presence of $Ru(bpy)_2CO_3$ complex. Shown are spectra obtained at 200 µM of $A\beta_{1\text{-}16}$ and 1.0 eq. of $Ru(bpy)_2CO_3$ prepared in PBS buffer (0.01 M, pH 7.4) at 37 °C. * His^6, His^{13} and His^{14}. † Tyr^{10}. Broadening of signals is likely due to precipitation.

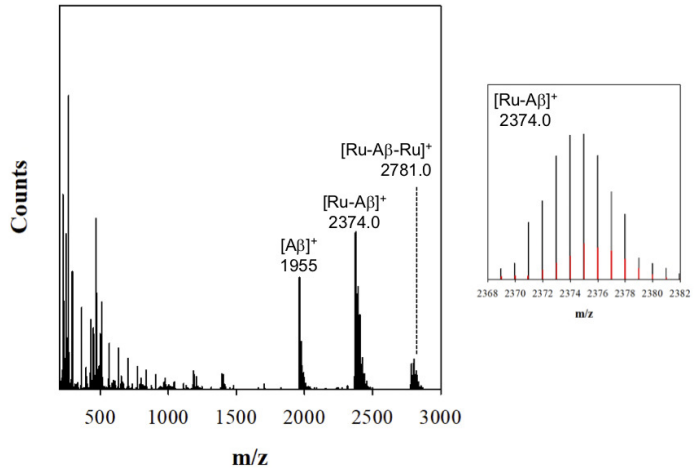

Figure A.6 ESI-MS of $Ru(bpy)_2CO_3$ and $A\beta_{1\text{-}16}$ indicating the adduct formation in the zoomed in region. In red the theoretical isotopic pattern. Samples were prepared in NH_4CO_3 buffer (20 mM, pH 9.0) and data was collected after the respective times for activation.

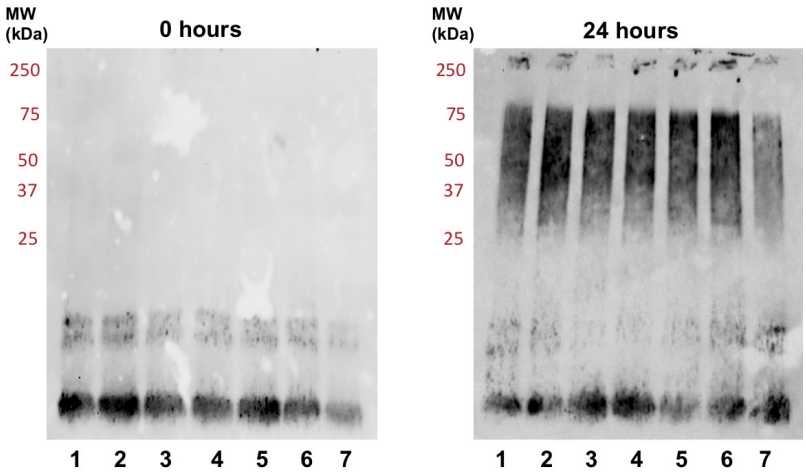

Figure A.7 Gel Electrophoresis/Western blot of 25 µM $A\beta_{1\text{-}42}$ and different concentrations of $Ru(bpy)_2CO_3$ in PBS buffer (0.01 M, pH 7.4) at 0 h and 24 h incubation with agitation at 37 ℃, using anti-Aβ antibody 6E10. Lane 1: $A\beta_{1\text{-}42}$; lane 2: $A\beta_{1\text{-}42}$ + 0.10 eq. Ru complex; lane 3 $A\beta_{1\text{-}42}$+ 0.25 eq. Ru complex; lane 4: $A\beta_{1\text{-}42}$+ 0.50 eq. Ru complex; lane 5: $A\beta_{1\text{-}42}$+ 1.0 eq. Ru complex; lane 6: $A\beta_{1\text{-}42}$+ 1.5 eq. Ru complex; lane 7: $A\beta_{1\text{-}42}$+ 2.0 eq. Ru complex.